ANL-6378
Reactor Technology
(TID-4500, 17th Ed.)
AEC Research and
Development Report

ARGONNE NATIONAL LABORATORY
9700 South Cass Avenue
Argonne, Illinois

CRITICAL EXPERIMENTS WITH THORIA-URANIA FUEL IN HEAVY WATER

by

W. C. Redman, S. G. Kaufmann,
K. E. Plumlee, and Q. L. Baird

including work done by

J. W. Armstrong, J. A. Beidelman, C. E. Cohn,
L. R. Dates, D. A. Daavettila, J. L. Helfrich,
E. Hellstrand, R. A. Mattson, and A. B. Rothman

Reactor Engineering Division

December 1961

Operated by The University of Chicago
under
Contract W-31-109-eng-38

DISCLAIMER

This report was prepared as an account of work sponsored by an agency of the United States Government. Neither the United States Government nor any agency Thereof, nor any of their employees, makes any warranty, express or implied, or assumes any legal liability or responsibility for the accuracy, completeness, or usefulness of any information, apparatus, product, or process disclosed, or represents that its use would not infringe privately owned rights. Reference herein to any specific commercial product, process, or service by trade name, trademark, manufacturer, or otherwise does not necessarily constitute or imply its endorsement, recommendation, or favoring by the United States Government or any agency thereof. The views and opinions of authors expressed herein do not necessarily state or reflect those of the United States Government or any agency thereof.

DISCLAIMER

Portions of this document may be illegible in electronic image products. Images are produced from the best available original document.

TABLE OF CONTENTS

TABLE OF CONTENTS

LIST OF FIGURES

LIST OF FIGURES

LIST OF TABLES

LIST OF TABLES

LIST OF TABLES

CRITICAL EXPERIMENTS WITH THORIA-URANIA FUEL IN HEAVY WATER

by

W. C. Redman, S. G. Kaufmann,
K. E. Plumlee, and Q L. Baird

ABSTRACT

The nuclear characteristics of a variety of small reactors composed of thoria-urania fuel in heavy water have been determined in a program of critical experimentation. The fuel element consisted of ceramic ThO_2-$U^{235}O_2$ pellets stacked to a height of 1.5 m within 0.787-cm-OD aluminum tubing. The pellets used most frequently were of 0.587-cm diameter and had a Th/U^{235} atom ratio of 25. Rods containing similar pellets with only half as much U^{235} were used to achieve small changes in the U^{235} content of the cores Some cores were assembled with 0.660-cm-diameter pellets having an atom ratio of 15. All cores were located in a 2-m-diameter tank containing D_2O.

Three distinct core structures were used, allowing measurements with uniformly distributed fuel rods, loading patterns compatible with the EBWR core geometry, and clustered lattice arrangements with D_2O, H_2O, and air surrounding the clustered fuel. Most of the cores assembled had some amount of radial D_2O reflector. A 0.3-m-thick bottom reflector composed of D_2O and aluminum was always present. For most of the assemblies, the control rods were fully withdrawn, criticality being achieved by adjustment of the water level. Observed critical dimensions and the results of the conventional reactivity, foil activation, and fuel substitution experiments used to determine core parameters such as p, ϵ, f, and τ, are reported. Information on void and temperature coefficients and control rod worth is included. No comparison of the experimental results with theoretical predictions is made nor are observations made on flux-trap systems of this composition included in this report.

I. INTRODUCTION

A. Nature of the THUD Program

From July 1957 to December 1959, Argonne's Zero Power Reactor Facility #7 (ZPR-VII) was used for the study of a variety of critical systems of thoria-urania fuel in heavy water. The term THUD was applied to this study and is derived from the chemical symbols for the principal ingredients, namely, thorium, uranium, and deuterium.

The investigation of the nuclear properties of this selection of materials was undertaken for several reasons. Oxide fuels, especially thorium-oxide, offer the prospect of achieving high burnup and are quite compatible with high-temperature water. Interest in the thorium cycle is based on the desirability of extracting the nuclear energy available in the more abundant fertile material. Good neutron economy is achievable with D_2O, and the lattice pattern in an optimum D_2O design is attractive for a forced-circulation reactor. Favorable operating characteristics had been observed in tests at Argonne for a boiling thoria-urania light-water system (BORAX-IV). It was anticipated that even greater stability would be achieved in a boiling reactor composed of a ceramic fuel in heavy water, because of the longer neutron lifetime and the smaller reactivity in steam.

The original objective of the THUD program was to design a loading of thoria-urania for subsequent insertion in Argonne's Experimental Boiling Water Reactor System (EBWR). At the time this program was initiated, the knowledge of the resonance escape probability and age for systems containing thorium was inadequate for the precision required in the computation of a thermal reactor. In addition, there was appreciable uncertainty regarding void coefficients of reactivity, a quantity of major importance in boiling systems. Consequently, an experimental program was undertaken to acquire both general information on lattice and criticality parameters, and data on void coefficients of reactivity. Fuel of two ratios of thorium to U^{235} was acquired, to achieve experimental flexibility and simultaneously to offset the disadvantage resulting from inadequate information on the properties of thorium-fueled reactors. At a later date, fuel of a third enrichment was obtained on an exchange basis from the Babcock and Wilcox Company, which was involved in a study of the properties of thoria-urania light-water assemblies.

The initial experiments performed in ZPR-VII were done in a geometry which duplicated that existing in the EBWR. However, it became apparent that the first loading of EBWR would occupy the facility for an extended period, because the conservative design of that system made feasible its operation at powers appreciably above the target level of 20 Mwt. Consequently, the THUD program turned from studies of a mockup nature to a systematic investigation of the properties of assemblies having simple geometry. At a later date, an investigation was made of more practical

clustered lattices of a variety of types thought to be of potential interest for exploitation of the advantages of a thoria-urania heavy-water system. Some measurements were also made for assemblies having a central moderating region.

The ZPR-VII facility had no special provisions for excluding air from contact with the heavy water. At the outset it was believed that the initial program with heavy water would not last for more than six months. Since EBWR was then operating with light water, it was felt that a complete clean-out of the EBWR system would not be practical when a heavy water loading was inserted, and consequently the heavy water from the THUD program could be used in EBWR. Thus, a slight contamination of this heavy water, during its use in ZPR-VII, would not be objectionable. As the scope of the program expanded and eventually even included experiments in which light water was introduced in the vicinity of clusters of this fuel, an appreciable contamination of the heavy water was inevitable. This variation in the heavy water purity complicates the interpretation of the experimental data.

B. Scope of the Report

This report is restricted to the experimental aspects of the THUD program. In general, only the methods, experimental procedures, and resulting data are presented. The large quantity of data obtained in the determination of reflector savings from flux plots and the relative photoneutron fraction from the shutdown flux decay rate makes this approach impractical for those measurements, and so only the derived values are reported in those cases. The interpretation of the experimental observations is complicated by the change in heavy water purity during the course of the program. For this reason, the analysis of the results will be presented in a subsequent report. Information on the flux-trap type of systems investigated will also be reported separately.

Some of the results obtained in the THUD program have been reported previously. Information obtained on the age and resonance escape probability during the first few months was reported at an AEC conference on thorium-fueled reactors.[1] Many of the results obtained during the first year of operation were included in a report presented at a United Nations Conference on Peaceful Uses of Atomic Energy.[2] During the course of the experimental program, there were several discussions of specific topics at the meetings of the American Nuclear Society.[3-9] The structure of the ZPR-VII facility has been described in the Hazards Summary Report[10] prepared to obtain approval for the operation of this facility for the THUD program, and the details of the instrumentation and control circuitry used for this system have also been reported.[11]

Whenever possible in the THUD program, the basic nuclear parameters ϵ, η, p, f, L^2, τ, λ_H, and λ_R were determined by independent

experimental means. This resulted in an overdetermination of these quantities, since the number of experimental relations exceeds the number of unknowns. It was hoped that this experimental approach would provide information on the relative merit and limitations of the various techniques of measurements commonly employed in critical assembly work.

Experiments performed in the THUD program to obtain information about lattice constants can be classified into four categories:

1. Observations directly interrelating lattice constants, so that if some are known by other means then the others can be evaluated. This is the type of information obtained by observation of the critical dimensions.
2. Direct determination of a particular basic lattice parameter with as little dependence on other constants as possible. Examples are foil activation measurements, which yield disadvantage factor, resonance escape probability, and reflector savings.
3. Investigations of reactor properties which are functions of the basic lattice constants, but which are related to the latter in an indirect way. Void coefficient of reactivity and control rod worth are examples of this type.
4. Measurements which provide knowledge useful for the interpretation of the other observations, such as spectral indices and delayed neutron yield.

Successive chapters of this report treat the experimental observations in each of these categories, following a description of the ZPR-VII facility and the fuel elements.

II. DESCRIPTION OF THE CRITICAL FACILITY AND CORE COMPONENTS

A. ZPR-VII

As a part of the evaluation of the ZPR-VII facility from the viewpoint of potential hazards, a detailed description of the mechanical features of this system was included in the Hazards Summary Report.[10] Subsequently, a separate report was issued on the instrumentation and control circuitry.[11] Here only the highlights of the ZPR-VII design will be reviewed. In the chapter describing clean critical experiments, details are given on the nature of the core structure used for those experiments. Likewise, the structural details of the core support are presented in the section describing the determination of reflector savings.

The ZPR-VII is a water critical facility of conventional design, being in simple form two tanks, a core tank and a storage tank, connected by fill and drain lines, with a pump and valves for transfer of water as desired. Of particular interest is the provision for precision adjustment of the water level through a variable level overflow, provision for electrical heating of the water in the dump tank to its atmospheric boiling point, and the use of pulleys and cables between the control rods and their drives to keep the top of the system relatively uncluttered.

The core tank and that core structure which duplicated the EBWR geometry are shown in Figure 1.

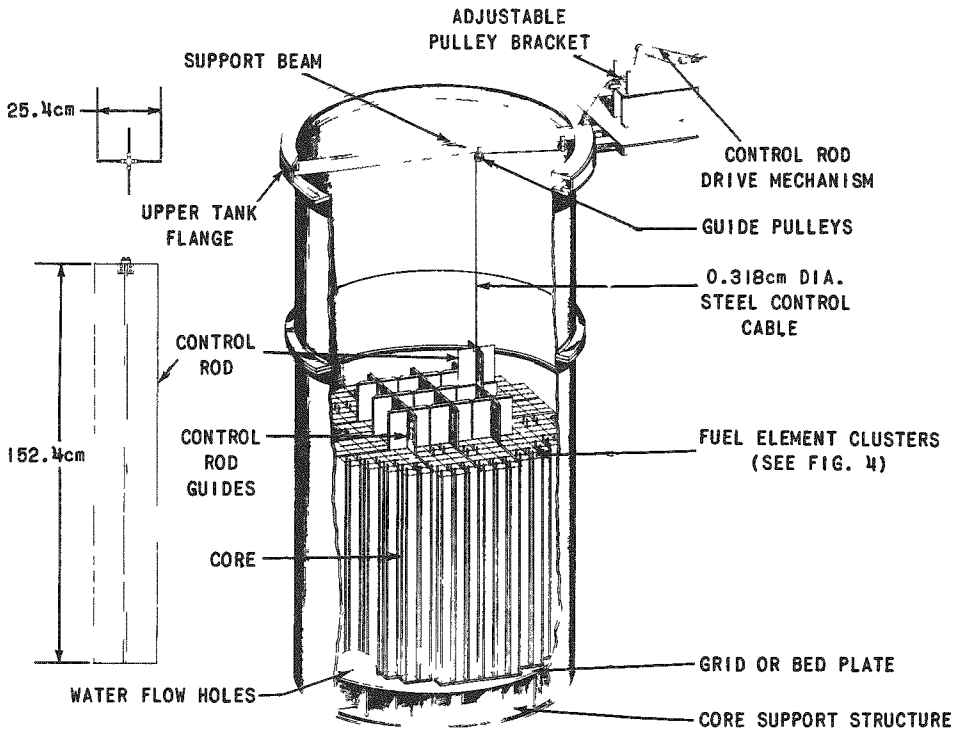

Fig. 1. EBWR Core Structure and Control Mechanism in ZPR-VII

The location of the core, very deep in the core tank, is a feature provided to reduce the complexity of a change in control rod location when operation with a top cover plate is required. The pattern of nine 25.4-cm-span cross rods and 10.16-cm-sq fuel elements of the EBWR structure is shown.

Another view of the control rod pattern is shown in Figure 2, a photograph taken prior to the insertion of fuel into this assembly. For reference purposes, a numbering system was used for the 3-by-3 array of control rods. Those at the corners were designated as No. 2, No. 4, No. 6, and No. 8. Rods No. 1, No. 3, No. 5, and No. 7 occupied the remaining peripheral locations, with the numbers in sequence around the periphery. The central rod was designated as No. 9.

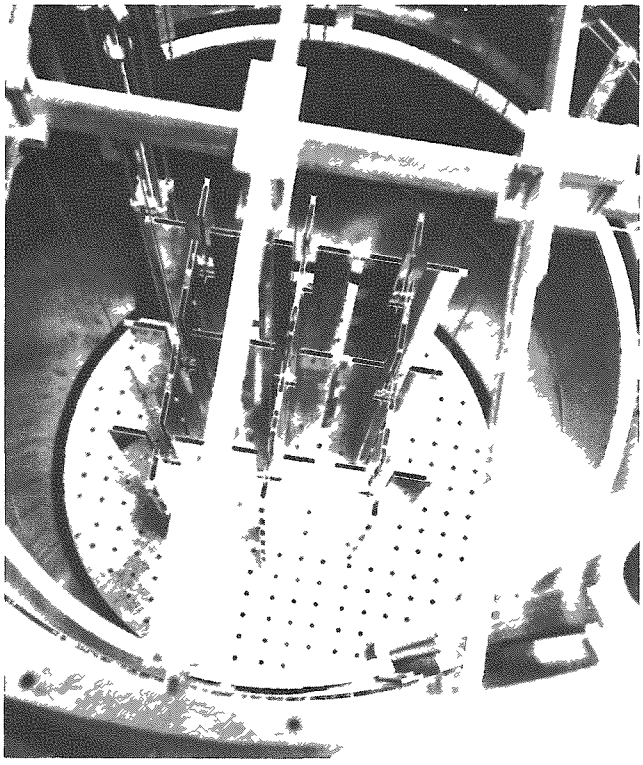

Fig. 2

ZPR-VII Core Tank Prior to Initial Loading

Most of the assemblies were made critical with the control rods completely removed from the moderator. For these assemblies it is necessary to adjust precisely the level of the water for criticality. This level is controlled through the variable level overflow standpipe, shown in the upper left hand corner of Figure 2. The position of the standpipe is transmitted to the control panel and displayed on a selsyn indicator. However, constant recirculation of the water causes a sizeable meniscus at the overflow of the standpipe, so that a difference exists between the actual water level and the indicated height of the overflow standpipe. The determination of the correction factor is described in Appendix A, and all of the data in this report have been corrected for this "zero" error in the standpipe position indicator.

The description of the ZPR-VII facility given in the Hazards Summary Report depicted the system as planned. Upon construction and initial operation of the facility, certain performance tests were made, and the need for a number of modifications became apparent. In order to update the description of the facility given in the Hazards Summary Report,[10] a summary of the observed performance and the modifications made to this facility is presented in Appendix A.

B. Description of the Fuel Elements

Considerations in connection with the design of a thoria-urania-D_2O loading for the EBWR determined the nature of the fuel elements procured for the THUD program. As a compromise among the nuclear, heat transfer, safety, and fabrication requirements, a fuel rod of 0.787-cm diameter was chosen. Aluminum and zirconium were specified as alternative cladding materials, but cost considerations led to the selection of aluminum for the critical experiments. With allowance for cladding thickness and pellet clearance, a diameter of about 0.6 cm remained for the fired thoria-urania pellets. Pellets with atomic ratios of 50/1 and 25/1 for fertile-to-fissile material were obtained for experimental flexibility.

For the interpretation of results of measurements in the THUD program, a knowledge of the dimensions, mass, chemical, and isotopic content of the fuel elements is required. Results of measurements of the properties of individual pellets, the groups of pellets within individual fuel rods and the pellet containment tubes are assembled in this section.

1. Fuel Pellets

Pellets were compounded from ThO_2 and U_3O_8 which were mixed, pelleted, and then fired to achieve a high density. In the firing the U_3O_8 is reduced to UO_2. The specifications for the fuel elements stated a minimum pellet diameter of 0.584 cm, with maximum diameter optional except that the pellets must fit without force into the aluminum containment tubes provided. The length was optional, and the pellets were to be loaded into the tubes to a length of 152.4 cm (+0.476 cm, -0 cm). Use of calcium fluoride (CaF_2), calcium oxide (CaO), or aluminum oxide (Al_2O_3) as a densifier was approved, provided that the amount in the fired body did not exceed 0.5% by weight. A maximum hydrogen content in the fuel pellets of one part in 5000 by volume was allowed.

Data are available on the weight and physical dimensions of the fuel, its chemical composition, and the isotopic composition of the uranium. Pertinent information from the supplier, from accountability records, and from physical, chemical, and nuclear measurements involving 350 pellets selected from about ten fuel rods are assembled in Appendix B.

The observed characteristics show the usual number of variables which might be encountered in the fabrication of small lots of material. The lot size was determined by criticality limitations and capacity of process equipment.

The weight of fuel pellets in the 1630 rods of 25/1 ratio ranged from 343 to 367 gm, with an average of 357.2 gm. Corresponding values for the 1525 rods of 50/1 material were 340, 359, and 349.8 gm. X-ray examination of a sample of the 25/1 fuel rods revealed that about 4% of the pellets were damaged, malformed, or separated from the adjacent pellet. Measurements on a selection of good 25/1 pellets gave diameters from 0.579 to 0.594 cm and densities from 8.37 to 8.90 gm/cm^3. From such results it was obvious that variations in fuel would result in spread of the experimental data, necessitating multiple measurements and averaging in those determinations which are sensitive to local fuel concentration.

Chemical analysis revealed that a very small fraction of the pellets had an abnormally high uranium content. This was confirmed by fission rate measurements on approximately 350 pellets, from which it is estimated that less than 1% of the 25/1 pellets and none of the 50/1 have a significant deviation from the specified uranium content. Spectrochemical analysis of a few pellets revealed trace amounts of elements other than thorium, uranium, and oxygen, but none was present in sufficient quantities to produce significant neutron absorption.

Toward the end of the THUD program, an exchange of fuel was arranged with a group at the Babcock and Wilcox Company's Atomic Energy Department. Their program involved a study of thoria-urania in light water, with fuel of 15/1 atom ratio. Because of the limited period for which their 15/1 fuel was available, no measurements were made of the physical or chemical properties of the pellets.

2. Fuel and Void Tubes

The 25/1 and 50/1 fuel pellets were contained within 0.794-cm-OD, 1100 (2S) aluminum tubing by means of 6061 aluminum end plugs which were brazed to the tubing. The tube length was 154.62 cm, $^{+0.16}_{-0}$ cm and with the end plugs inserted had a total length of 157.48 cm. As ordered, the tubing had an outer diameter of 0.793 cm, $^{+0}_{-0.015}$ cm, and a wall thickness of 0.081 cm, $^{+0.010}_{-0}$ cm.

Similar tubes of thinner wall having a removable O-ring-sealed top plug were obtained for use in void coefficient experiments, and these were later used to contain the Babcock and Wilcox 15/1 fuel pellets. Specified dimensions for the tubing were 0.793-cm, $^{+0}_{-0.015}$ cm OD, 0.036-cm wall, and 155.3-cm length. The bottom plugs were identical with those of the fuel

tubes except for the added diameter of the inserted portion required because of the thinner tube wall. With the top plug inserted, the total length was the same as for the fuel tubes.

The average weights of the fuel and void tubing were 81.525 and 34.49 gm, respectively. Using an aluminum density of 2.70 gm/cm^3 and lengths of 154.7 and 155.3 cm, respectively, the following set of diameters, consistent with the specifications for the tubing, are obtained:

	Fuel Tube	Void Tube
Outer diameter	0.787 cm	0.787 cm
Inner diameter	0.610 cm	0.718 cm

The bottom plug weighed 2.5 gm, the fixed top plug 2.1 gm, and the removable top plug 2.0 gm.

Samples of the fuel and void tubes were analyzed spectrochemically for the known impurities in 1100 aluminum and for other materials having a high thermal-neutron-absorption cross section. These results are given in Table I. Also included are similar data for the control rod guides, which were constructed of the same material as the end plugs. For comparison, the nominal amounts of alloying elements in 6061 aluminum and a plausible distribution of 1% impurities present as an upper limit in 1100 aluminum (>99% aluminum) are indicated.

Table I

RESULTS OF SPECTROCHEMICAL ANALYSIS OF THUD STRUCTURAL COMPONENTS

(in wt-%)

	1100 Aluminum			6061 Aluminum	
Element	1% Impurities	Fuel Tube	Void Tube	Alloying Elements	Control Rod Guide
B		<0.0001	0.01		<0.0001
Cr		<0.01	<0.01	0.25	
Cu	0.15	0.02	0.07	0.25	0.3
Fe	0.37	1	0.8		
Cd		<0.0001	<0.0001		<0.0001
Mg		0.004	0.008	1.0	
Mn	0.04	0.01	0.008		0.08
Si	0.37	0.1	0.1	0.6	
Ti		0.03	<0.01		
Zn	0.07	0.04	<0.03		

NOTE: Accuracy estimated as order of magnitude.

Bowing of the fuel tubes when loaded with fuel pellets met the specification that it not exceed 0.24 cm for the entire length of the fuel rod.

3. Recommended Constants for Fuel Rods

As a basis for subsequent calculations, the set of values presented in Table II is recommended. The data presented there were derived from the chemical and mass spectrographic analyses of four fuel pellets (Table XLV), the averages of the fuel weights reported by the supplier, the specified length of the column of pellets within the fuel tubes, the average diameter of the 103 pellets which were weighed and measured (Table XLIII), and the fuel rod and void tube dimensions derived from the weights and specified dimensions for these tubes. Data given for the 15/1 fuel were obtained from BAW-1191.(12)

Table II

PROPERTIES OF THUD FUEL RODS

Cladding (1100 Al, 0.787-cm OD)	50/1		25/1		15/1	
Clad thickness, cm	0.089		0.089		0.034	
ID, cm	0.610		0.610		0.719	
Physical Description of Fuel						
Weight, gm	349.8		357.2		434.6	
Length, cm	152.64		152.64		152.40	
Diameter, cm	0.587		0.587		0.660	
Effective density, gm/cm^3	8.476		8.655		8.35	
Chemical Composition	wt-%	gm	wt-%	gm	wt-%	gm
Thorium	85.925	300.6	84.13	300.51		355.9
Uranium	1.905	6.66	3.71	13.25		
U^{235}*		6.21		12.35		24.04
Oxygen	12.15		12.15			
Other	0.02		0.01			
Ratios for Th-U^{235}						
Weight	48.41		24.34		14.80	
Atom	49.03		24.65		15.00	

*Isotopic distribution for 50/1 and 25/1 fuel, in wt-%:

U^{234} - 0.96; U^{235} - 93.18; U^{236} - 0.46; and U^{238} - 5.40.

C. Additional Core Structure

Two other items, namely, fuel element clusters and control rod guides, introduced sufficient material into some of the critical assemblies to warrant consideration in the analysis of the data. Details regarding the presence and location of these components are included in the descriptions of the clean critical assemblies. Some information on the structure and quantity of material is presented here.

A control rod guide consists mainly of four 182.9 cm x 26.7 cm x 0.318-cm 6061 aluminum sheets bent to form a right angle of 182.9-cm height and spaced by 1.27-cm-wide blocks of aluminum to form a 1.27-cm-wide cross-shaped channel in which the 25.4-cm-span cruciform rods may move. The total weight of a guide was 16.92 kg, of which approximately 16.48 kg was contained in the 5-ft-high region coinciding with the fuel pellets.

The structure of a fuel element cluster used for experiments in EBWR geometry is depicted in the section on clean criticals (see Figure 4). With the exception of eight steel drive pins used to fasten the tie rods to the shoulder pins, locating pins, and lifting studs, all material was 6061 aluminum. The total weight of 799.2 gm was distributed as follows:

2 locating pins	12.0 gm, total
2 shoulder pins	10.0
1 support plate	82.0
4 grid spacer rings	1.4
3 element positioning grids	36.0
4 tie rods	620.0
4 lifting studs	36.0
8 steel drive pins	1.8
	799.2

III. CLEAN CRITICALS

Of special interest in terms of interpretation of the data obtained in a program of critical experimentation are those assemblies which are uniform in composition and arrangement of the constituents, simple in core and reflector geometry, and free of control materials. These are termed clean criticals. In this chapter the observed critical dimensions for assemblies satisfying these three criteria are presented.

A. General Characteristics

Clean critical experiments have been performed with three different types of core structures, and the results are segregated on this basis in the material which follows. However, there are certain characteristics which all of these assemblies have in common, namely, the reflector geometry, experimental procedures, and degree of reproducibility.

1. Reflector Geometry

All of the assemblies were made in the 205.7-cm-diameter tank described previously, and so the outer radius of the radial heavy water reflector was constant. Each of the three different core structures rested on the same base plate and supporting structure. Thus the bottom reflector consisted always of the same 30-cm-thick combination of materials, mainly heavy water and aluminum with slight amounts of stainless steel and void. Detailed information on the spatial variation of these constituents of the bottom reflector is given in the section on reflector savings. For most of the assemblies reported, only a portion of the fuel and core structure was immersed in heavy water. Thus the top reflector varied markedly in lattice structure and size; however, the relatively low amount of fuel per unit volume of reflector in these assemblies made the results far less sensitive to the effect of reflection of neutrons from above the water level than exists for light water systems.

2. Procedure

The standard operating procedure required that a critical condition for each loading be first achieved by adjustment of control rod position. There followed an alternate lowering of the water level and withdrawal of the control rods, with attendant observation of the reactivity state of the assembly, until all control rod tips were above the top of the water. Experience showed that the reactor was insensitive to control rods hanging more than about 10 cm above the water level. Consequently, a minimum of 15-cm clearance was established for the clean experiments, subject to the limit of 164 cm on the height above the base of the core to which the control rods could be withdrawn. Nine control rod guides were present in the experiments with EBWR core geometry, but this number was reduced to four following loading No. 86.

Two alternative procedures were used to establish the critical water level for the clean systems. The less common one involved the observation of the positive reactor period for a minimum of two supercritical water levels, conversion to reactivity, and a linear extrapolation of a reactivity versus water level curve to zero reactivity. Limitations exist because of uncertainties in the period-reactivity relationships and the effect of reactivity shifts due to temperature and geometry effects; nonetheless, the result of this procedure was usually in very close agreement with the usual method of adjustment of the water level to achieve a critical condition.

For many of the types of cores assembled, critical dimensions were determined for a range of height-to-diameter ratios. This provided a means to determine buckling and reflector savings, independently of flux-distribution measurements, in the following way. The geometrical buckling for a cylindrical system is

$$B_g^2 = \left(\frac{\pi}{H}\right)^2 + \left(\frac{2.405}{R}\right)^2 = \left(\frac{\pi}{H}\right)^2 \left[1 + \left(\frac{2.405\ H}{\pi R}\right)^2\right] \quad .$$

Here H is the actual core height H_c plus the bottom (λH_1) and top (λH_2) reflector savings, and R the actual core radius R_c plus the radial reflector savings λ_R. From partial differentiation, $-\delta B^2 = (2\pi^2/H^3)\,\delta H =$

$[2\,(2.405)^2/R^3]\,\delta R$, and $\frac{H}{R} = \sqrt[3]{\left(\frac{\pi}{2.405}\right)^2 \frac{\delta H}{\delta R}}$. Substitution of this in the equation for geometrical buckling yields

$$B_g^2 = \left(\frac{\pi}{H}\right)^2 1 + \left(\frac{2.405}{\pi}\ \frac{\delta H}{\delta R}\right)^{2/3} \quad .$$

Solving for the critical water level gives

$$H_c = \frac{\pi}{B_g} \sqrt{1 + \left(\frac{2.405}{\pi}\ \frac{\delta H}{\delta R}\right)^{2/3}} - (\lambda H_1 + \lambda H_2) \quad .$$

This is the equation for a straight line of slope π/B and intercept $(\lambda H_1 + \lambda H_2)$.

Thus values of $\overline{H}_c$ and $\sqrt{1 + \left(\frac{2.405}{\pi}\ \frac{\Delta H_c}{\Delta R_c}\right)^{2/3}}$ from successive pairs of observations in the sequence of geometrical criticals can be plotted to yield the geometrical buckling and axial reflector savings. Implicit in such a treatment of the clean critical data is an assumption that the reflector savings are independent of core dimensions.

3. Reproducibility

Precise reproducibility of the observed critical dimensions was precluded by the large number of variables, such as residual neutron source, heavy water purity, temperature, position of the components, and fuel content of fuel rods.

The presence of delayed photoneutrons due to interaction of fission product gamma rays with the deuterium in the heavy water makes the apparent criticality of the reactor sensitive to the power level and to the operational history of the fuel rods comprising the assembly. The yield of neutrons from spontaneous fission was relatively small. To establish the power level at which this built-in source of variable intensity would have a negligible effect on the determination of criticality, the apparent critical position was observed as a function of power level. It was more convenient to make such observations in terms of position of a control rod inserted in the core, and this procedure was repeated for significant changes in the geometry or composition of the core. The results of the first determination, for loading No. 13, are illustrated by Figure 3. The power level was first increased and then decreased in steps. The central control rod had an average worth of 0.15% $\Delta k/k$ per cm over this range of apparent critical positions. An increase in the Instrument Channel No. 5 log level chart reading of 5.13 divisions corresponded to a factor of 2 increase in power level. For this loading a reading of 45 on Channel No. 5 indicated a core power of approximately one watt.

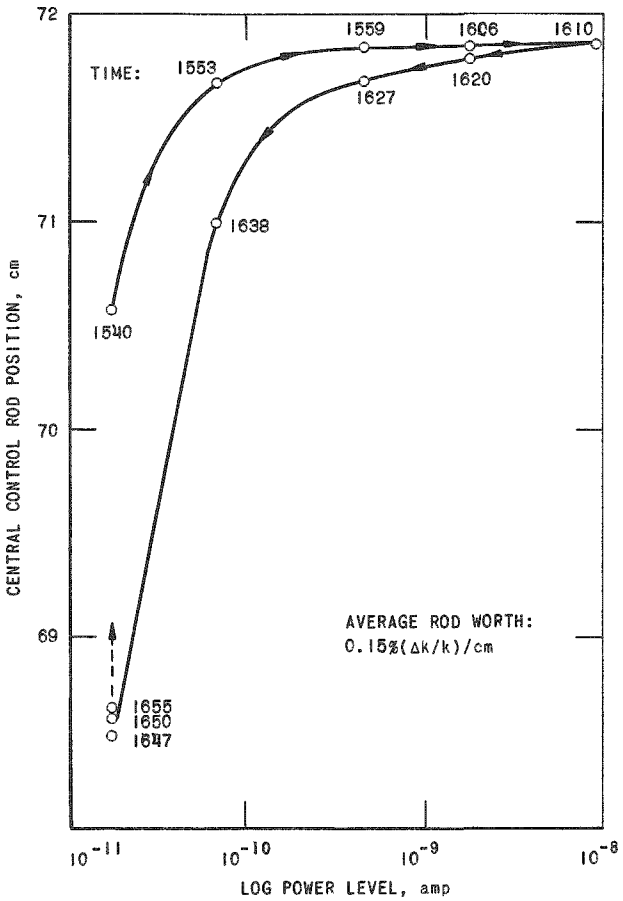

Fig. 3. Dependence of Apparent Criticality on Reactor Power Level.

Because of the gradual change in heavy water purity during these measurements, certain assemblies were rebuilt occasionally to provide data on the reactivity effect of the change in heavy water concentration. However, there are other effects which contributed to the failure to reproduce the earlier critical conditions. Following loading No. 12, a thermocouple was added to the ZPR-VII system and so information on temperature variations was available. The core structures were in general sufficiently rigid and the record of

loadings quite detailed, so significant errors are not expected from these sources. However, some displacement of fuel rods is possible, particularly during a water dump, because of the clearance between fuel rods and the holes in the grid plates. Also, there always exists the possibility of errors in location of fuel rods in a reconstructed assembly.

The appreciable variation in fuel content among the rods does present a potential source of error in achieving a reproducible loading. Records of location of specific fuel rods were never kept, and after an estimate of the errors introduced in the analysis of results by random selection of rods, the recording of the actual elements in the reactor was abandoned. Random selection of the large number of rods loaded into the core served to minimize asymmetries of loading, as demonstrated by the following information on the amount of U^{235} per quadrant for two representative early loadings:

No. 6		No. 14	
1691.9 gm	1690.4 gm	2493.8 gm	2497.9 gm
1687.7	1697.9	2501.8	2503.3

These and similar results for subsequent loadings soon led to elimination of records of uranium content of the cores.

Systematic errors due to variations among the fuel rods are detectable when only a few rods are involved in a loading change. Table III illustrates this with results obtained in some of the last systems assembled.

Table III

CRITICALITY SHIFTS PRODUCED BY FUEL ROD EXCHANGE

Loading Number	Date	Temperature (°C)	Critical D_2O Level (cm)	Change
459	12/10/59	22.5	149.48	Reference loading
460	12/11/59	22.8	148.49	30 central rods & date
461	12/11/59	22.8	148.35	30 central rods
462	12/11/59	22.8	148.34	32 peripheral rods
462	12/16/59	22.4	148.18	date
463	12/16/59	22.2	148.74	30 central rods

The change in critical height with exchange of about 10% of the total number of rods is given for a core composed of 331 rods of 25/1 fuel with a 3.81-cm triangular pitch. In this example, temperature and time were only minor variables.

B. Assemblies with EBWR Geometry

The first core structure provided in the ZPR-VII facility duplicated that existing in the Experimental Boiling Water Reactor (EBWR). In EBWR, a 3 x 3 square array of 25.4-cm-span cruciform control rods with a center to center spacing of 32.4 cm are positioned within a core composed of 10.16-cm-sq fuel elements. The THUD program version of core structure is visible in the cutaway view of the core tank (see Figure 1).

The detailed structure of the aluminum fuel element assemblies and aluminum-clad fuel rods used in the THUD program is shown in Figure 4. Element assemblies consisting of perforated material with 0.794-cm holes on a 0.953-cm triangular spacing held by hollow corner tubes provide a means for assembling a variety of fuel rod lattices conveniently. Actually, all but one of the clean criticals assembled with the EBWR-type structure had a single triangular fuel rod pitch of 1.906 cm. This core structure was also used extensively for voided and poisoned lattice experiments, which are reported later in Section V-A.

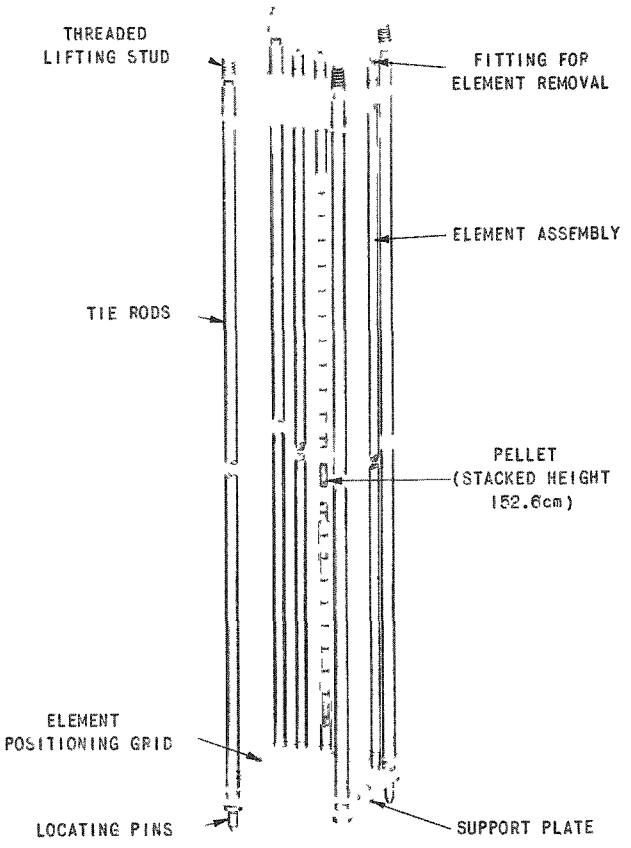

Fig. 4. Fuel Rod Assembly for EBWR Core Geometry.

Application of the term "clean" to these criticals requires some qualification. The loading pattern used in a typical fuel element cluster is shown in Figure 5. It contained 28 fuel rods and from zero to a maximum of 33 void tubes. Also shown are representative boundaries as defined by the peripheral rods in specific critical assemblies. Note that the water channels associated with the control rod pattern contributed certain structure deviating from an ideal lattice and making a smooth periphery difficult to achieve at times. Use of the standard 9.84-cm-sq-clusters at a 10.16-cm spacing contributed to a lesser extent to the inhomogeneity.

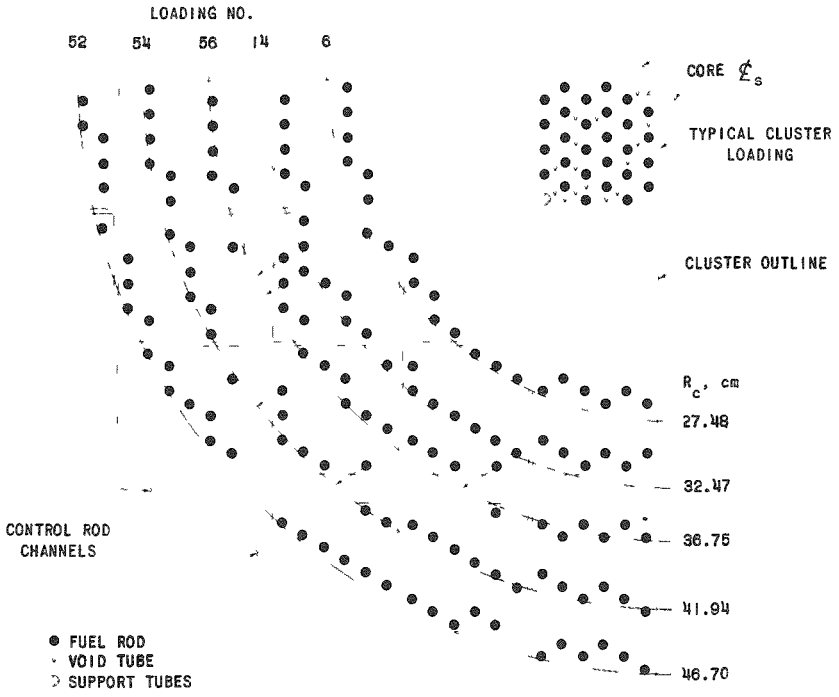

Fig. 5. Representative Core Loading in EBWR Geometry.

Table IV summarizes the critical water heights and radii for the clean criticals of 25/1 fuel in EBWR geometry. All of the assemblies had cylindrical geometry except loading No. 81, which was the reference assembly for a single clustering experiment with the EBWR core geometry.

Table IV

CLEAN CRITICALS OF 25.1 FUEL IN EBWR GEOMETRY

Loading Number	Date	Number of Rods	kg U^{235}	Radius R_c (cm)	Height H_c (cm)	Temperature (°C)	Area Rod (cm^2)
6	7 8 57	568	6.768	27.483	152.40		4.18
10	7/10 57	629	7.515	28.656	137.16		4.10
12	7/17 57	688	8.228	29.819	126.16		4.06
13	7 18 57	748	8.943	30.934	118.69	29.2	4.02
14	7 24 57	836	9.997	32.474	109.80	28.9	3.96
19	8 1 57	836		32.474	109.65	28.9	3.96
71	11 8 57	836	10.027	32.474	111.02	22.5	3.96
15	7 26 57	924	11.052	34.917	101.60	28.3	4.15
16	7/29 57	1012	12.125	36.862	95.28	28.3	4.22
60	10 14 57	1013	12.142	36.876	94.89	22.1	4.22
58	10 4 57	1013	12.142	36.751	94.82	22.8	4.19
59	10/11 57	1013	12.142	36.751	95.33	23.3	4.19
55	10/ 4 57	1164	13.975	39.402	85.71	22.8	4.19
54	10/ 3/57	1316	15.820	41.941	80.15	23.9	4.20
53	10/ 3 57	1468	17.666	44.193	75.73	23.9	4.18
52	10 1 57	1616	19.464	46.701	72.55	23.3	4.24
81	1/ 7/ 58	1008		36.53*	96.47	18.3	4.16

* Equivalent radius for 64.77-cm^2-lattice

Thirteen of the assemblies were investigated in two sequences of experiments, and the others recorded were subsequent reconstructions of loadings Nos. 14, 16, and 56. Loading No. 60 was a repeat of loading No. 16, but an extra fuel rod was present unintentionally. Loadings Nos. 56 and 59 contained the same number of rods as loading No. 60, but with the fuel rods positioned in a slightly more compact arrangement.

Included in Table IV are the number of rods for each loading and the computed area per rod. The latter depends on a knowledge of the core radius. The radius of a uniform core is readily evaluated from the cell area and the number of rods. However, the irregularities of the EBWR-type core loadings have resulted in a more arbitrary determination of critical dimensions. The radius was determined from the average of measurements of the location of each peripheral fuel element plus a correction per peripheral rod for an increment of water calculated as half that amount associated with a fuel pin on a 1.905-cm triangular spacing. This procedure was necessary because the presence of control rod guide channels, corner posts in the element clusters, and spacing of the element clusters prevented the assembly of a true 1.905-cm lattice core. If one assumes a unit cell composed of nine fuel clusters and one-half of each of the bounding water channels, a figure of 4.16 cm^2/rod results. This is in reasonable agreement with the actual values given in the table. The equivalent radius given for loading No. 81 was obtained from the cross-sectional dimensions of 64.77 x 64.77 cm, which include half the width of the bounding control rod guide channels.

Two additional clean critical assemblies were made in EBWR geometry at the end of the THUD program, with the following results:

Loading Number	Number of Rods	Radius, (cm)	Height, (cm)	Temperature, (°C)
467	821	28.659	122.45	22.7
468	710	26.651	151.74	22.8

These values cannot be compared directly with observations in Table IV because the fuel rods were loaded in a true 1.905-cm triangular pattern, subject to a slight displacement of some of the fuel rods at the boundaries of the fuel element clusters. Recall that the fuel rods in the assemblies reported in Table IV had a 1.905-cm triangular pitch only within the individual fuel clusters and that the gaps between the clusters and at the control rod position produced an average cell area somewhat greater than the 3.14-cm^2 value for a 1.905-cm pitch. Nor are these two assemblies directly comparable with the results reported later for uniform lattices, since the fuel element clusters introduced appreciably more aluminum into the core than existed with the uniform grids. The radii given for these two loadings were calculated from the 1.905-cm pitch and the number of fuel rods.

C. Single Fuel Rods in Uniform Geometry

Upon completion of the EBWR-oriented measurements, the ZPR-VII core structure was modified to accommodate a variety of uniform lattice patterns in a central 61-cm-sq region. The individual 9.84-cm-sq element clusters which were used initially to fill the central region were replaced by one large 61-cm-sq cluster composed of three sheets of perforated aluminum attached to a 0.953-cm-thick aluminum base plate by rods at the edges. The perforations were 0.794 cm in diameter on a 0.953-cm triangular lattice spacing. This arrangement did not differ appreciably from the manner in which fuel elements were formerly positioned. Elimination of the four corner posts associated with each 9.84-cm-sq cluster, the irregularity due to the spacing of the clusters, and the cross rod channels and guides made feasible the assembly of cores with truly uniform fuel rod patterns.

The dimensions of the central region were determined by the location of the four corner cross rod guides of the 3 by 3 EBWR control rod pattern which were already installed in the ZPR-VII facility. Previous experiments had used the central cross rod and the four cross rods having their centers on lines passing through the blades of central cross rod. In Section II-A, rods were identified as Nos. 1, 3, 5, 7 and 9. The guides for these rods were removed to allow insertion of the new central fuel rod holder, and so the corner cross rods Nos. 2, 4, 6 and 8 were used for subsequent experiments.

The central section contained slightly over 4800 holes into which fuel rods could be placed. With the amount of fuel available it was not possible to achieve a critical assembly with either the 25/1 or 15/1 fuel rods at the closest pitch of 0.953 cm, but assemblies with fuel of each of these enrichments were constructed for multiples of 2, 3, 4, and 6 times this basic unit of triangular pitch. For future convenience, this unit of 0.953 cm ($\frac{3}{8}$ in.) is designated as "a_0." Figure 6 is a photograph of the $3a_0$ lattice in the uniform core structure. The two tubes shown within the core were present for some oscillator experiments.

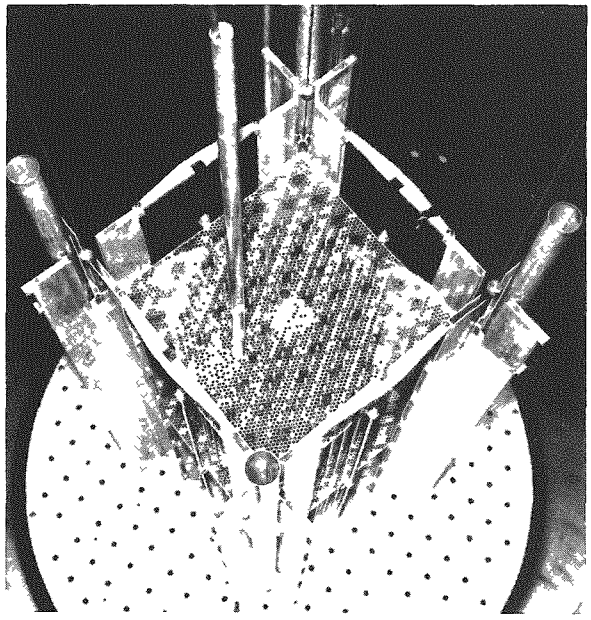

Fig. 6. Typical Core of Single Fuel Rods with Uniform Spacing.

Table V summarizes the observed critical configurations of single fuel rods assembled in the uniform core structure within the ZPR-VII system. The number

of fuel rods and critical water height are given, as well as the loading number, date, and moderator temperature. All assemblies were cylindrical. The radii are not given since they are readily calculated from the number of fuel rods and the cell area, equal to $\frac{1}{2}\sqrt{3}$ times the square of the triangular pitch. The one exception to this existed for loading No. 178, for which the nominal pitch of $6a_0$ was exceeded slightly. For this loading there were 30.09 cm^2/rod instead of the 28.28 cm^2/rod characteristic of a $6a_0$ pitch. Note that a sequence of assemblies was constructed for each lattice except the ones of 25/1 fuel with ~ $6a_0$ pitch. For several of the assemblies with 25/1 fuel, measurements were repeated at intervals during the THUD program. Three reconstructions which were not critical are included in this table.

Table V

CLEAN CRITICALS OF SINGLE FUEL RODS IN UNIFORM GEOMETRY

Loading Number	Date	Number of Rods	Height (cm)	Temperature (°C)
25/1 Fuel, $2a_0$ Pitch				
90	2/28/58	665	150.88	
89	2/28/58	685	145.40	
455	12/ 8/59	685	159.13	21.7
91	3/ 3/58	745	132.84	
233	11/13/58	745	135.08	20.0
456	12/ 9/59	745	139.09	21.9
92	3/ 3/58	805	123.53	
93	3/ 3/58	867	115.95	
161	7/ 7/58	925	111.05	23.1
94	3/ 4/58	926	110.03	
162	7/ 8/58	945	109.30	25.0
262	2/19/59	977	104.70	18.9
95	3/ 4/58	1009	103.30	
269	3/ 3/59	1526	76.74	18.3
25/1 Fuel, $3a_0$ Pitch				
103	3/11/58	325	148.22	19.4
231	11/12/58	325	>157	
104	3/11/58	353	133.79	19.7
105	3/12/58	375	125.20	20.0
232	11/12/58	375	132.21	21.1
106	3/13/58	405	115.81	20.0
107	3/13/58	421	111.85	20.6
108	3/14/58	461	103.70	20.0

Table V (Cont'd.)

Loading Number	Date	Number of Rods	Height (cm)	Temperature (°C)
25/1 Fuel, $4a_0$ Pitch				
117	3/24/58	257	154.97	19.4
118	3/25/58	266	147.61	19.4
457	12/10/59	266	>178	22.2
119	3/25/58	283	137.08	20.0
120	3/26/58	299	129.35	19.7
458	12/10/59	299	>178	22.2
463	12/16/59	331	148.74	22.2
464	12/16/59	339	143.66	22.3
25/1 Fuel, ~$6a_0$ Pitch				
178	8/25/58	932	113.61	24.4
244	1/15/59	1082	104.33	19.7
15/1 Fuel, $2a_0$ Pitch				
388	8/19/59	345	132.97	26.4
385	8/18/59	366	123.04	25.8
381	8/11/59	421	104.58	25.3
382	8/14/59	495	90.16	25.6
384	8/18/59	593	78.90	25.8
383	8/14/59	687	71.78	26.2
15/1 Fuel, $3a_0$ Pitch				
403	9/ 8/59	163	150.81	25.8
402	9/ 8/59	190	115.47	25.6
401	9/ 4/59	321	72.38	23.0
400	9/ 4/59	429	59.73	26.1
15/1 Fuel, $4a_0$ Pitch				
407	9/14/59	139	127.32	25.3
405	9/11/59	163	103.05	25.6
404	9/11/59	247	72.79	25.4
15/1 Fuel, $6a_0$ Pitch				
411	9/23/59	134	137.15	25.1
410	9/23/59	147	122.10	25.1
409	9/23/59	176	103.58	24.7

Figure 7 illustrates the degree to which a circular cross section could be achieved in the uniform core structure. Shown there are the rod patterns which existed in the smallest and largest cores of 25/1 fuel rods with $2a_0$ pitch. The calculated radii calculated from the number of rods and the pitch are also indicated on these loading diagrams.

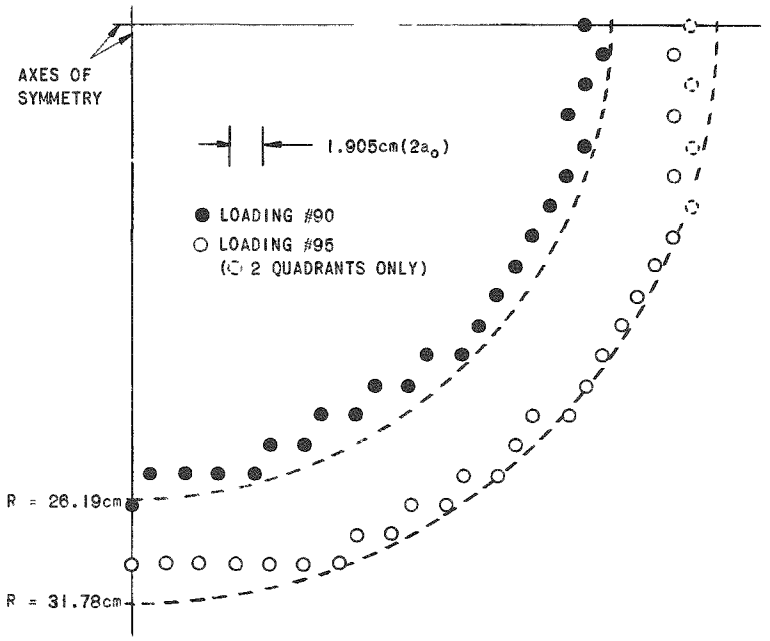

Fig. 7. Loading Patterns for Two Cores of 25/1 Fuel Rods at $2a_0$ Pitch.

Not as many assemblies were made with 25/1 fuel rods at a $4a_0$ spacing as for $2a_0$ and $3a_0$, because of the size limit imposed by the dimensions of the central uniform grid. Observations on a series of four assemblies at $4a_0$ spacing are recorded in Table V. The limited size of the central region resulted in a displacement of 5 of the peripheral elements in loadings Nos. 119 and 120 from the ideal pattern to a $3a_0$ spacing. For loading No. 120 and some subsequent loadings this central 2-ft-sq uniform region was extended slightly by the addition of perforated sheets at the edge. Note also that the first $4a_0$ critical assembly listed required 2.57 cm of top reflector for criticality.

Core Structure in Low Fuel Density Loadings

For criticality with 25/1 fuel at a $6a_0$ spacing, a region much larger than the uniform central grid was required. Measurements with the 25/1 fuel for the $\sim 6a_0$ spacing were first made in a core structure composed of a combination of the uniform grid material and fuel element clusters from the EBWR-type structure. A precise uniform spacing of fuel rods was not

achieved and so the clusters were later replaced by additional perforated sheeting of the type used in the region bounded by the four corner control rod guides.

The first core structure used to achieve a nominal $6a_0$ spacing contained nine sections arrayed 3 x 3. Four control rod guide channels separated the corners about the central section, creating 1.905-cm openings. The four diagonal sections were rounded (or the edge staggered) to fit the 205.7-cm-ID reactor tank; each of the other four parts was 62.2 cm sq horizontally and 152.4 cm high. The central section, one side, and one corner section were formed from large sheets of the uniform grid material, and the remainder was made up of standard 9.84-cm-sq THUD fuel element clusters.

The clean critical in this structure, loading No. 178, presented some uncertainties which resulted in rebuilding the core in a more precise fashion. The lattice spacing in No. 178 was not entirely uniform at the boundaries of the sections, so that the average area surrounding each fuel pin was about 30.09 cm^2 instead of the ideal lattice requirement of 28.28 cm^2. Nevertheless, the spacing was ideal in all regions of high statistical weight, with nearly 0.4 of the total importance being in the central 62.2-cm-sq grid region. The term "6^+a_0" is used to indicate this core structure.

The revised core structure for the $6a_0$ spacing as used for loading No. 244, was constructed of large grid sheets and was uniformly loaded, except for the slight displacement of a few fuel rods near the openings for the control rod guides. The revised core structure contained a significantly smaller amount of aluminum. The distribution of this structural material is compared for the two arrangements in Table VI.

Table VI

WEIGHT (in kg) OF ALUMINUM CORE STRUCTURE IN $6a_0$ LATTICE EXPERIMENTS

Item	Loading No. 178	Loading No. 244
4 control rod guides	65.92	65.92
4 posts for center grid	1.23	1.23
1 center midplane grid	.73	.73
6 top and bottom grid sheets	3.54	-
168 fuel element assemblies*	113.40	-
18 top and bottom grids	-	10.88
28 clusters as grid supports	-	18.90
Total weight	184.82	97.66
No. of fuel rods in clean critical	932	1082
Average weight per cell	198.3 gm	90.3 gm

* Weight of support plates locating pins, shoulder pins, steel drive pins, and half of lifting studs excluded.

D. Clean Criticals with Clustered Fuel

The structure of the grids used for positioning single fuel rods in both the EBWR and the uniform geometries made feasible the investigation of lattice arrangements in which fuel rods were arranged in regions of high fuel density ($1a_0$ pitch), these regions being separated from each other by pure moderator regions. In this section are described a variety of critical experiments on lattices of clusters of the 25/1 fuel in these grids. At a later date, a core structure more representative of a practical D_2O reactor design was introduced to allow additional clustered fuel experiments. In these more extensive measurements, fuel enrichment and cluster coolant were also varied, but there was less of a range of pitch and number of fuel rods per cluster. These results are also presented in this section.

1. Clustering in EBWR Geometry

A single clustering experiment was performed in the reactor core arrangement which contained fuel element clusters separated by cross rod guide channels. Each of the 36 fuel rod assemblies filling the core area bounded by the guides for control rods Nos. 2, 4, 6, and 8 contained 28 fuel rods uniformly distributed in a $2a_0$ triangular lattice within each assembly. In a previous description[2] this arrangement has been termed the "slightly clustered" system. This name indicates that the fuel rods are uniformly arranged within an assembly, and that the pattern is repeated on 10.16-cm centers to form a square lattice, interrupted occasionally by 1.905-cm-wide water channels.

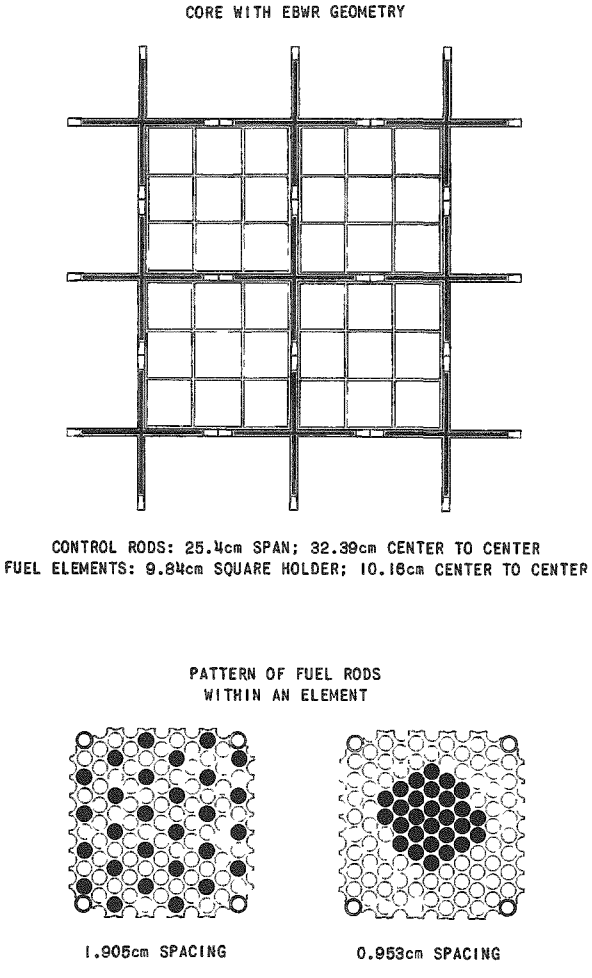

Fig. 8. Core Structure for Clustered Fuel Experiment in EBWR Geometry.

For this core of square cross section, containing 1008 fuel rods, a critical water level of 96.47 cm was observed (Loading No. 81). Next, the 28 rods contained in each assembly were grouped at the center of the assembly, in a $1a_0$ triangular pattern. These arrangements of fuel are illustrated in Figure 8. An average of four determinations of the critical water height yielded a value of 107.87 cm, indicating a significant loss of reactivity as a consequence of the clustering.

2. Clustering in Uniform Geometry

Three types of clustered experiments were performed in the 61-cm-sq perforated aluminum grid arrangement. In the first set, the ratio of moderator volume to fuel volume was kept constant. In the second, the number of fuel rods within each cluster was varied for four different cluster pitches. In the final sequence of assemblies, the critical water heights for certain hollow clusters of fuel were observed for a single cluster pitch. The experimental details and results are presented below.

a. Constant V_M/V_F

For the sequence of assemblies with constant moderator-to-fuel volume ratio, a uniform $2a_0$ lattice was assembled as a starting point. The number of fuel rods was chosen to fill the central uniform region with a lattice of circular cross section, subject to the restriction that successive clustering steps of three adjacent fuel-bearing regions would result in a core of moderately close conformance to circular cross section and leave no surplus fuel pins. This number was 945 fuel rods.

Table VII summarizes the sequence of fuel-clustering experiments, performed over a period of one month because of frequent interruptions for related measurements.

Table VII

CLUSTERING OF 945 RODS INITIALLY IN A $2a_0$ UNIFORM LATTICE

Loading Number	Date	Status	Critical Height (cm)
162	7/ 8/58	Initial lattice	109.30
163	7/11	Clusters of 3 adjacent rods	107.01
167	7/21	Clusters of 3 adjacent clusters of 3	106.63
167	7/28		106.25
168	7/28	Shift of some peripheral clusters	105.89
169	7/28	Split of some peripheral clusters	105.16
175	8/ 4		105.87
175	8/ 5		105.92
176	8/ 6	Clusters of 3 adjacent clusters of 9	94.77
176	8/ 7		94.82
177	8/ 8	4 peripheral clusters split into 6	96.34*

Temperature Range: 23.6 to 25.0°C

* 8 indium foils present

The sequence included a few variations in the arrangement of the clustered elements. Figure 9 shows the manner in which the clustering was accomplished. Two adjacent fuel rods were moved toward a third to provide the first clustered arrangement. This resulted in a slight shift in the center of the core; the direction of motion of the fuel in subsequent clusterings was varied to minimize the resultant displacement of the core center. In the next step, two clusters of three were moved toward each third cluster and the nine fuel rods were arranged in a diamond-shaped cluster. For the cluster of nine rods, the cross section of the core was subsequently smoothed by moving peripheral clusters. In the first step, loading No. 168, several peripheral clusters were relocated, and in the second step, loading No. 169, circular symmetry was achieved by splitting all peripheral clusters. For the final cluster of fuel, two adjacent clusters of 9 were moved toward a third nearby cluster and the 27 fuel elements rearranged in the pattern shown in Figure 9. This resulted in the cluster arrangement shown in Figure 10. The modified shape of several of the peripheral clusters was necessary because of the boundaries of the uniform grid. An attempt was made to circularize this final lattice by removing nine rods from each of the four shaded clusters and clustering them on the X-X' axis, with the result that for loading No. 177 there were six clusters of 18 elements each. The resultant change in water height includes the slight poisoning effect of eight indium foils present in the observation reported.

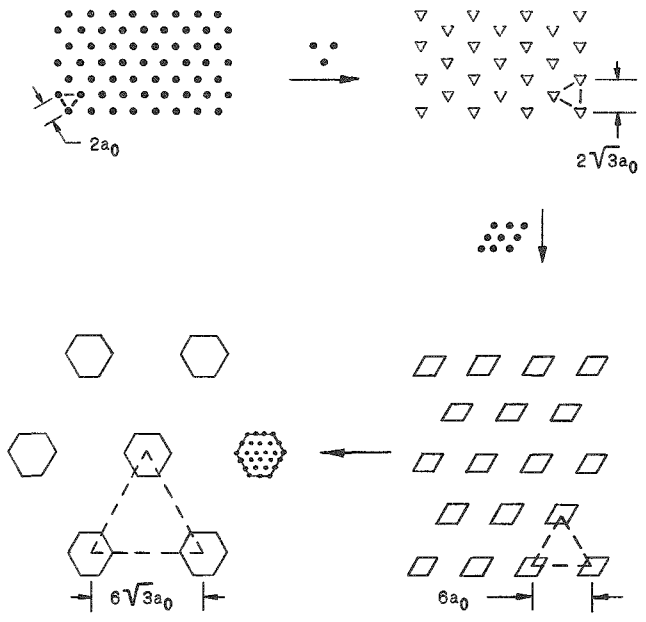

Fig. 9. Successive Steps in Clustering with Constant Moderator-to-fuel Volume Ratio.

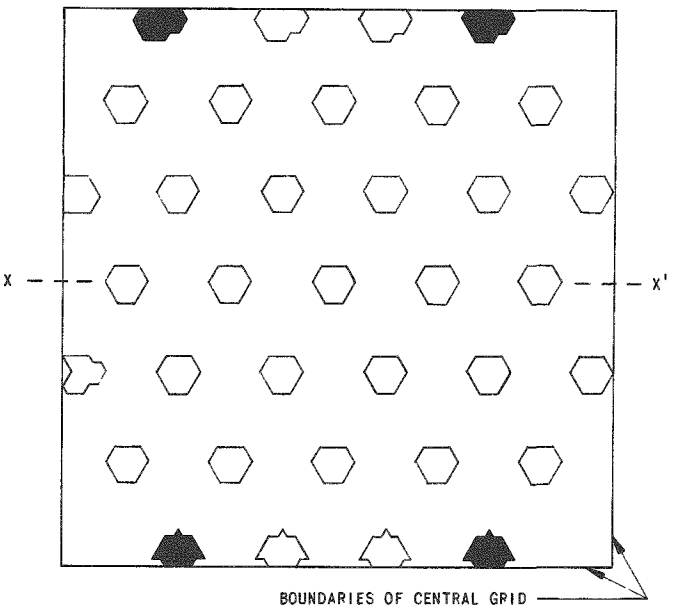

Fig. 10. Pattern of Fuel Rods in Core of Largest Clusters for Constant V_M/V_F Sequence.

No large change occurred in the first two steps, namely, the clusters of three and of nine fuel rods. For the clustering of three adjacent groups of nine rods, however, there was an appreciable gain in reactivity, in contrast with the observation for the slightly clustered system, in which clustering of 28 adjacent rods resulted in a loss of reactivity. The significant differences in these two systems are the ratio of moderator to fuel volumes and the aluminum content, as follows:

	Volume Fractions	
Constituent	$2a_0$ Uniform	Slightly Clustered
Fuel	0.0882	0.0667
Moderator	0.9118	0.9333
D_2O	0.8462	0.8379
Aluminum	0.0587	0.0902
Void	0.0069	0.0052

b. Variable Pitch and Rods per Cluster

The next investigation of clustered assemblies had three objectives:

1. to check an apparent discrepancy observed in the first two clustering experiments;

2. to extend the range of information relating the parameters of importance, namely, the number of rods per cluster, the spacing of the clusters, and the critical buckling; and

3. to obtain information directly on uniform systems of less than $2a_0$ lattice spacing.

The clustering of the fuel in the "slightly clustered" system (EBWR geometry) resulted in a loss of reactivity. Subsequent experiments, involving the clustering of a $2a_0$ uniform lattice of fuel, resulted in a gain in reactivity. The significant differences in these two systems were the ratio of moderator to fuel volumes and the aluminum content. Qualitatively, these variations did not seem of sufficient significance to explain the observed differences in reactivity effects. Thus, a primary objective of the additional clustering experiments was to test the validity of these previous observations.

A practical design for heavy water power reactor involves a clustered fuel arrangement. Hence, it was desirable to extend the THUD program to provide data of use for the design of a practical system. Thus, the second objective of the additional experiments was to establish how clustering of fuel and spacing of clusters affected the reactivity.

Finally, the uniform-lattice experiments had included spacings of from two to six units of the basic spacing of 0.953 cm ($1a_0$). Calculations had indicated a rapid decrease in buckling for lattices of less than $2a_0$ pitch, but the amount of fuel available was inadequate to assemble a critical system with a one-unit lattice spacing. Hence, an indirect approach involving large clusters of fuel, only slightly separated, would provide some information on systems with a moderator to fuel ratio less than that for a two unit lattice.

Procedure

The previous clustering experiments had been performed in a manner which required the shifting of a large quantity of fuel for each observation. For these next experiments, a simplified procedure allowed the assembly of successive lattices at a more rapid rate. Thus, some 27 clustered assemblies were made critical in a period of approximately two weeks.

The uniform lattice extended over an area 61 cm sq at the center of the core tank. In addition, there were approximately 1560 usable fuel rods of the 25/1 thorium to U^{235} atom ratio on hand. These two factors established limits on the geometry and composition of systems that could be assembled. Clusters of fuel rods with center-to-center spacings of $8a_0$, $10a_0$, $15a_0$, and $24a_0$ were assembled in a triangular pattern. At the same time, uniform lattices of $2a_0$ and $3a_0$ spacing were reassembled to determine the magnitude of reactivity changes associated with the gradual contamination of the heavy water.

The selection of particular cluster spacings was guided by the desire that the central region be filled to the extent consistent with maintaining a reasonable semblance of circular cross section for the core. This was accomplished most readily by the assembly of cores of hexagonal cross section, and so the number of clusters for the several pitches represented the number of lattice points in hexagons of increasing radius, namely, 7, 19, 37 and 61. Actually, only 60 such clusters could be fitted into the central region for the closest pitch investigated, and so the cross section of this core was hexagonal with one corner cluster removed.

For a particular lattice spacing, approximately the maximum number of rods available were inserted with $1a_0$ spacing in clusters around the lattice points. The experimental procedure involved observing the critical water height, with control rods withdrawn, for successive steps in which a few rods were removed from the periphery of each cluster. This procedure resulted, first, in a gain in reactivity and, later, in increasing loss, until it was no longer possible to go critical within the limits available for water height and control rod withdrawal. The accompanying diagram, Figure 11, indicates two of the sequences of removal of fuel, showing the steps between hexagons containing 19 and 37 rods and between those of 7 and 19 rods. All of the 20 different clustered patterns involved arrangements as near circular as could be achieved without relocating fuel pins.

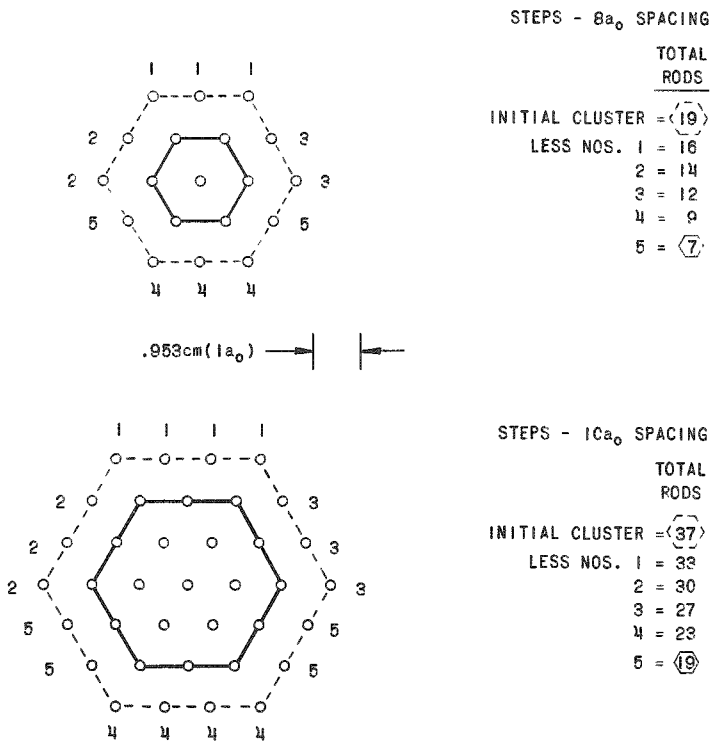

Fig. 11. Sequence of Fuel and Rod Removal in Representative Clustering Experiments at Constant Pitch.

Table VIII summarizes the geometrical characteristics of the clustered systems studied. Dividing the clustered lattice pitch by the square root of the number of rods in the cluster yields the spacing that would be achieved if all of these rods were distributed uniformly throughout a core of the same effective radius as that associated with the clustered system. The range of equivalent uniform pitch achieved in these critical assemblies is included in this table.

Table VIII

GEOMETRICAL CHARACTERISTICS OF CLUSTERED SYSTEMS

Loading Numbers	Lattice Pitch (a_0 = 0.953 cm)	Number of Clusters	Core Radius (cm)	Number of Rods Cluster	Equivalent Uniform Pitch
198 to 207	$10a_0$	37	30.40	12 to 42	2.88 to 1.54 a_0
208 to 216	$15a_0$	19	32.72	23 to 82	3.13 to 1.66 a_0
217 to 220	$24a_0$	7	31.78	147 to 217	1.98 to 1.63 a_0
221 to 230	$8a_0$	60	30.99	6 to 25	3.26 to 1.60 a_0

Results for Solid Clusters

Table IX summarizes the observed critical water heights for each of these clustered systems. For two of the assemblies a range of heights is reported. This is the result of the limit on the height to which the four control rods located at the corners of the central uniform region could be withdrawn. The higher value corresponds to the critical water level, the lower to the position for the four control rods. The former value is applicable if the control rods are worthless; the latter applies if they are sufficiently strong to function as a blanket. The former corresponds more closely with the actual situation.

Table IX

OBSERVED CRITICAL WATER HEIGHTS

Lattice	$8a_0$		$10a_0$		$15a_0$	
Temperature, °C	20.3 to 22.5		21.7 to 22.2		21.7 to 21.9	
	Rods per Cluster	H_c, cm	Rods per Cluster	H_c, cm	Rods per Cluster	H_c, cm
	25	140.13	42	162.38 to 165.53	82	125.48
	22	124.28	37	140.13	73	118.26
	19	114.17	33	128.16	61	113.39
	16	108.41	30	121.96	52	112.80
	14	106.86	27	117.60	44	115.54
	12	107.35	23	114.86	37	122.00
	9	114.41	19	116.31	33	127.89
	7	130.30	16	120.84	27	145.87
	6	146.00	12	139.03	23	162.15 to 172.52

Table IX includes observations for only three of the four pitches studied. For the $24a_0$ pitch, criticality was not achieved. Observed inverse multiplications for four assemblies of this pitch are recorded in Table X. These values pass through a minimum in the same manner that the other sequences have a minimum for the critical height, indicating that, for the diameter of the system assembled with this $24a_0$ spacing, criticality would not have been achieved if additional fuel pins had been removed.

Table X

RECIPROCAL MULTIPLICATIONS FOR CORES OF $24a_0$ PITCH

Number of Rods/Cluster	215.7*	200	169	147
(Counting Rate)$^{-1}$	4.29	3.23	3.00	3.43

* 6 clusters of 217, and 1 of 208

Because of the long-time lapse between these measurements and the original measurements on uniform systems, some of the uniform systems were reassembled to provide a measure of the effect of light water contamination during the intervening eight months. For convenient comparison, these observations and the earlier results, already reported in Table V, are repeated in Table XI. These losses in reactivity are not due solely to a change in absorption and moderation resulting from a contamination of the D_2O. A lack of precise reproducibility on a short-term basis leads to an additional uncertainty in these values. For example, there are also included in Table XI two measurements on what was believed to be the same core loading of 19 clusters of 37 fuel rods each on a 15-unit lattice spacing, corresponding to an equivalent lattice spacing of $2.47a_0$. This appreciable loss in reactivity, in less than ten days, is presumably a measure of the errors associated with the reassembly of a particular loading.

Table XI

COMPARISON OF CRITICALITY FOR UNIFORM LATTICE CORES OF 25/1 FUEL

Lattice	Loading Number	Date	Number of Rods	H_c(cm)	Temperature (°C)
$3a_0$	103	3/11/58	325	148.22	19.4
$3a_0$	231	11/12/58	325	Not critical	
$3a_0$	105	3/12/58	375	125.20	20.0
$3a_0$	232	11/12/58	375	132.21	21.1
$2a_0$	91	3/ 3/58	745	132.84	
$2a_0$	233	11/12/58	745	135.08	20.0
$=2.47a_0$*	213	11/ 5/58		122.00	21.7
$=2.47a_0$*	234	11/14/58		124.74	20.6

* $15a_0$ spacing for 19 clusters of 37 rods each.

Results for Annular Clusters

Immediately following the solid-cluster fuel experiments performed with the uniform grid in ZPR-VII, a brief investigation of the effect of tubular-type fuel clusters was performed. Table XII summarizes the observations of critical height as fuel was removed in steps from the center of the clusters of 37 fuel rods arranged in a $15a_0$ triangular lattice.

Table XII

CRITICALITY WITH TUBULAR ARRANGEMENT OF FUEL IN ASSEMBLY OF 19 CLUSTERS WITH $15a_0$ TRIANGULAR PITCH

Loading Number	Rods per Cluster	Description	H_c (cm)	T (°C)
234	37	Uniform cluster	124.74	20.6
235	36	Central pin out	124.71	19.4
236	30	Central 7 pins out	127.56	19.4
237	24	Ditto, plus 6 of next ring	137.82	20.3
238	18	Central 19 pins out	171.35	20.6
239	37	Uniform cluster	124.54	21.1

3. Practical Clustered Lattices

In a practical heavy water power reactor using fuel of the THUD type, a separation of the coolant in the immediate vicinity of the fuel from the bulk of the moderator is desirable to reduce the power expended in pumping. Because of the limitation on the size of pressure vessel which can be fabricated, a pressure-tube type of design is attractive for D_2O reactors. This also allows the use of coolants other than D_2O. To obtain data of use in the design of such systems, a new core structure was provided for the ZPR-VII facility.

Design of the Core Structure

The mechanical design of the new core structure required was strongly influenced by a desire to minimize changes in the existing core structure and to use materials already on hand so as to reduce the delay in performing these experiments. It was decided that the control rod positions would not be altered. In order to use control rods Nos. 2, 4, 6, and 8, it was necessary to adopt a square lattice pattern. Two spacings of clusters, 10.795 cm and 12.978 cm, satisfied the requirements that a uniform loading pattern be achieved with no interference from the rod guides and that the systems investigated have a practical spacing. The 10.8-cm-sq lattice coincided with the pattern of fuel elements used in the EBWR and was equivalent in regard to cell area to a $12.2a_0$ triangular lattice spacing.

The 13.0-cm-sq lattice corresponded to a $14.6a_0$ triangular spacing. These values fall within the range of measurements made previously, namely, those for $8a_0$, $10a_0$, and $15a_0$ triangular lattice pitches.

The selection of cluster sizes was influenced by the previous results, by the tubing available, and by considerations of what might constitute a practical reactor design. There was on hand sufficient 6061 aluminum tubing to fabricate 39 cluster tubes of 6.191-cm ID, 0.159-cm wall, and 13 of 6.033-cm ID, 0.159-cm wall. Into a tube of 6.033-cm ID could be fitted a cluster of 31 fuel rods with $1a_0$ spacing, in the form of a hexagon with the corner pins removed.

The maximum number of fuel rods per cluster was selected to achieve a core of circular cross section and maximum radius, consistent with the limit on the number of fuel rods available and with having a reasonable number of cluster tubes involved. For the two spacings which could be assembled, patterns of 52 clusters for the 10.8-cm sq lattice and 49 for the 13.0-cm-sq lattice were provided. For the tighter lattice, the central 36 positions contained the four control rod guides, plus four clusters on each of the four faces of this square to provide a core of reasonably circular cross section. For the larger spacing, a 7 x 7 cluster square with the four corner clusters moved to the faces of the square provided a useful pattern.

Perforated aluminum sheet was used to insure a uniform $1a_0$ triangular spacing of fuel rods within the cluster tubes. Snap rings placed on two of the fuel rods served to position the three grids in each fuel cluster. Each fuel cluster contains an "O"-ring-sealed threaded plug in its base plate. This plug fixed the position of the fuel cluster by insertion in a close-fitting hole within a special 0.953-cm-thick baseplate provided to achieve the two desired lattice spacings. This baseplate was 111.8 cm square and contained 84 holes on a 10.8-cm-sq lattice spacing and 65 with 13.0-cm spacing.

The length of the cluster tubes was 182.9 cm. This insured that moderator water could not flow in over the top, since there was inadequate heavy water to fill the core tank to this height above the baseplate. For a 167.6-cm height of water, 6.13 kg of heavy water were displaced by a cluster tube. The weight of a cluster tube with the three grid plates was 1.59 kg. Each fuel rod weighed 0.45 kg. Consequently, there was no probelm due to buoyancy, as long as a minimum of eleven fuel rods was present in each cluster.

Although these fuel cluster tubes had slightly more than a 6.35-cm-diameter bearing surface on the baseplate, a device for achieving a precise lattice spacing at the top of the cluster was provided. This consisted of a plate, for each of the two spacings to be studied, containing 7.62-cm-diameter holes at the proper lattice pitch. This plate was supported by projections from the control rod guide channels, and special rings which

slipped over the fuel cluster tubes projecting through this top plate centered the fuel tubes within the 7.62-cm-diameter holes. Thus it was possible to remove individual fuel cluster tubes without disturbing the location of this top plate.

Figures 12 through 15 provide a brief review of this core geometry. Figure 12 shows the arrangement of fuel clusters for the cores of maximum size assembled with 10.8- and 13.0-cm-sq lattice spacings. Cores of 24, 32, 44, and 52 clusters were studied with the 10.8-cm spacing, and arrays of 21, 25, 29, 37, and 49 clusters in the 13.0-cm pattern. Figure 13 is a photograph of a core with 44 clusters having a 10.8-cm spacing. In Figure 14, the pattern of fuel rods within the cluster tubes is shown. Measurements were made with assemblies of 19, 25, and 31 fuel rods in each cluster. Figure 15 is a photograph of a cluster of 31 fuel rods and a cluster tube.

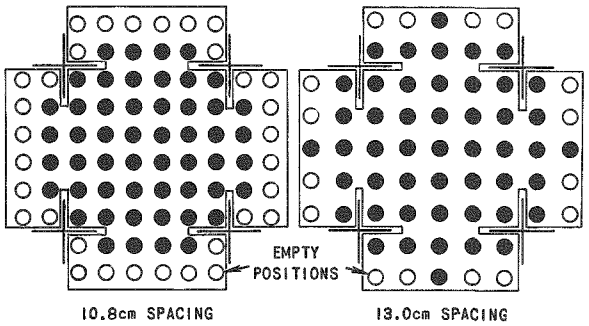

Fig. 12

Patterns of Clusters in Practical Lattices for Cores of Maximum Diameter.

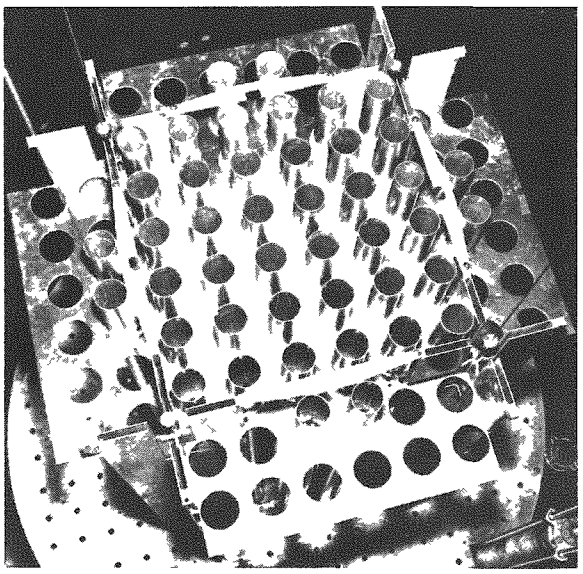

Fig. 13. Core of 44 Clusters with 10.8-cm Spacing.

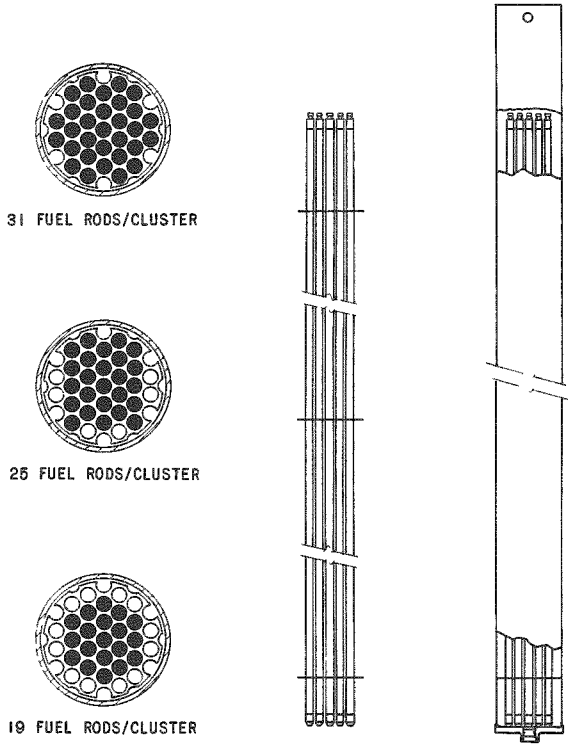

Fig. 14. Pattern of Fuel Rods within Cluster Tubes.

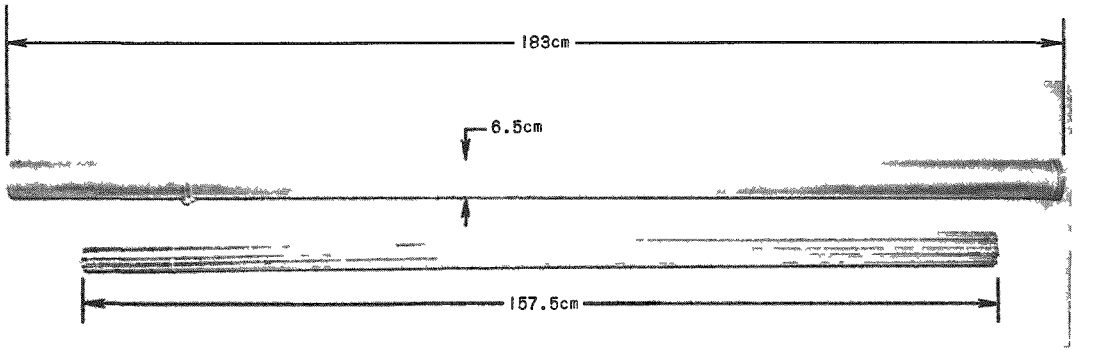

Fig. 15. 31 Fuel Rod Cluster and Cluster Tube.

Experiments with 25/1 Fuel

Subject to the reactivity restrictions imposed by the number of fuel rods and/or the maximum of 52 clustered tubes available, critical assemblies of each of the possible combinations of lattice pitch (10.8 cm and 13.0 cm), fuel rods per cluster (19, 25, and 31), and moderator within the clustered tube (D_2O, H_2O, and none) were constructed.

It was planned to use the two sizes of cluster tubes in a three-to-one ratio throughout the sequence of experiments, but trouble with leaky bottom plugs prevented this in some of the early assemblies. Whenever light water was used in the cluster tubes, the fuel rods and tubes were removed and dried thoroughly before proceeding with those assemblies.

Malfunctioning of the reactor tank thermocouple prevented measurement of temperatures for these assemblies prior to loading No. 318. From the temperatures measured at the corresponding dates in the previous year, it is estimated that the temperature was 19 to 20.5°C.

For those clustered assemblies having heavy water within the fuel tubes, assemblies of several sizes were constructed, primarily to provide information on the manner in which the differential water worth changed with core height. For each assembly, the critical water height and the doubling time associated with a small increase in this height were observed. Tables XIII and XIV describe the various loadings and record the observed critical water height and the radius calculated from the lattice pitch and the number of clusters.

Certain explanatory remarks are included in these tables to point out limitations applicable to these data. Values reported for two of the assemblies with 25 fuel rods per cluster have been corrected for the presence of perturbing effects, in one case, that of a single cluster from which the bottom plug was not removed, and in the other case for the

presence of certain foils. These corrections were based on critical heights observed for similar assemblies and the differential water worth curves. The data for differential core worths are reported in Table XXIII.

Table XIII

CRITICALITY DATA FOR 10.8-cm-sq LATTICE

Date	Loading Number	Number of Clusters (Small-Large)	Contents of Clusters	R_c (cm)	H_c (cm)	Footnote
31 fuel rods /cluster						
3/27/59	297	44 (11-33)	D_2O	40.41	86.54	
3/30/59	298	32 (8-24)	D_2O	34.44	108.84	
3/30/59	299	24 (6-18)	D_2O	29.85	147.80	
4/22/59	334	24 (6-18)	D_2O	29.85	148.49	
3/27/59	296	44 (11-33)	Air	40.41	109.13	
3/27/59	295	32 (8-24)	Air	34.44	145.53	
3/27/59	294	24 (6-18)	Air	29.85	>170.	
3/26/59	293	24 (6-18)	H_2O	29.85	123.01	(1)
4/24/59	335	24 (6-18)	H_2O	39.85	125.26	
25 fuel rods/cluster						
3/31/59	300	32 (8-24)	D_2O	34.44	114.50	
3/31/59	301	32 (8-24)	Air	34.44	168.86	
4/ 1/59	303	32 (8-24)	H_2O	34.44	136.04	(2)
19 fuel rods/cluster						
4/13/59	320	52 (13-39)	D_2O	43.92	89.87	
4/13/59	321	44 (11-33)	D_2O	40.41	100.03	
4/14/59	322	32 (8-24)	D_2O	34.44	133.48	
4/13/59	319	52 (13-39)	Air	43.92	123.2	
4/10/59	318	52 (13-39)	H_2O	43.92	>170.	(3)

(1) From three pairs of D_2O-H_2O critical levels: 126.11 and 109.22, 122.73 and 125.73; 123.0 and 123.19

(2) From three pairs of D_2O-H_2O critical levels: 141.20 and 114.30, 135.23 and 153.67; 135.94 and 137.16.

(3) H_2O at 152.40 cm.

Table XIV

CRITICALITY DATA FOR 13.0-cm-sq LATTICE

Date	Loading Number	Number of Clusters (Small-Large)	Contents of Clusters	R_c (cm)	H_c (cm)	Footnote
31 fuel pins/cluster						
3/19/59	278	49 (12-37)	D_2O	51.26	75.74	
3/19/59	279	37 (6-31)	D_2O	44.53	86.56	
3/20/59	282	29 (6-23)	D_2O	39.42	100.58	
3/23/59	283	21 (5-16)	D_2O	33.55	136.68	
3/18/59	277	49 (12-37)	Air	51.26	84.56	(1)
3/20/59	280	37 (6-31)	Air	44.53	98.95	
3/20/59	281	29 (6-23)	Air	39.42	116.26	(2)
3/25/59	290	29 (6-23)	H_2O	39.42	108.71	(3)
3/24/59	287	21 (5-16)	H_2O	33.55	161.71	(4)
25 fuel pins/cluster						
4/6/59	309	49 (12-37)	D_2O	51.26	81.58	(5)
4/6/59	308	37 (9-28)	D_2O	44.53	94.31	
4/3/59	306	25 (6-19)	D_2O	36.60	131.65	(6)
4/3/59	307	21 (5-16)	D_2O	33.55	167.54	
4/6/59	310	49 (12-37)	Air	51.26	94.32	
4/6/59	311	37 (9-28)	Air	44.53	110.90	
4/2/59	304	37 (9-28)	H_2O	44.53	141.90	(7)
19 fuel pins/cluster						
4/8/59	315	49 (12-37)	D_2O	51.26	95.01	
4/8/59	314	37 (9-28)	D_2O	44.53	113.46	
4/9/59	316	29 (7-22)	D_2O	39.42	143.94	
4/7/59	312	49 (12-37)	Air	51.26	110.38	
4/7/59	313	37 (9-28)	Air	44.53	134.67	
4/10/59	317	49 (12-37)	H_2O	51.26	~170.	(8)

(1) At least 3 tubes leaked (through bottom plugs).

(2) One cluster out of position ~5 cm at base of core.

(3) From three pairs of D_2O-H_2O critical levels: 108.51 and 144.78, 108.67 and 119.38, 108.71 and 109.22 cm.

(4) H_2O at 144.78 cm.

(5) Corrected by -0.29 cm for 1 voided cluster at periphery.

(6) Corrected by -1.50 cm for foils present.

(7) From two pairs of D_2O-H_2O critical levels: 142.47 and 137.16 and 141.86 and 142.24 cm.

(8) H_2O at 152.40 cm.

Figure 16 displays the critical dimensions for all of the assemblies made with 31 fuel rods per cluster. It is apparent that, for all assemblies, removal of the heavy water moderator in the fuel zone results in a loss of reactivity, but the effect of light water is dependent upon the lattice spacing, indicating the competition between the moderation and absorption effect of light water.

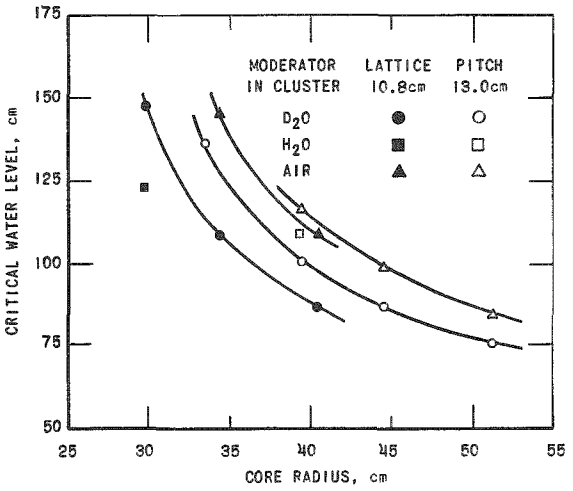

Fig. 16.

Critical Dimensions for Practical Clustered Lattices with 31 25/1 Fuel Rods per Cluster

Experiments with 15/1 Fuel

While the 15/1 fuel was available, a few of the practical clustered lattices were reconstructed with the fuel of higher enrichment. The observed critical water heights for the various loadings are given in Table XV. These results are also presented graphically in Figure 17, in which the critical heights are plotted as a function of the core radius calculated from the lattice pitch and the number of clusters. The removal of the heavy water from the fuel zone results in a loss of reactivity. The effect is more pronounced for the 19-rod clusters.

Some scatter exists in the values at small radii for the cluster arrangement studied most thoroughly, namely, the voided cluster of 31 fuel rods. It is thought that this is the result of pronounced deviations from a circular core cross section for the assemblies composed of only a few clusters and that the same effect would have been observed for the other cluster conditions if a comparable number of systems had been assembled. To illustrate this difficulty, the patterns of cluster arrangement is included in Table XV. For the fuel of lower enrichment, a larger number of clusters was required and such a fluctuation was less pronounced in the observations with 25/1 fuel.

Data obtained for the measurements of differential water worth for these systems are included in Table XXIII.

Table XV

CRITICAL HEIGHTS FOR 15/1 CLUSTERED CORES OF 13.0-cm-sq PITCH

Number of Clusters (Large-Small)	Void		D_2O-Filled	
	Loading Number	H_c (cm)	Loading Number	H_c (cm)
31 Rod Clusters				
37 (28-9)	415	60.45		
29 (22-7)	416	66.83		
25 (19-6)	417	72.59	429	64.41
21 (16-5)	418	79.22		
16 (12-4)	422	101.12	427	85.83
13 (10-3)	419	118.59		
12 (9-3)	423	139.17	425	116.97
11 (9-2)	421	157.33		
19 Rod Clusters				
37 (28-9)	438	72.67	441	63.70
25 (19-6)	437	90.86	440	78.64
16 (12-4)	436	137.26	439	115.82

Temperature range: 23.2-24.9°C
Duration of experiments: 10, 7 to 10, 16/59

Cluster patterns:

11 12 13 16

37 29 25 21

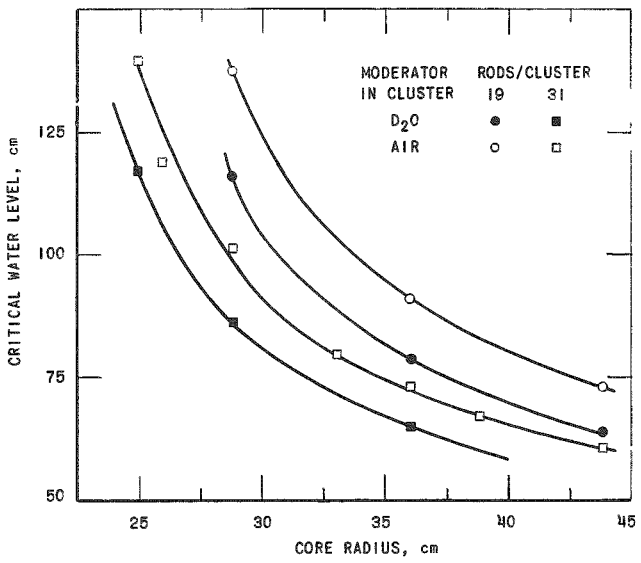

Fig. 17

Critical Dimensions for Clustered Cores of 15/1 Fuel Rods.

IV. BASIC PARAMETERS

In many of the clean critical assemblies, measurements were made to provide information about the nuclear parameters which occur in the various few-group theoretical descriptions for the behavior of neutrons in thermal reactors. The sections of this chapter describe experiments performed to determine reflector savings, age, resonance escape probability, thermal utilization, and fast fission effect.

A. Reflector Savings

Data for the determination of reflector savings for the THUD cores have been obtained by a variety of experimental techniques. Indirect methods for determining the axial reflector savings from the results for the geometrical critical sequences and from the differential water worth measurements are discussed in Sections III-A-2 and IV-B-1, respectively. Obviously, a combination of the values for the axial reflector savings obtained by those procedures with the observed critical dimensions would yield values for the radial reflector savings. In this section, the direct determination of bottom reflector savings and some information on radial reflector savings from measurements of neutron flux distribution patterns are reported. Also included are two types of experimental data from which values of the differential worth of the top reflector can be derived.

1. Reflector Savings from Flux Plots

In this method of determining reflector savings, the measured axial flux distribution of thermal neutrons is fitted to a cosine function over that portion of the core sufficiently distant from the reflector that perturbations due to the reflector are negligible. Similarly, the radial reflector savings are determined by fitting a J_0 function to the central portion of the observed radial flux distribution. Both counter traverses and activation techniques were used for the measurement of the flux distributions.

a. Experimental Procedure

Fuel rods, gold, dysprosium, indium, and manganese were each used at various times as the neutron detector in the activation method. Initially, the residual activity in irradiated fuel rods provided a measure of the neutron flux distribution. It was desirable to use a new fuel rod for each measurement, so that the background activity of the rod was both low and uniform along its length. After all available fuel had been used in the various core loadings, the flux distribution patterns were determined with gold wire of 0.13-cm diameter. The strong resonance absorption by gold necessitated duplicate sets of measurements, one with a bare wire, the other with a cadmium tube surrounding the wire. It was feasible to make these irradiations simultaneously, at symmetric locations within the reactor.

In order to halve the number of segments of wire or foils to be counted and calculated to yield a value for reflector savings, a switch to a dominantly thermal neutron detector, in the form of dysprosium dispersed in aluminum, was made at a later date. Foils (of 0.635-cm diameter) of this material were taped to aluminum strips. Indium foils and manganese-iron wires, encased in cadmium, were also used at times as epithermal detectors in radial flux distribution measurements, primarily to eliminate the confusion caused by thermal flux peaking in the heavy water radial reflectors of cores with small diameter.

Gamma-ray scintillation counting was the method normally used to measure the neutron activation of the wires and foils. Since the measurement of flux distributions by the activation technique involves a large number of routine counting operations, an automatic wire-scanning device was designed and constructed to measure and record the activity of 1-in. increments of the gold and manganese-iron wires. The mechanism, after measuring the activity of one segment of the wire, advances to the next segment and repeats the measurement, the activity of each increment being printed on a paper tape. When the last inch of the wire had been counted, the mechanism returned to the first part of the wire and repeated the series of counts. For the foil measurements, an automated counting system employing six commercial sample changers was used, with recording of pertinent data on IBM cards for subsequent processing.(13)

In the second method used to measure flux distributions, a 0.95-cm-diameter, 6.35-cm-long, U^{235}-coated fission counter having a sensitive length of 3.2 cm was moved in 2.5-cm steps by one of the spare control rod drive mechanisms within a water-tight aluminum tube running vertically through the core. The signal from this counter was fed into one counting channel (pre-amplifier, amplifier, and scaler) while pulses from a stationary counter were fed into another channel. The second counter served to monitor changes in the reactor power, and would stop both scalers when a predetermined number of counts had accumulated. The reactor's instrument channel I, a BF_3 counter located outside the core tank, was used as this monitor channel. The position of the fission counter as it was moved through the core was indicated by the control console selsyn associated with the particular control rod drive mechanism which was used to move the counter. Measurements were made with the fission counter both bare and cadmium covered.

A least-squares cosine or J_0 curve fit to each observed thermal neutron flux distribution was made by either GEORGE or an IBM 704 computer. Use of background and reference decay foils in the foil-counting equipment allowed more of the data manipulation to be performed by the computer than for the case of the wire-scanning equipment described above. The difference between the intercepts of the fitted curve with the distance axis and the actual location of the edges of the

core gave the reflector savings. In most cases, equally good fits were obtained by using various central portions of the distribution data, and in these cases the average value for the reflector savings was taken. Actual values are reported separately below for the axial and radial measurements.

b. Axial Reflector Savings

Relatively more attention has been given to the determination of axial reflector savings by the technique of measuring flux distribution. The reasons were twofold:

1) The flux peaking in the radial reflector caused a major distortion of the J_0 distribution in the cores of small diameter. This effect was of minor consequence for axial measurements.

2) The complexity of the structure used to support the fuel rods would introduce an appreciable uncertainty in any calculation of the axial reflector savings.

Figure 18 shows the total, thermal, and epithermal distributions of radial flux measured with gold wires for a typical core assembled in the EBWR structure. The pronounced thermal flux peaking in the reflector almost flattens the thermal distribution in the core. Figure 19 shows the sizeable and abrupt variation of the volume fractions of aluminum and heavy water in the immediate vicinity of the base of the core, due to the positioning and support structure for the fuel rods. Note also that there is some variation of these volume fractions among the three types of structure used in the THUD experiments.

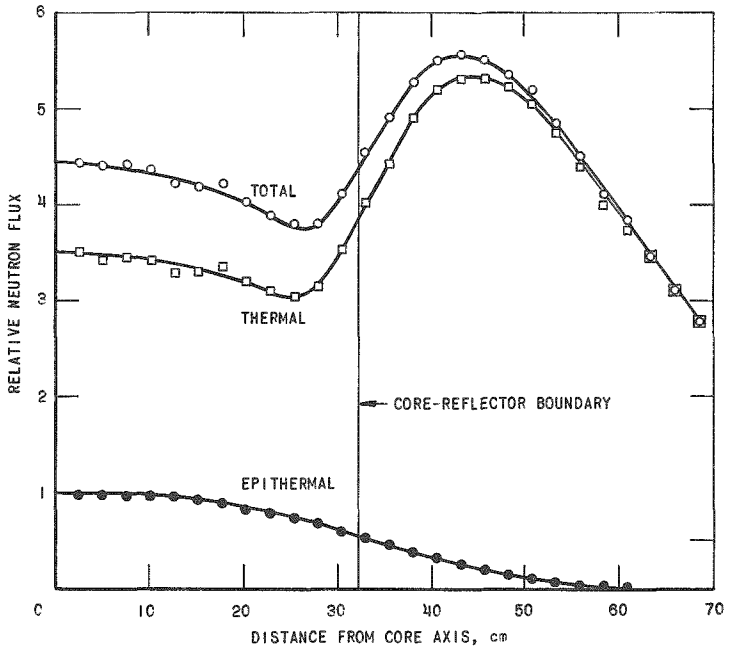

Fig. 18

Typical Radial Distribution of the Neutron Flux

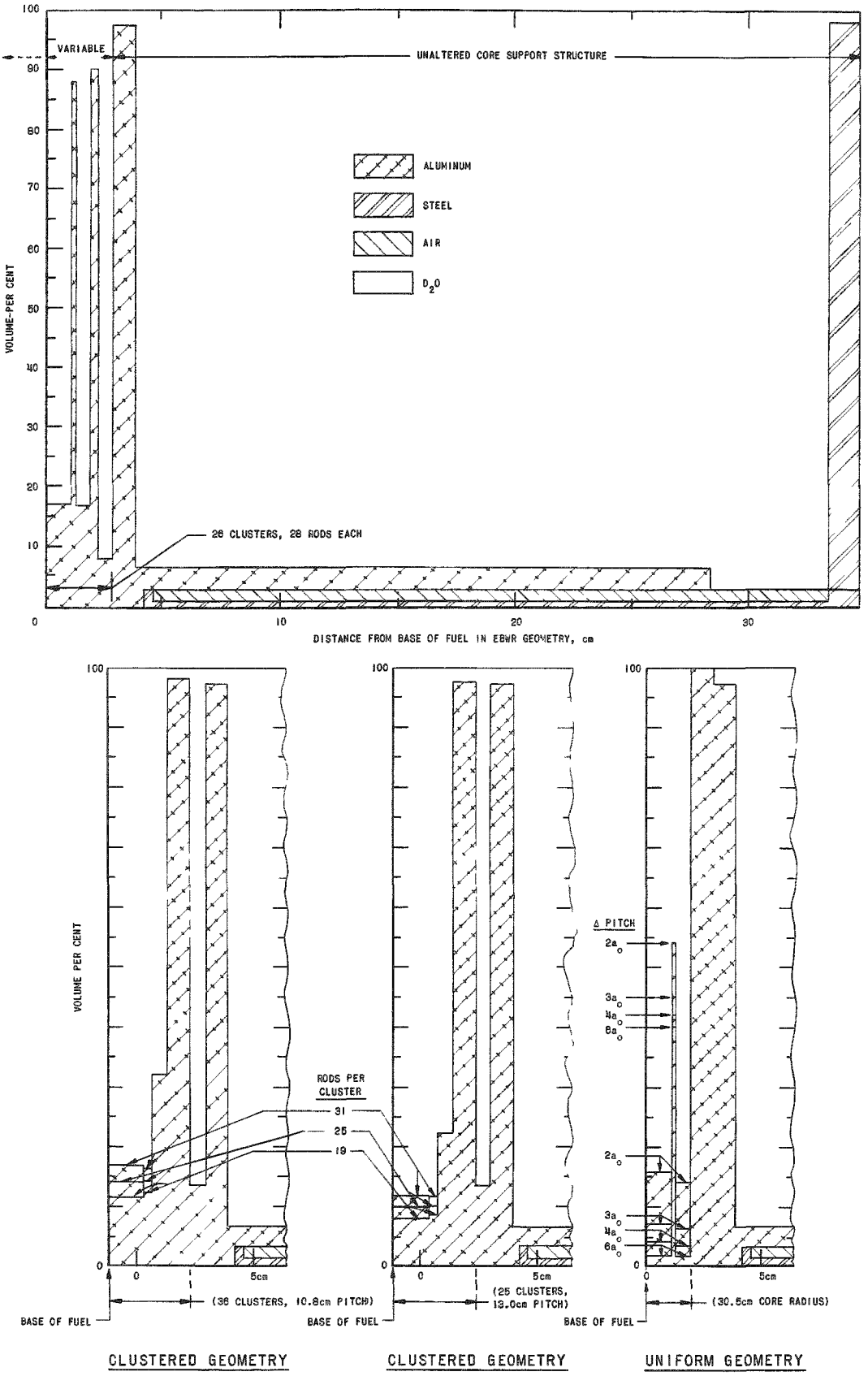

Fig. 19. Initial and Alternate Compositions of Bottom Reflector

Axial flux plots were made for the "slightly clustered" system (EBWR geometry, $2a_0$ triangular pitch) with 25/1 fuel, and for all of the uniform lattices with fuel of both the 25/1 and 15/1 enrichments except for the $4a_0$ lattice of 25/1 fuel. Values for the axial reflector savings, as determined from the least-squares fitting of the observed axial flux distributions are assembled in Table XVI.

Table XVI

AXIAL REFLECTOR SAVINGS FROM FLUX DISTRIBUTIONS

Loading Number	Identification[a]	Date	Critical Height (cm)	Reflector Savings λ_H (cm)	Detector
EBWR Structure, 25/1 Fuel, Partial Top Reflector					
43	C.C. #14[c]	9/4/57	161.09	40.69	Counter
44	C.C. #14	9/4/57	160.35	33.93	Counter
EBWR Structure, 25/1 Fuel, No Top Reflector					
52	C.C.	10/1/57	72.77	16 48	Au
60	C.C.	10/16/57	95.55	21.49	Au
61	C.C. #15	10/21/57	104.83	23.44	Au
66	F.S.	11/1/57	132.26	21.97	Au
71	C.C.	11/11/57	111.13	24.77	Counter
73	C.C. #15	11/22/57	108 51	28.80	Counter
73	C.C. #15	11/22/57	108.51	24.49	Counter
80	C.C. #14	12/23/57	115.77	18.44	Au
80	C.C. #14	12/23/57	115.77	18.52	Counter
80	C.C. #14	1/3/58	111.18	18.97	Counter
Uniform Lattice, 25/1 Fuel					
100	$2a_0$, C.C. #91	3/7/58	138.81	21.87	Au
100	$2a_0$, C.C. #91	3/10/58	133.02	22.73	Counter
108	$3a_0$, C.C. #108	3/14/58	104.11	19.74	Counter
109	$3a_0$, C.C. #103	3/19/58	149.78	17.42	Counter
184	6^-a_0, F.S.	9/15/58	150.29	19.08	Dy
184	6^-a_0, F.S.	9/15/58	148.51	18.70	Dy
184	6^+a_0, F.S.	9/18/58	151.00	18.29	Dy
184	6^+a_0, F.S.	9/24/58	149.33	18.78	Dy
184	6^+a_0, F.S.	10/2/58	146.33	18.06	Dy
242	#244, less 10 peripheral rods	12/15/58	106.12	18.92	Dy
244	$6a_0$, C.C.	1/15/59	104.60	19.46	Dy
248	$6a_0$, F.S.	1/20/59	138.51	16.43	Dy
249	$6a_0$, F.S.	1/21/59	153.49	18.42	Dy
Uniform Lattice, 15/1 Fuel					
381	$2a_0$, C.C.	8/12/59	105.93	20.1 18 8	Dy Cd-In-Cd
401	$3a_0$, C.C.	9/8/59	72.47	19.1 16.9	Dy Cd-In-Cd
407	$4a_0$, C.C.	9/14/59	128.79	18.0 17.2	Dy Cd-In-Cd
411	$6a_0$, C.C.	9/24/59	137 97	17.6 14.0	Dy Cd In-Cd

[a] Contained 24 empty and 9 D_2O-filled void tubes per cluster in addition to fuel.

[c] C.C. - Clean Critical, F.S. - Fuel Substitution Assembly.

Included there are the loadings for which the flux distribution measurements were made, a brief identification of the core in terms of loadings described in Sections III-B, III-C, and IV-C, the critical water level, the method of measurement, and the total axial reflector savings, as determined from the data-fitting procedure. Figure 20 shows a representative axial flux distribution with the cosine curve as fitted by the machine computation.

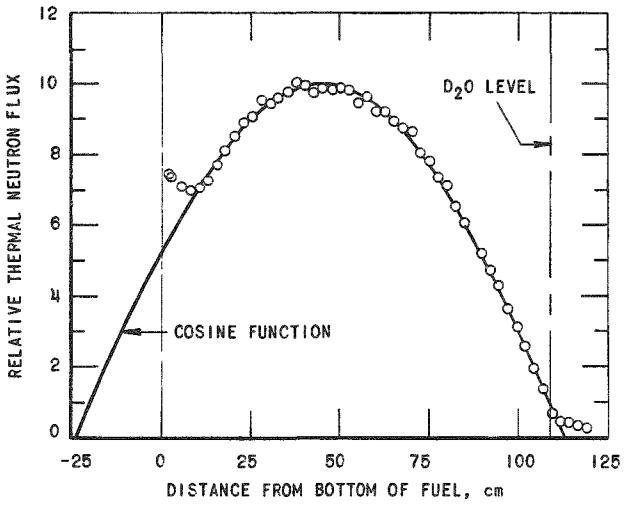

Fig. 20

Typical Axial Flux Distribution of Thermal Neutrons

Except for two cores with voids (loadings Nos. 43 and 44), the heavy water level was below the top of the fuel so that the upper reflector consisted of fuel, aluminum, control rods, and structural members, all in air above the water level. The tabulated values of reflector savings usually represent the average of the values given by several equally good fits for various portions of the total axial distribution of the thermal flux. Since the computation of reflector savings did not involve the determination of the center of the flux distribution, only the total of the top and bottom values is recorded in Table XVI. A slight error in locating the effective center of the observed flux distribution causes a significant change in the value for the top reflector savings. Consequently, to determine the bottom reflector savings from the data presented in this table, the contribution of the unreflected top portion of the core should be removed by subtraction of the calculated extrapolation distance, $0.71\,\lambda_{tr}$.

All of the measurements made with U^{235} fission counters required two separate runs, since it was necessary to determine both the thermal and epithermal component of the flux. For the observations with the cadmium-covered detector, the nuclear poisoning effect of the cadmium produced a significant change in the critical water height, and this height was also appreciably more dependent on detector position than for the bare counter. The critical water level existing for the bare counter measurements is the one reported in the table and is the one that was used in calculating the reflector savings from the least-squares fit of the

experimental data. A similar situation existed for the first two determinations by the gold-wire method, but subsequent gold-wire measurements made use of the flux symmetry which existed in the core for simultaneous irradiation of bare and cadmium-covered gold wires.

c. Radial Reflector Savings

In lieu of a sequence of geometrical criticals for the uniform lattices of maximum pitch assembled in the ZPR-VII core tank, the flux-distribution technique was applied, with moderate success, to the determination of radial reflector savings for those dilute cores having only a thin radial reflector. The results, coupled with the acquisition of a foil-counting system of greater capacity, led to a subsequent attempt to measure radial reflector savings for the sequence of uniform lattices with 15/1 fuel. For these latter measurements, resonance detectors were inserted radially at the same time that the axial measurements reported at the end of Table XVI were made.

The results of four irradiations of radially placed foils in the $6^{+}a_{\theta}$ (5.89-cm) pitch arrangement of the 25/1 fuel and two in the reassembly having the exact $6a_{\theta}$ pitch are given in Table XVII.

Table XVII

RADIAL REFLECTOR SAVINGS FROM FLUX-DISTRIBUTION MEASUREMENTS IN UNIFORM LATTICES OF 25/1 FUEL WITH $6^{+}a_{0}$ AND $6a_{0}$ PITCH

Loading Number	Date	Detector	Direction	Extrapolated Radius* (cm)	Average (cm)
$6^{+}a_{0}$ Pitch, 94.48-cm Radius					
184	9/12/58	Dy	NW Radius	108.38	
			NE Radius	104.50	
			SE Radius	104.50	
			SW Radius	103.96	
					105.33
184	10/2/58	Dy	NW Radius	108.20	
			NE Radius	105.41	
			SE Radius	108.99	
			SW Radius	104.47	
					106.77
191(=186)	10/23/58	Dy	Dispersed		104.83
184	10/10/58	Cd-Mn-Cd	NE Radius	103.53	
			SE Radius	103.89	
			SW Radius	99.09	
					102.16
$6a_{0}$ Pitch, 98.69-cm Radius					
248	1/20/59	Dy	E-W Diameter	105.51	
			NE-SW Diameter	108.46	
			N-S Diameter	106.15	
					106.71
249	1/21/59	Dy	E-W Diameter	107.47	

*Distance from center of core to the extrapolated zero-flux fit of the experimental data.

All of the cores were ones which existed during fuel-substitution experiments. Bare dysprosium-aluminum foils or cadmium-covered manganese wires were placed on core diameters for all but one of the irradiations. The foils and wires were mounted on steel or aluminum strips for traverses, and were inserted as nearly as possible along a radius or diameter 75 cm above the bottom of the core. In the remaining case, dysprosium-aluminum foils located in void tubes were placed in an identical pattern between the fuel rods within a cell, to reduce the influence of local flux perturbations.

Because of irregularities in the fuel rod pattern at the periphery (and to a lesser extent within the core) for the assemblies with $6^{+}a_0$ pitch, the flux center was not coincident with the geometric center of the core. This complicated the J_0 least-squares fitting, particularly for the dispersed arrangement of foils. Flux shapes in the $6^{+}a_0$ lattice were somewhat flattened in comparison with a J_0 function. This resulted in a tendency of the fitted center to shift away from the center of the core, in order to permit a better fit at the periphery. Diametrical traverses were divided into paired radial traverses, permitting a better fit to all data points and improving the reproducibility in the measurement of the distance from the geometric center to the position of the extrapolated zero flux.

The slight disagreement among the results from the three distinct techniques for determination of flux distribution represented by the values reported in Table XVII is considered to be inherent in the experimental methods employed. The dysprosium-aluminum foils were susceptible to local flux perturbations, since they were not located at equal distances from surrounding fuel rods. The dispersed foil arrangement eliminated scatter in the data due to the varying proximity of individual fuel rods by the selection of midpoint locations in the triangular lattice, but this prevented locating the foils in radial or diametrical lines, since there were relatively few triangles having 25/1 fuel rods at all corners. There would have been a problem of orientation had the more frequently occurring type triangle, composed of one 50/1 and two 25/1 fuel rods, been chosen. The data for each quadrant were grouped to provide enough data points for a good Bessel fit. This procedure permitted the use of geometrical radii for each foil, although some errors were evident because the flux center did not coincide with the geometric center. The manganese wires were encased in 0.203-cm-OD, 0.102-cm-ID cadmium tubing which resulted in a change of ~13 cm in the critical D_2O height. The uncertainties regarding the weighting factors for four such radial tubes which overlapped near the center of the core prevented a reliable assessment of the reactivity effects. The significant difference (3.5 cm) in extrapolated radii between the cadmium-covered manganese and the bare dyprosium-aluminum is attributed to the different spectra sampled.

No evidence of flux asymmetry was observed in the reconstructed assembly ($6a_0$), and the values reported were the result of fitting the flux patterns observed for foils placed on diameters of the two cores. A direct comparison with the results for the 6^+a_0 pitch core should not be made, because of the slight difference in fuel element spacing and the difference in core diameters.

Table XVIII summarizes the radial reflector savings determined from radial flux measurements for the uniform lattices with 15/1 fuel. Most of the radial distributions were obtained with cadmium-covered indium rather than dysprosium. In the smaller cores, the reflector peak distorted the thermal flux to such an extent that a fit could not be made to data obtained with the dysprosium foils.

Table XVIII

RADIAL REFLECTOR SAVINGS FROM FLUX-DISTRIBUTION MEASUREMENTS IN UNIFORM LATTICES OF 15/1 FUEL

Loading Number	Identification*	Date	Core Radius (cm)	Reflector Savings (cm)	Detector
381	$2a_0$, C.C.	8/12/59	20.52	16.9	Cd-In-Cd
401	$3a_0$, C.C.	9/8/59	26.88	14.25	Cd-In-Cd
407	$4a_0$, C.C.	9/14/59	23.58	12.73	Cd-In-Cd
411	$6a_0$, C.C.	9/24/59	34.73	14.4 22.1	Cd-In-Cd Dy

*C.C. = Clean Critical

2. Reflector Savings for a Top Reflector

Measurements were undertaken to determine the worth of the top reflector as a function of thickness, primarily to provide experimental data for comparison with calculations of reflector savings for the THUD lattices. Such information was advantageous from the theoretical viewpoint because the top reflector was relatively free of irregularities in composition, and the nature of the ZPR-VII system made experimental data easy to obtain. Two experimental methods were used for uniform lattices of 25/1 fuel with $3a_0$ triangular pitch and for mixtures of 25/1 and 50/1 fuel with the 6^+a_0 pitch, one a direct dynamic measurement of the worth of different layers of top reflector and the other an extension of geometrical critical experiments to assemblies having various amounts of top reflector.

a. Method for Differential Water Worth

The method for determining experimentally the total reactivity worth of the top reflector as a function of thickness requires a measurement of the differential water worth at various critical heights. Integration of the curve $\delta\rho/\delta H$ as a function of the reflector thickness, H, yields the total reactivity worth of the reflector, ρ, as a function of thickness. This procedure assumes that the differential water worth is independent of small changes in the core radius and that the worth of a given water slab as measured here will remain constant when the slab is part of a complete top reflector.

Values of the differential water worth for top reflector thicknesses up to 17 cm were obtained by stepwise removal of a total of 17 fuel rods from a $3a_0$ triangular lattice arrangement of 25/1 fuel rods which was approximately critical with the water level at the top of the fuel. These steps, together with the doubling time observed when the critical water level was increased by a small amount, are recorded in Table XIX. The significance of the column labelled "Final Critical Height" and the reason for missing entries are explained in Section IV-B.

Table XIX

CRITICAL DIMENSIONS AND DOUBLING TIME DATA FOR TOP-REFLECTED $3a_0$ PITCH LATTICES OF 25/1 FUEL

Loading Number	Date	Number of Rods	Initial Critical Height (cm)	Increment (cm)	Final Critical Height (cm)	Doubling Time (sec)
148	6/19/58	324	152.67	1.270		58.47
159	6/30/58	322	154.71	1.016	154.64	79.8
			154.64	1.778		37.99
151	6/20/58	320	155.65	1.270	155.60	56.93
			155.60	1.778		36.82
150	6/20/58	316	158.78	1.016	158.67	87.1
			158.67	1.778		45.03
149	6/19/58	312	162.75	1.270	162.71	79.55
			162.71	1.778		54.40
158	6/27/58	312	163.98	1.778	163 91	54.65
154	6/25/58	310	163.04	1.016	162.99	137.65
			162.99	2.032	162.99	58.35
			162.99	1.270		132.75
156	6/26/58	310	166.14	1.778	165.99	60.75
			165.99	2.540		41.75
152	6/23/58	309	166.29	0.762	166.04	186.9
			166.04	1.778		79.7
157	6/27/58	308	166.62	1.778	168.55	77.5
			168.55	2.540		52.95
155	6 26/58	307	169.77	1.270	169.70	129.4
			169.70	2.032		79.3

Similar but less extensive data for assemblies composed of a mixture of 25/1 and 50/1 fuel with the $6^{+}a_0$ triangular pitch, loadings Nos 186 to 190, are reported at the end of Table XXII, a collection of differential water worth data for cores of uniform structure. Loadings Nos. 186 to 190 are described in Table XXIV.

b. Buckling Compensation Method

The second method used for an experimental determination of the relationship between top reflector savings and reflector thickness is based on observation of the decrease in core radius required to maintain criticality when the top reflector thickness is increased. Since the buckling remains constant, the increase in the radial buckling is equal to the decrease in the axial buckling, and hence to an increase in axial reflector savings. The average radius of the core can be calculated by knowing the lattice and the number of fuel pins present. The core radius R and the top reflector savings λ_T are related by the definition of the critical geometrical buckling:

$$B^2 = \left(\frac{\pi}{H + \lambda_B + \lambda_T}\right)^2 + \left(\frac{2.405}{R + \lambda_R}\right)^2 ,$$

where λ_R is the radial reflector savings. Rearrangement gives

$$\lambda_T = \frac{\pi}{\sqrt{B^2 - \left(\frac{2.405}{R + \lambda_R}\right)^2}} - (H + \lambda_B) .$$

The critical assembly data of Table XIX are amenable to this type of treatment. Note that the maximum core radius was 27.01 cm, resulting in a radial reflector thickness of 75.86 cm. The decrease in core radius was only 0.72 cm, and so the change in radial reflector thickness, and hence change in radial reflector savings, was negligible.

A similar set of data on geometrical criticals is available in Table XX for a $6^{+}a_0$ pitch lattice of a mixture of 25/1 and 50/1 fuel. Because the core nearly filled the ZPR-VII tank, the change in radial reflector savings which resulted from the decrease in core size from 94.48 to 81.41 cm, with a corresponding increase in radial reflector thickness from 8.39 to 21.46 cm, must be taken into account. For these data, a more fruitful procedure would be to use the top reflector savings, as determined from the measurements of differential water worth for loadings Nos. 186 through 190, to evaluate the radial reflector savings as a function of thickness of the radial reflector. These results would provide a check on the values obtained from radial flux plots in loadings Nos. 191 and 184, as given in Table XVII.

Table XX

GEOMETRICAL CRITICALS FOR MIXED FUEL RODS AT $6^{+}a_0$ PITCH

Loading Number	Date	Number of Fuel Rods 25/1	Number of Fuel Rods 50/1	Height (cm)	Temperature (°C)
191	10/23/58	712	220	153.14	22.8
192	10/24/58	680	214	154.69	22.8
193	10/24/58	648	206	155.58	22.9
194	10/24/58	616	198	157.56	23.0
195	10/24/58	584	190	160.20	23.1
195	10/27/58	584	190	159.97	22.5
196	10/27/58	548	184	164.36	22.2
197	10/27/58	518	174	171.32	22.2

B. Differential Water Worth

For many of the critical assemblies, the period resulting from the addition of a small amount of water to the critical reactor was observed, to provide information on the neutron age.

1. Relation to Age

In the formulation of age-diffusion theory, the observed differential reactivity is related to the neutron age by

$$\frac{\delta\rho}{\delta H} = \frac{\varepsilon}{\delta H}\left[1 - \frac{(1 + L^2B^2)\, e^{\tau B^2}}{k_\infty}\right] = \frac{2\pi^2}{(H + \lambda_H)^3 k}\left(\tau + \frac{L^2}{1 + L^2B^2}\right) .$$

Rearrangement gives the following expression for the age τ, in terms of the observed differential reactivity and quantities known from other experiments:

$$\tau = \frac{(H + \lambda_H)^3 k}{2\pi^2}\,\frac{\delta\rho}{\delta H} - \frac{L^2}{1 + L^2B^2} .$$

When period measurements were made for two or more assemblies of the same composition but different ratios of height to diameter, a slope-intercept type of data treatment yields information on the axial reflector savings as well. Rearrangement of the above equation shows how the age and axial reflector savings can be evaluated from the intercept and slope of the resulting graph:

$$H = \frac{2\pi^2}{k}\left(\tau + \frac{L^2}{1 + L^2B^2}\right)^{1/3}\left(\frac{\Delta\rho}{\Delta H}\right)^{-1/3} - \lambda_H \quad .$$

In this simple analysis it is assumed that the axial reflector savings is not a function of core height; in practice, however, the large extrapolation required restricts the accuracy of the determination of λ_H by this method.

2. Experimental Procedure

Because of the relatively low rate of flow of water allowed in the ZPR-VII system for a core near a critical condition, the experimental procedure used for measurements of differential water worth differed somewhat from that followed in control rod calibrations by the usual rod bump-period method. After achieving a clean critical condition at a power level sufficiently high to make the long-term delayed photoneutron contribution negligible, the standpipe was raised by the amount desired for the increment of water level. Water was added until it had reached the height corresponding to the new standpipe level, and this added reactivity was counterbalanced by moving a single control rod into the core. The reactor was held critical at a much lower power level for a minimum of 5 min, to achieve equilibrium for both the delayed-neutron emitters and the water level. The control rod was then withdrawn from the core at the maximum allowed speed; normally, the rod was completely withdrawn by the time that the power level reached its original value. In this way the power level could be observed over several doubling times without raising the residual background of radioactivity in the core to an undesirable level. A preliminary value for the doubling time generally was available from the log level recorder, but the values reported here are the average of the doubling times obtained from a semilogarithmic plot of the trace of the two linear level recorders. The detectors were all neutron-sensitive ionization chambers, uncompensated for the current due to gamma radiation.

3. Results

The observations for systems assembled in the EBWR, uniform, and clustered core structures are collected in Tables XXI, XXII, and XXIII, respectively. These tables include the equilibrium critical heights observed before and after each determination of the differential reactivity, the change in water height made for the measurement, and the average doubling time. Details of the assemblies in which these measurements were made are given in the tables of clean critical data in Chapter III and those for the fuel-substitution experiments in Section IV-C.

Table XXI

DIFFERENTIAL WATER WORTH NEAR CRITICAL FOR EBWR CORE STRUCTURE

Loading Number	Initial Critical Height (cm)	Increment (cm)	Final Critical Height (cm)	Doubling Time (sec)
Clean Criticals 25/1 Fuel				
14		0 813	110 922	29 64
		1 245	109 474	13 16
	109 474	0 737	109 487	34 50
	109 487	0 978	109 500	21 85
15	101 600	0 737	101 600	26 68
	101 600	0 965	101 600	16 81
16	95 288	0 953		14 10
	95 250	0 533		39 84
	95 263	0 762		20 72
19	109 639	0 762		30 18
52	72 547	0 508	72 550	18 42
	72 550	0 635	72 550	12 31
	72 550	0 762		8 47
		0 508	73 927	20 06
53	75 730	0 508	75 730	22 49
	75 730	0 762		10 89
54	80 150	0 508	80 112	23 39
	80 112	0 635	80 086	16 65
	80 086	0 762		12 62
55	85 712	0 635	85 712	19 98
	85 712	0 762	85 700	14 98
	85 700	0 889		11 55
56	94 844	0 762	94 806	20 99
	94 806	0 762	94 806	22 39
59	95 352	0 508	95 314	40 2
	95 314	0 762		25 25
60	94 894	0 508		41 1
71	111 028	0 762	111 023	36 6
	111 023	1 016	111 023	23 5
	111 023	1 270		15 5
81	96 457	0 508		44 75
		0 762		23 0
Clustered Geometry 25/1 Fuel				
82	107 887	0 508	107 848	60 0
	107 887	0 508	107 848	57 8
	107 848	1 016		21 15
Mixture of 25/1 and 50/1 Fuel				
63	114 465	0 381	114 325	106 8
	114 325	0 762	114 325	57 05
	114 325	1 143		27 55
64	119 037	0 508	118 796	82 9
	118 796	1 016	118 796	46 3
	118 796	1 270		30 3
65	123 762	0 508	123 736	95 42
	123 736	1 016	123 723	37 9
	123 723	1 397		22 83
66	127 940	0 762	127 889	66 40
	127 889	1 524		22 92
67	140 068	0 762	140 035	80 63
	140 035	1 524	140 018	31 03
	140 018	1 143		51 08
68	148 044	1 143	147 942	58 75
	147 942	1 524	147 955	43 3
	147 955	2 032	147 942	26 85
69	118 440	0 762	118 237	60 7
	118 237	1 143	118 262	42 6
	118 262	1 397		19 5
	118 301	1 524	118 275	20 18
	118 275	1 143	118 262	26 05
	118 262	0 762	118 339	51 57
	118 339	0 381		149 6
70	114 668	1 270	114 600	18 2
	114 600	1 270	114 605	18 6
	114 605	1 016		28 73

Table XXII

DIFFERENTIAL WATER WORTH NEAR CRITICAL FOR UNIFORM CORE STRUCTURE

Loading Number	Initial Critical Height (cm)	Increment (cm)	Final Critical Height (cm)	Doubling Time (sec)
$2a_0$ Pitch, 25/1 Fuel				
90	150.901	1.524	150.851	47.5
	150.851	2.794		19.42
89	145.453	1.270	145.352	53.6
	145.352	2.032	145.390	29.16
	145.390	2.794		15.49
92	123.53	0.762	123.520	57.97
	123.520	1.524	123.520	20.07
	123.520	1.143		33.08
93	115.95	1.270	115.95	22.63
95	103.340	0.762	103.353	35.70
	103.353	1.016	103.353	21.70
	103.353	1.270		14.30
$3a_0$ Pitch, 25/1 Fuel				
103	148.247	1.524	148.234	34.24
	148.234	2.286	148.184	17.89
	148.184	0.762		106.2
104	133.820	1.016	133.731	42.28
	133.833	1.778		16.56
105	125.222	0.762	125.197	51.85
	125.197	1.143	125.197	28.94
	125.197	1.524		18.06
106	115.799	0.762	115.824	39.33
	115.799	0.508	115.811	77.89
	115.811	1.016		26.84
107	111.874	0.762	111.849	35.43
	111.849	0.508	111.836	70.34
	111.836	1.016		24.20
108	103.708	0.508	103.696	51.39
	103.696	0.889	103.696	22.10
	103.696	0.711		32.54
$4a_0$ Pitch, 25/1 Fuel				
118	147.625	1.270	147.599	37.09
	147.599	0.762	147.599	87.00
	147.599	1.778		23.53
6^+a_0 Pitch, 25/1 Fuel				
178	113.005	0.254	113.055	138.78
	113.055	0.762	113.208	36.69
	113.208	1.016	113.106	21.54
	113.284	1.270		13.23
	113.563	0.508	113.538	58.40
	113.538	1.016		17.95
	113.640	0.762	113.627	29.36
	113.627	1.016	113.627	19.17
	113.627	1.270	112.116	12.65
$2a_0$ Pitch, 15/1 Fuel				
385	123.038	1.016		44.30
381	104.585	0.635		54.40
382	90.157	0.635		31.47
383	71.780	0.381		36.55
$3a_0$ Pitch, 15/1 Fuel				
402	115.468	1.524		15.98
401	72.377	0.191		78.33
400	59.726	0.142		80.06
$4a_0$ Pitch, 15/1 Fuel				
407	127.318	1.270		29.67
405	103.048	1.270		10.68
404		0.284	72.791	38.01
$6a_0$ Pitch, 15/1 Fuel				
409	103.581	1.270		10.34
Cluster of 27 25/1 Fuel Rods, $6\sqrt{3}\,a_0$ Pitch				
177	96.342	0.508	96.342	49.63
	96.342	1.016		16.42
$2a_0$ Pitch, Mixture of 25/1 and 50/1 Fuel				
98	128.346	1.016	128.321	47.35
	128.321	1.524	128.321	26.19
	128.321	1.778		20.09
$4a_0$ Pitch, Mixture of 25/1 and 50/1 Fuel				
121	148.920	1.270	148.895	39.53
	148.895	1.905	148.895	21.34
	148.895	0.762		91.33
6^+a_0 Pitch, Mixture of 25/1 and 50/1 Fuel				
179	118.491	1.016		19.94
	118.542	1.016		20.17
180	123.838	1.016		25.96
181	130.175	1.016		30.565
183	146.101	1.016	146.164	47.275
	146.164	1.524		26.575
184	148.514	1.524		26.62
	142.926	2.032		13.27
	144.831	1.778		17.22
	145.821	1.524		23.30
	147.676	1.524		23.86
185	149.479	1.778		21.11
186	152.298	1.524	152.171	30.23
	152.171	2.032		23.29
187	156.185	1.524	156.159	33.87
	156.159	2.540		15.57
188	159.906	1.524	159.791	44.80
	159.791	2.540		23.28
189	165.049	2.540	164.998	31.70
	164.998	1.524		72.52
190	167.640	2.032		58.06
	167.792	1.778		56.35

Table XXIII

DIFFERENTIAL WATER WORTH NEAR CRITICAL FOR CLUSTERED CORE STRUCTURE

Loading Number	Initial Critical Height (cm)	Increment (cm)	Doubling Time (sec)	Contents of Clusters
10.8-cm Pitch, 25/1 Fuel				
31 rods/cluster				
297	86.538	0.635	22.71	D_2O
298	108.839	1.270	16.26	D_2O
299	147.803	2.540	18.17	D_2O
296	109.131	1.016	19.76	Air
295	145.529	1.778	24.39	Air
293	123.000	1.524	35.80	H_2O
25 rods/cluster				
300	114.496	0.762	44.97	D_2O
301	168.859	2.540	50.40	Air
303	141.199	1.524	58.38	H_2O
	135.230	2.540	21.05	
	135.941	2.540	24.35	
19 rods/cluster				
320	89.865	0.635	23.90	D_2O
321	100.025	0.635	31.63	D_2O
322	133.477	1.524	27.54	D_2O
319	123.241	1.651	10.20	Air
13.0 cm Pitch, 25/1 Fuel				
31 rods/cluster				
278	75.743	0.508	19.36	D_2O
279	86.563	0.635	20.68	D_2O
282	100.584	0.762	25.89	D_2O
283	136.677	1.270	36.07	D_2O
277	84.557	0.254	31.025	Air
	84.506	0.635	8.99	
280	98.946	0.762	19.56	Air
281	116.256	1.016	22.75	Air
290	108.712	1.016	32.50	H_2O
25 rods/cluster				
309	81.559	0.635	15.58	D_2O
308	94.310	0.635	27.74	D_2O
310	94.323	0 762	15.30	Air
311	110.896	0.762	28.80	Air
304	142.469	2.540	24.85	H_2O
	141.859	3.353	15.86	
19 rods/cluster				
315	95.009	0.635	25.01	D_2O
314	113.462	1.016	21.46	D_2O
316	143.942	2.540	11.87	D_2O
312	110.376	1.016	15.07	Air
313	134.671	1.270	23.41	Air
13.0-cm Pitch, 15/1 Fuel				
31 rods/cluster				
419	118.593	0 762	45.10	Air
418	79 223	0.508	20.58	Air
417	72.593	0.381	25.58	Air
416	66 827	0.254	37.37	Air
415	60.452	0.254	31.05	Air
425	116 942	0.762	47.85	D_2O
427	85.827	0.508	31.03	D_2O
429	64 414	0.254	38.96	D_2O
19 rods/cluster				
438	137.262	1.270	28.88	Air
437	90.856	0.508	27.57	Air
436	72.669	0.254	44.67	Air
439	115.824	1.016	27.43	D_2O
440	78.638	0.381	29.97	D_2O
441	63.703	0.254	30.25	D_2O

Various methods were used to terminate the excursion. When only a single period determination was desired, or when the measurement was the last of a sequence, the reactor was shut down by either a hand scram or a power level trip signal. When the period measurement was made as an incidental part of a foil irradiation, the assembly was restored to a critical state at a high power level. When a subsequent period measurement was planned, the system was also restored to a critical condition, but at a power level approximating that used in the initial leveling of the reactor. The tables of data of differential core worth give either an initial critical height (single period or last of a sequence), or a final critical height (foil irradiation), or both (measurement other than the last of a sequence). Some of the "final" values for the critical height

represent the same measurement as the initial value for a subsequent doubling-time measurement. Some shifting of the critical position in successive runs was noted occasionally, in spite of the precaution that all critical settings were established at a moderately high power level.

In Table XXIII, the "Final Critical Height" column has been omitted, since a sequence of period measurements in the clustered geometry was made only for loading No. 277. Where more than one value is reported elsewhere in this table, the loading had been modified between measurements. This applies to measurements made when the clusters were filled with light water. The footnotes of Tables XIII and XIV for the clustered clean critical data give information on the H_2O level in the clusters during these period measurements.

Some additional data on differential water worth are given in Table XIX for top-reflected cores with 25/1 fuel rods at a uniform $3a_0$ pitch; in Table XXXII for voided cores of 25/1 fuel in EBWR geometry; in Table XXXIV for clustered cores containing thorium sheets; and in Table XL and XLI for the cores which were heated for temperature coefficient measurements.

4. Data Treatment

The differential reactivity at a particular water level can be obtained in two ways, provided there exists a minimum of two observations for different increments. An average of the observed $\Delta\rho/\Delta H$ values gives one value, and the slope of a graph of the reactivity as a function of water level provides the second. These two methods of averaging are of comparable precision, but together and with similar values at other heights they serve to better define the actual differential worth. As a matter of interest and as an indication of the accuracy of the latter method, the critical water height indicated by the intercept was usually in good agreement with the observed height. For that comparison a tentative inhour equation was used to convert the observed doubling times to reactivity. However, a conversion of the data of Tables XXI, XXII and XXIII is not included here, because of the need for additional analysis of the variation of the effective delayed photoneutron fraction with core structure and geometry.

C. Fuel-substitution Experiments

The addition of a neutron poison to a critical assembly provides a means to evaluate certain nuclear parameters from the observed reactivity effect. In a water system, the change in critical dimensions resulting from the addition of a known amount of soluble poison is sometimes observed to provide information on both the neutron age and the resonance escape

probability. In the THUD program, a modification of this procedure was employed, because of both a desire to avoid contamination of the heavy water and the availability of fuel of two enrichments.

1. Method

As used in the THUD program, the technique of fuel substitution or variation enrichment starts with a clean critical of partial core height containing only fuel of the higher enrichment available, the 25/1 thorium to U^{235} atom ratio fuel. Lower enrichment (50/1) fuel is substituted for a portion of the 25/1 fuel as uniformly as possible throughout the core, and the new (higher) critical water height is observed. This procedure is continued until submersion of almost the full 1.5-m length of the fuel rods is required for criticality.

It is of interest to indicate the manner of treatment of the experimental observations, using the two-group age-diffusion criticality equation as a simple model. This equation,

$$k_{eff} = 1 = k_\infty e^{-\tau B^2}/(1 + L^2 B^2) \quad ,$$

may be written in the form

$$\ln\left(\frac{1 + L^2 B^2}{f^{25}}\right) = - \tau B^2 + \ln (\eta^{25} \epsilon p) \quad ,$$

which has the linear form $y = ax + b$. The known fuel concentration and the observed critical water height are combined with the core radius, reflector savings, and pertinent cross sections to evaluate $\ln[(1+L^2 B^2)/f^{25}]$ and B^2 for each loading. Corresponding pairs of values define a curve whose slope and intercept yield values of τ and p, respectively, provided η^{25} and ϵ are known.

2. Core Patterns and Results

Several types of core geometries have been studied by the fuel-substitution experiment. The first was a slightly clustered arrangement containing 28 fuel rods in a 1.905-cm ($2a_0$) triangular spacing, repeated on a 10.16-cm-sq pattern with a superimposed grid of control rod guide channels. This pattern corresponds to the structure of EBWR, and representative fuel arrangements are shown in Figure 5. The structure for the uniform lattices studied subsequently is shown in Figure 6. Triangular patterns of single fuel rods spaced 1.905, 2.858, 3.81, 5.72, and 5.89 cm ($2a_0$, $3a_0$, $4a_0$, $6a_0$, and 6^+a_0) apart were assembled in the uniform region bounded by control rod guide channels Nos. 2, 4, 6 and 8. A single clustered lattice composed of nine fuel rods at $6a_0$ spacing was also investigated.

The radius of each system was adjusted to achieve initial criticality at approximately two-thirds full-core height. The total number of rods involved depended upon the lattice spacing. Several substitution steps were made, with up to ~30% of the total rods being replaced except in one case, for one system in which only 11% of the fuel was substituted. The number of low-enrichment fuel rods and the observed critical water heights for these sequences of fuel substitutions are given in Table XXIV. These data are self-explanatory, but some additional information is required in regard to the pattern of low-enrichment rods.

Table XXIV

CRITICAL WATER LEVELS IN FUEL SUBSTITUTION EXPERIMENTS

Loading Number	25 1 Rods	50 1 Rods	Critical Height (cm)	kgU^{235} 50 1	kgU^{235} 25 1
FBWR Geometry					
63	836	30	114.48	0.1795	9.618
64	772	64	119.05	0.3833	9.211
65	740	96	123.77	0.5747	8.828
66	716	120	127.91	0.7183	8.541
67	660	176	140.08	1 0536	7.873
68	634	208	148.06	1.245	7.512
69	776	60	118.31	0.3535	9.313
70	804	32	114.68	0.1916	9.639
71	836	0	121.02	0	10.027
$2a_0$ Uniform					
95	1009	3	103.35	0	12.1374
96	937	72	109.88	0.4325	11.2729
97	865	144	117.86	0.8724	10.4077
98	793	216	128.33	1.3055	9.5410
99	720	288	141.95	1.7453	8.6633
$3a_0$ Uniform					
110	461	0	103.67	0	5.5411
111	426	35	110.73	0.2106	5.12e0
112	394	67	118.63	0.4026	4.7378
113	359	102	129.73	0.6132	4.31e0
114	327	134	143.18	0.8059	3.93e1
$4a_0$ Uniform					
120	299	0	129 35	0	3.5915
121	265	34	148 90	0.2053	3 1825
122	273	26	143.52	0.1568	3.2795
123	282	17	137.97	0 1022	3.3876
124	289	10	134.45	0 0601	3.4720
125	299	0	129.59	0	3.5919
$6a_0$ Uniform					
244 2	1082	0	104.51		
245-1	1018	64	110.64		
246-1	948	134	118.08		
247-1	881	201	126.85		
248 1	813	269	138.15		
249-1	748	334	153.00		
6^+a_0 Uniform					
178 19	932	0	113.79		
179-1	894	38	118.49		
180-1	856	76	123 84		
181-1	818	114	130.15		
182-1	780	152	137.35		
183 1	742	190	146.10		
184-38	742	190	145.80		
185-1	722	210	149.48		
186-1	712	220	152 30		
187-1	702	230	156.18		
188-1	692	240	159.91		
189-1	682	250	165.07		
190-1	678	254	167.64		
$6a_0$ Pitch Clusters of 9 Rods					
169	945	0	105.16		
170	871	74	113.21		
171	825	120	118.97		
172	751	194	130.71		
173	705	240	139.95		
174	679	266	146.25		
175	945	0	105.87		

The substitution pattern used for the $3a_0$ and $2a_0$ pitch uniform lattices is illustrative of the care taken to insure that a representative exchange of fuel was made for each step. The pattern of substitution in the assembly with a $3a_0$ triangular lattice is shown in Figure 21, in which the numbers 1, 2, 3, and 4 designate the four steps of substitution of the low-enrichment fuel. Figure 22 shows the pattern in which the elements of lower enrichment were placed within the $2a_0$ core. The entire loading pattern was divided into rows of seven rod groups, and single pins from alternate groups were removed in steps, shown as 1, 2, 3, and 4 in the portion of the core depicted. The steps correspond to exchange of approximately 7% of the fuel each time.

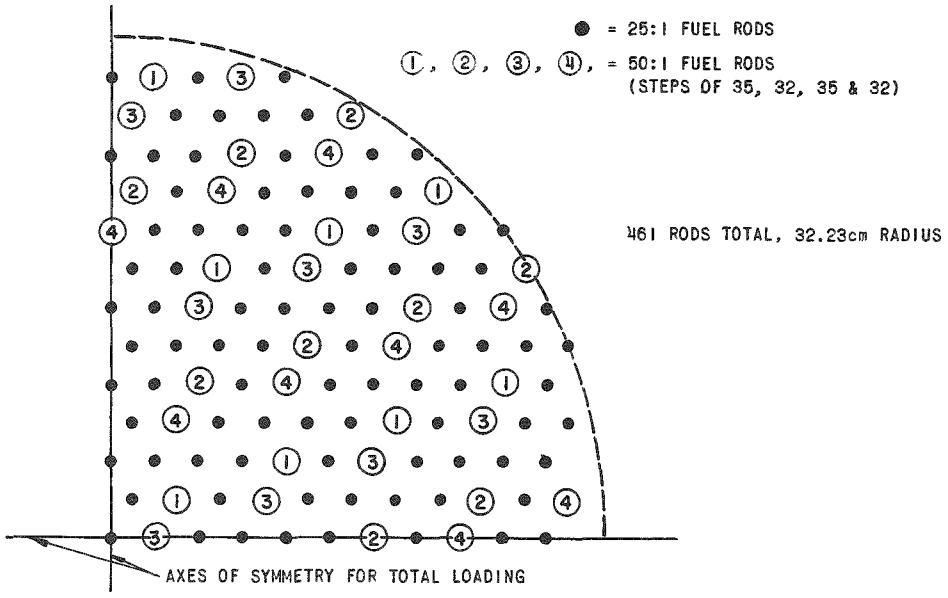

Fig. 21. Pattern of Fuel Substitutions Steps in the Uranium $3a_0$ Lattice.

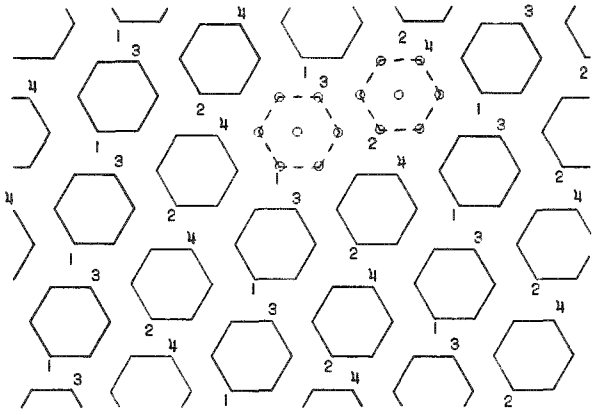

Fig. 22

Steps for Fuel Exchange in the Uniform $2a_0$ Core

For the uniform lattice with $4a_0$ pitch, the presence of control rod guide channels at the corners of the central region would have complicated the construction of clean lattices of radius larger than that of loading No. 120. Consequently, the sequence of fuel-substitution experiments recorded in Table XXIV involved only a maximum substitution of 11.4% low-enrichment rods. Because of the small number of rods present, the exact pattern of rod substitution is more important here than for the preceding experiments on systems of $2a_0$ and $3a_0$ spacing. The actual loading pattern and the order in which rods were interchanged is depicted in Figure 23. The average radial locations of the increments of fuel substituted in these measurements are as follows:

Loading Change	Number of Rods	R (cm)
125 → 124	10	23.0
124 → 123	7	29.5
123 → 122	9	23.5
122 → 121	8	24.9

The effectiveness of a fuel rod is not strongly dependent upon position in this core, since the effect of the D_2O reflector is to produce pronounced flattening of the flux in the core.

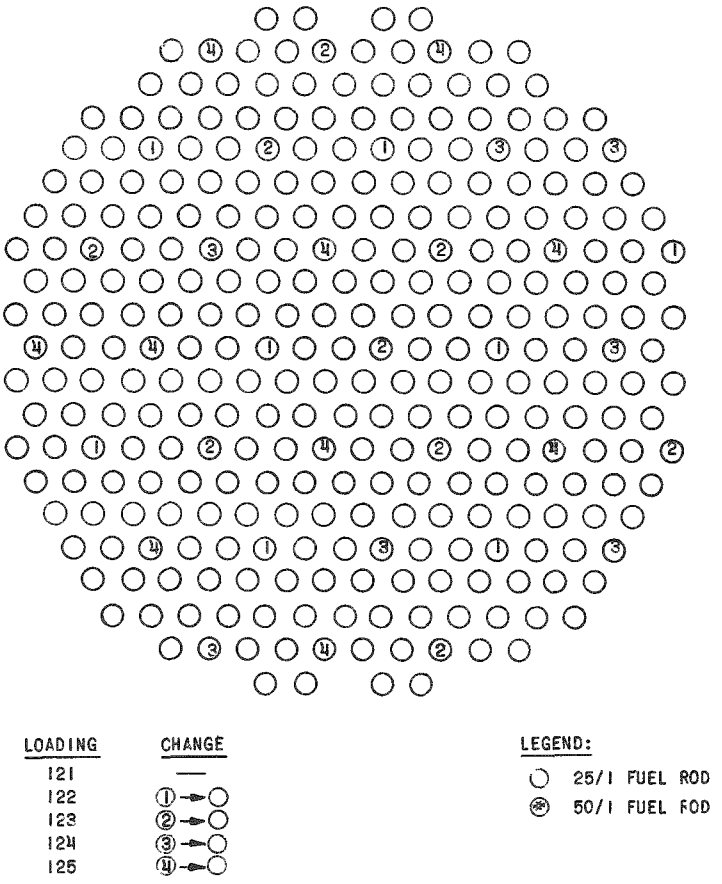

Fig. 23. Distribution of Low Enrichment Rods in the $4a_0$ Lattice Core

Structural details of the two different core geometries which approximated a $6a_0$ triangular spacing have been given previously in the chapter on clean criticals. Fuel-substitution experiments were performed with each. These were routine for the second core structure, that having a precise $6a_0$ pitch. For the initial assembly of 5.89-cm (6^+a_0) pitch, the sequence of substitution steps included assemblies having a top reflector.

The core composed of clusters of nine fuel elements having a pitch which yielded the same moderator-to-fuel volume ratio as a uniform $2a_0$ lattice was used as a starting point for a fuel-substitution experiment. In this sequence of fuel substitution a total of 28% of the original fuel was replaced by the rods of lower enrichment.

D. Cadmium Ratio of Thorium

The cadmium ratio for the thorium in the fuel rods was measured for a variety of core configurations, as a means to establish the resonance escape probability. Scintillation-counting techniques were used to determine the relative activation of bare and cadmium-covered thorium foils irradiated in fuel rods.

1. Relation to Resonance Escape Probability

The method used for the determination of the resonance escape probability by foil activation techniques is similar to that developed for use in critical assemblies containing U^{238} as the fertile material.[14,15] Modifications were required in the counting techniques because of the use of thorium, and in the interpretation of the observed cadmium ratios because of appreciable neutron leakage from the small, heavy water critical assemblies.

The relation between the measured cadmium ratio and the resonance escape probability is easily visualized on the basis of the usual representation of the neutron life history in a thermal reactor. For each thermal neutron absorbed, $\eta f \epsilon$ fast neutrons are produced. Through scattering, these neutrons are degraded in energy toward the resonance region. A fraction $(1 - L_0)$ escapes, so that $\eta f \epsilon L_0$ neutrons actually reach the resonance energy range. While traversing the resonance range, the fraction $(1 - L_1)$ escapes, so that the quantity $\eta f \epsilon L_0 L_1 (1 - p)$ are absorbed in the resonance range and the quantity $\eta f \epsilon L_0 L_1 p$ are degraded toward thermal energy. A fraction $(1 - L_2)$ of those leak and so only the quantity $\eta f \epsilon L_0 L_1 p L_2$ reach thermal. Once again a fraction $(1 - L_3)$ leak from the reactor, and of the remainder a fraction f are absorbed in the fuel. Of the $\eta f \epsilon L_0 L_1 L_2 L_3 p f$ neutrons absorbed in the fuel, only the fraction

$$F = \frac{\sum_a^{Th}}{\sum_a^{Th} + \sum_a^{U^{235}}}$$

are absorbed in the thorium.

In this terminology, the ratio of the resonance to thermal energy capture by thorium is

$$\frac{\eta f \epsilon L_0 L_1 (1 - p)}{\eta f \epsilon L_0 L_1 L_2 L_3 p f F} = \frac{1 - p}{L_2 L_3 p f F} \quad .$$

Experimentally,

$$\frac{\text{thorium resonance captures}}{\text{thorium thermal captures}} = \frac{\text{cadmium-covered Th foil activity}}{\text{bare Th foil activity - cadmium-covered Th foil activity}} = \frac{1}{CdR - 1}$$

in terms of the cadmium ratio, CdR. Therefore, the measured cadmium ratio is related to p by

$$\frac{1}{CdR - 1} = \frac{1 - p}{L_2 L_3 p f F} \quad .$$

Rearrangement gives

$$p = \frac{1}{1 + fFL_2L_3\left(\frac{1}{CdR - 1}\right)} \quad .$$

Substitution of age-diffusion theory formulation of the nonleakage probabilities and replacement of fF by the thermal utilization for thorium,

$$f^{Th} = \left(\frac{\sum_a^{Th}}{\sum_a^{total}}\right)_{thermal} \quad ,$$

puts this relation in the form

$$p = \left[1 + \frac{f^{Th}}{CdR - 1} \cdot \frac{e^{-B^2\tau_R}}{1 + L^2B^2}\right]^{-1} \quad .$$

Here τ_R is the neutron age from the lowest thorium resonance at 22 ev to thermal energy. Obviously, the values derived for p are dependent upon a knowledge of several other parameters, and so only the observed cadmium ratios are reported in this section.

2. Determination of Th^{233} Activity

Neutron capture by thorium results in the following decay chain:

$$Th^{232}(n, \gamma)Th^{233} \xrightarrow[22.4m]{\beta,\gamma} Pa^{233} \xrightarrow[27d]{\beta,\gamma} U^{233} \xrightarrow[1.6 \times 10^5\ y]{\alpha}$$

The thermal capture cross section is approximately 7.5 b, so detection of the Th^{233} decay is the only practical way to detect the capture reaction for irradiations made in a zero-power reactor.

Th^{232} is naturally radioactive and is, in general, in equilibrium with the members of its decay chain. By scintillation counting of a thorium foil, it was found that the gamma spectrum of the natural radioactivity had two distinct peaks, one at the characteristic x-ray energy of 89.5 kev and the other at 235 kev. The time dependence of the gamma radiation from irradiated thorium foils was studied with a continuous scanning device. It was found that the general gamma activity was increased considerably over the natural background activity, and that the X-ray peak at 89.5 kev had also increased. The peak at 235 kev could no longer be distinguished. Both the peak at 89.5 kev and the general activity decreased with time after irradiation until the same activity level existing before activation was reached.

The intensity of the 89.5-kev peak, plotted as a function of time after irradiation in Figure 24, shows the decay patterns characteristics of a short-lived radioactive substance mixed with a very long-lived substance. The decay curve was asymptotic with the residual activity level after approximately 3 hr. Subtraction of the residual activity from each point yielded a half-life of 22.5 min, in agreement with the reported value for the half-life of Th^{233}. Depending upon the activation level, this decay was clearly discernible for from three to seven half-lives. Since this was satisfactory for the proposed measurements, no attempt was made to improve upon this technique for the detection of neutron capture by thorium.

3. Measurements

Thorium metal foils, 0.584 cm in diameter and 0.025 mm thick, were used. The foils were encased in aluminum foil for protection ranging from 0.01 to 0.03 mm, for protection against recoiling fission fragments. These showed no measurable penetration by fragments from the fuel. The foils were positioned between two fuel pellets, at the estimated position of maximum axial flux, and assembled in a standard 1.5-m column of fuel pellets contained in a void tube, as shown in Figure 25. A void tube was used instead of the standard fuel tube in order to provide the necessary clearance for a cadmium covering.

The cadmium cover was made from stock sheeting. A tube was made by rolling a flat piece so that there would be approximately 0.8-mm overlap at the seam. Cadmium discs, 0.584 cm in diameter, were placed in the tube but separated from the thorium foils by a single fuel pellet, to prevent streaming of the resonance neutrons.[16]

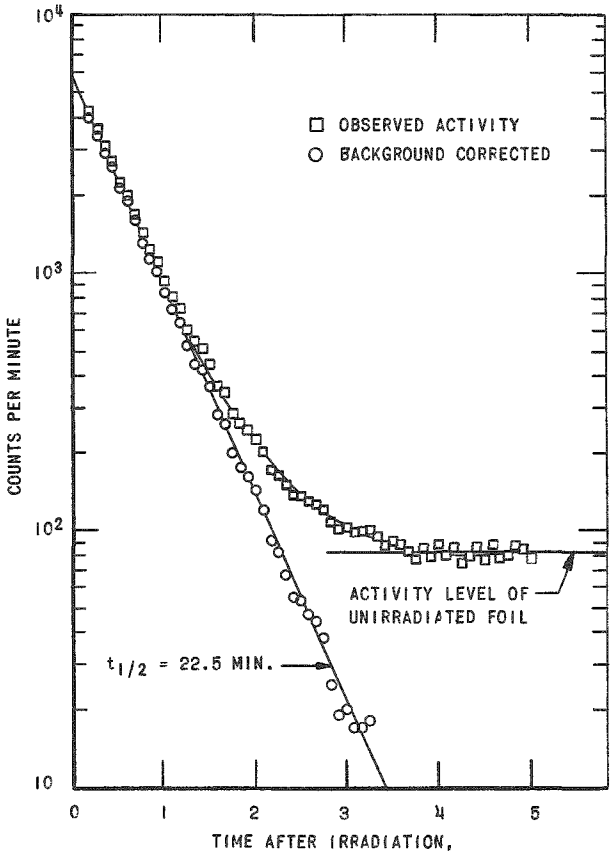

Fig. 24

Half-life Determination for 90 kev X-Rays from Neutron-Irradiated Thorium.

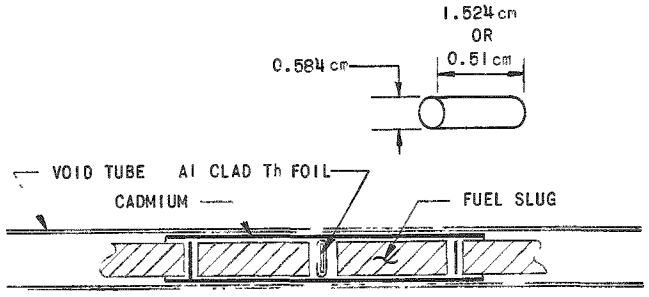

NOTE: NOT TO SCALE; CLEARANCES ENLARGED FOR CLARITY

Fig. 25

Arrangement for Measurement of the Cadmium Ratio of Thorium Foils.

Irradiation of bare foils was accomplished by using the same type of aluminum cladding but eliminating the cadmium cover. In this case, the foil and its adjacent pellets were held in axial alignment by cellulose tape around the pellets.

For the measurements of the thorium-cadmium ratio with 25/1 fuel, 0.028-cm cadmium covers and 1.524-cm fuel separators were used. With 15/1 fuel, 0.051-cm cadmium covers and 0.51-cm fuel separators were used. This difference in fuel separator size should not influence the observed ratios.[16] However, the 1/v correction to be made to the values of p computed from the observed cadmium ratios does depend on the cadmium thickness.

Gamma radiation from the activated foils was detected with a NaI crystal, 5 cm in diameter and 5 cm thick, attached to a 5-cm photomultiplier tube. The foil was positioned by positive mechanical stops at a distance of 2.9 cm from the crystal face and concentric with the crystal axis within 0.8 mm. The method of mounting of the foil allowed an axial uncertainty of no more than 0.1 mm. Thus the counting geometry was quite reproducible throughout the measurements. The discriminator was set so that a 40-kev window was centered on the 90-kev activity peak. Preliminary studies showed that the window width could be varied over rather wide limits (up to 140 kev) without appreciably affecting the signal-to-noise ratio or the background-corrected half-life.

The power level and length of irradiation were adjusted to yield a minimum activity level of 5,000 cpm for the bare foil at the end of the activation. The activity of the foils was followed for a minimum of three half-lives and the background correction was derived from an unactivated foil. The capture rates were determined directly from the measured activity of the Th^{233} produced. Since the foils were pure metallic thorium, their weight ratios were used to determine the relative number of thorium atoms per foil.

The resulting cadmium ratios are given in Table XXV. With the exception of three values obtained in EBWR geometry and one in the uniform grid pattern, the results are based on measurements for a single pair of foils. The error limits indicated for these four values are average deviations calculated from the number of separate measurements indicated in parentheses.

E. Measurement of Disadvantage Factors

Interpretation of the observed criticals in terms of the usual parameters requires a knowledge of the local variation of the neutron flux. Although this can be calculated, there exists an uncertainty in regard to the acceptable degree of approximation to transport theory. Consequently, measurements were made in a variety of THUD criticals to provide a basis for comparison with the values calculated by several approximations.

1. Experimental Details

It was assumed (and later verified) that any local variations in the epithermal flux would be of negligible proportions, and so it was sought to establish in the experimental measurements the ratio of the average thermal fluxes in the moderator and fuel. The activation of suitable materials in the form of wires and foils, positioned to sample the flux in these two regions, provided the means to determine this quantity, termed the disadvantage factor for the fuel.

Table XXV

CADMIUM RATIOS FOR THORIUM FOILS WITHIN FUEL RODS

EBWR Geometry (25/1 Fuel)

Pattern of 28 Rods	Position in Cluster	CdR
$2a_0$ uniform	center	$2.111 \pm 0.059^{(10)}$
$2a_0$ uniform	edge	$3.002 \pm 0.030^{(3)}$
a_0 clusters	center	$2.200 \pm 0.117^{(3)}$
a_0 clusters	edge	1.885

Uniform Grid

Pitch	CdR, 25/1 Fuel	CdR, 15/1 Fuel
$2a_0$	1.717	1.486
$3a_0$	2.835	2.239
$4a_0$	4.09	3.127
$6a_0$	$5.47 \pm 0.69^{(2)}$	5.471
$2\sqrt{3}\,a_0$*	2.07	

Clustered Geometry (15/1 Fuel, 13.0-cm sq Pitch, Voided Clusters)

Number of Fuel Rods	Position in Cluster	CdR
19	1st ring	2.729
19	2nd ring (edge)	2.761
31	center	1.842
31	2nd ring	1.964
31	3rd ring (edge)	1.981

*3 rod clusters

a. Techniques of Flux Measurement

Because of the rapid variation of flux with position and the relatively small dimensions of many of the lattice cells, activation methods were used exclusively for the determination of the average neutron fluxes

in the moderator and fuel. Both integral measurements and the integration of the spatial variation of flux was used for the fuel and moderator regions, and a variety of neutron-detection materials were used.

The average flux within the fuel region of a representative core cell was usually determined by irradiation of foils placed between fuel pellets. These foils matched the diameter of the pellets and were wrapped for the total flux measurements in 0.025-mm aluminum to prevent their contamination by fission products. When the nature of the foil material required a determination of the epithermal portion of the induced activity, the foils were encased in 0.28-mm-thick cadmium. Pellet separations of approximately 0.13 and 0.76 mm, respectively, existed with the aluminum and cadmium-covered foils. In order to provide the additional clearance needed for the covers, the fuel pellets were contained in a void tube during such irradiations.

In a few cases, single sheets of foil material were cut to coincide with the exact cell outline. A fuel rod was severed, the foil centered between the two parts, and the severed portions butted together to hold the foil in place during the irradiation. The portion of the foil coinciding with the fuel pellets was punched out, in order to separate the activity produced by the flux in the fuel region. More often though, the foil in the fuel region was inserted in the rod and the foil in the moderator region was located as a collar around the rod in the same plane. For fuel clusters, foils were placed in several rods.

The use of a single foil as a detector for the moderator flux was convenient for the lattices of small pitch, but the more common procedure in these measurements of the disadvantage factor involved the activation of very small amounts of the detector material positioned on radii extending from the center of the cell to the corner and the flat portion of the cell boundary. Wires, strips of foil material, and small foils attached to strips of aluminum were used at various times. With few exceptions, use was made of the symmetry of the core to accomplish all irradiations of bare and cadmium-covered detector foils simultaneously.

b. Foil Materials

Gold, uranium, manganese, copper, and dysprosium were used successively for the determination of the relative thermal neutron fluxes in the moderator and fuel. The majority of values to be reported for the disadvantage factor is based on differential flux measurements with dysprosium. However, some details on the difficulties encountered in the use of these other detectors are recounted here to provide a basis for assessing the magnitude of the error associated with the earlier measurements. Factors which contributed to the eventual selection of dysprosium as the most suitable detector are revealed in the discussion which follows.

Gold foils and wire were used in the first measurements because of their availability in uniform dimensions and their high chemical and isotopic purity. The induced activity was convenient for β and γ counting, and also for autoradiography. However, certain edge effects with gold foil proved to be objectionable. These were attributed to the large resonance absorption and to the density of gold, which led to higher activation at the boundaries of foil than elsewhere. A second objection was the local depression of epicadmium activation of gold by resonance absorption in the fuel pins. The following tabulation gives those resonance levels in thorium and uranium which approximate those in gold.

Element	Resonance Energy E_R, ev	$\sigma_t(E_R)$, b	Remarks
Au	4.9	30,000	Principal Resonance
	60.	570	
U^{235}	4.9	200	
	6.4	500	
	7.2	250	
U^{234}	5.2	16,000	
Th^{232}	60.	150	

These data show the probability that the resonance activation was shadowed by nearby resonance absorption in U^{235}, U^{234}, and Th^{232}. Thus, the epicadmium activity of the gold foil would be influenced by its location relative to the fuel pellets.

A few measurements were made with U^{235}, in the form of foils of the metal, foils of an alloy with aluminum, and fuel pellets. The use of metallic uranium detectors was complicated by surface oxidation, by natural radioactivity, by long-lived fission products which prevented frequent re-use of the foils, by variable half-life, and by complicated spectra. The alloy eliminated the oxidation and attendant contamination problem but introduced the possibility of variations in U^{235} content. Direct fission product counting of irradiated fuel pellets was also tried, although the pellets increased the background count rate unduly because of the mass of material involved.

Manganese-iron wire and foil were used for a brief period as convenient substitutes for bare U^{235} foils. Although the resonance integral of manganese is different from that of U^{235}, a close similarity in bare-foil flux patterns resulted. The manganese data were better in regard to reproducibility and scatter than those obtained with U^{235}.

Copper foil and wire were also used, because of their availability and purity. Resonance absorption and epicadmium flux depressions were not apparent, but the copper required irradiation at a rather high power level, which generally resulted in some degree of compromise in the foil activity obtained. Counting of copper activation by beta-detection equipment was not as reliable as with gold and manganese. The annihilation gamma radiation resulting from positron interactions may have complicated both beta and gamma counting of copper.

In an investigation of the epithermal flux within a lattice cell, it was found that the activation of cadmium-covered foils was inversely related to the amount of cadmium in the vicinity. This was attributed to a reduction in the fission rate in the nearby fuel, due to the absorption of thermal neutrons by the cadmium. Subsequently, the correction for epicadmium activation was based on measurements with a single, small, cadmium-covered foil in the fuel, until the adoption of dysprosium as the flux detector.

Dysprosium was known to have a very high cadmium ratio for activation. Consequently, to bypass the problem of flux depression by cadmium and also to reduce the number of measurements required for a disadvantage factor determination, some tests were made to determine the feasibility of utilizing a dysprosium-aluminum alloy as a thermal neutron detector. A dysprosium-aluminum alloy containing about 3.7 wt-% dysprosium was acquired from the American Electrometals Division of Firth-Stirling, Inc., in sheets 0.23 mm thick.

Dysprosium had been reported to be essentially a $1/v$ absorber. The isotope Dy^{164} (28.2% abundant) has a thermal activation cross section of about 2600 b for formation of an isomeric state of Dy^{165} (1.3-min half-life) and of about 1000 b for formation of the ground state of Dy^{165}. The isotope Dy^{165} beta decays to Ho^{165} with a half-life of 2.32 hr. Irradiation of a sample of the alloy in CP-5 yielded a half-life in excellent agreement with the reported value. This test also revealed that, after giving the 1.3-min isomeric state a few minutes to decay, there is no observable effect of impurity activation to influence measurements made with an ordinary beta counter for at least 8 hr after irradiation (test ended at 8 hr).

A second measurement was made in which both copper and dysprosium foils were irradiated in aluminum and cadmium covers. Utilizing these data and the known resonance integral of copper, a value of about 100 b was obtained for the resonance integral of Dy^{164}. No correction was made for the effect of self-shielding. More recently, a value of 420 ± 50 b has been observed[17] for the epithermal activation integral of Dy^{164}. If Dy^{164} were a $1/v$ absorber, it would have a resonance integral of about 1300 b.

Consequently, the activation cross section of Dy^{164} is less than $1/v$ above the cadmium cutoff, and possibly so in the thermal region as well.

In order to test the uniformity of the dysprosium distribution in the alloy, four 9 x 15-cm sheets were inserted as nearly as possible in the center of the ZPR-VII core and irradiated. Autoradiographs were then made of each sheet. Density traces of these autoradiographs made with a recording microphotometer revealed that the variation in the distribution of the dysprosium was, at most, 4% in any one sheet. They also showed that there were no sharp discontinuities in the distribution. Foils of 1.27-cm diameter were punched from the corners of each of the four sheets previously irradiated. Using a rotating wheel to assure the same flux for each foil, these were irradiated in a neutron beam. Beta counting of these foils revealed a variation of dysprosium density of from 2% to 5% in each sheet, and as much as 9% from one sheet to another. For this reason, such an intercalibration was made for all foils used in the disadvantage factor measurements.

The errors inherent in intercalibration partially offset the advantage of the low epicadmium activation. The $3.7 \pm 0.3\%$ dysprosium-aluminum alloy was otherwise highly satisfactory, being readily activated and β counted, and so it was used henceforth.

c. Detection of Foil Activity

The activity produced in the detector materials was determined mainly by beta counting with scintillation detectors. To avoid complicated geometrical corrections, ribbons, wires, and the larger foils used in integral-type determinations were cut into small segments prior to counting. The activity patterns in a few of the latter were determined by an autoradiographic method. Gamma-scintillation counting was used primarily for the detection of fission product activity.

Pilot "B" plastic scintillator sealed to photomultiplier tubes gave good counting efficiency without undue difficulty because of background counts, shielding, and counting geometry. Gamma-activity counting was less susceptible to errors arising from foil-surface activation such as the gold resonance produces, surface blemishes resulting from oxidation of uranium and manganese foils, and irregular shape as with fuel pellets. However, the gamma-activity measurements were more sensitive to environmental conditions than the beta determinations. These conditions resulted in drifts in detector sensitivity and in fluctuating backgrounds, partly from capture gamma radiation due to neutrons produced during reactor operation, penetration of the detector shields by radiation from the foils stored in the sample changer, and electrical noise. Beta and gamma counting were done by scintillation counters adjusted for low

discrimination, except for the U^{235} foils. These were gamma counted with approximately 1-Mev discrimination to reduce the background counting rate due to natural radioactivity. The manganese, copper, and dysprosium activities were not counted with satisfactory efficiency by gamma detectors.

Standard decay corrections were applied to copper, gold, dysprosium, and manganese. The U^{235} fission activities were plotted and time corrected graphically. Time corrections were minimized by repeatedly counting related traverses in sequence, then decay correcting each traverse to approximately the time when half the set had been counted. Counter dead-time corrections were negligible for the count rates utilized. Activities for the differential type of measurements were corrected for foil weight except for the dysprosium-aluminum foils, for which intercalibration data based on activation were used.

For one of the first measurements using foils which covered the entire cell area, the irradiated materials were placed on a photographic plate to determine the relative flux distributions. The autoradiographs of irradiated gold and manganese foil were scanned by a recording microdensitometer* to obtain detailed flux shapes for this purpose. The chart records for three or four evenly spaced diametrical traverses were smoothed to eliminate irregularities due to recorder band spread, emulsion defects, and edge effects.

Exposure of Kodak type M plates by irradiated foils produced reasonably linear curves of opacity versus exposure. The variations appeared random, but their magnitude made statistical averaging a necessity. A check of the linearity was made with each plate scanned. The opacities were compared with beta-counter data for the entire foil, and also with punched-out segments. In the case of gold foil, two or more images of each piece were obtained, differing in time and extent of exposures.

Numerous errors may arise in autoradiography. However, the statistical averaging produced well-defined flux shapes which could not be obtained otherwise. Errors were minimized by standardized developing and reading of the images. The easily comparable results, such as cadmium ratios, were equivalent to those obtained by beta counting. No further use was made of this method, because of limits set by irregularities in the emulsion and the range of activity detectible.

2. Results for Uniform Lattices of Single Fuel Rods

In the treatment of the data obtained from foils activated in lattices of single fuel rods, the disadvantage factor was taken as the ratio of the average thermal neutron flux in the D_2O moderator to that in the fuel rod. The flux in the aluminum cladding of the rod was ignored. The results are assembled in Table XXVI. The method used for the determination is also given. When more than one measurement was made, the separate values are recorded.

*Leeds and Northrup Scanning Microdensitometer Cat. No. 6700 P-1, Ser. No. 677877, plus a millivolt recorder.

Table XXVI

EXPERIMENTAL DISADVANTAGE FACTORS FOR SINGLE ROD LATTICES

	50/1 Fuel		25/1 Fuel		15/1 Fuel	
Δ Pitch	Value	Method	Value	Method	Value	Method
$2a_0$			1.10	Au and Mn, photo.	1.23	Dy, integral
$3a_0$			1.17	Cu, integral	1.32	Dy, integral
			1.18	Cu, integral		
			1.27	Cu, integral		
$4a_0$					1.31	Dy, diff.
$6a_0$	1.14	Dy, diff.	1.28	Dy, diff.	1.36	Dy, diff.
	1.12	Dy, diff.	1.24	Dy, diff.		
	1.12	U^{235}, CdR	1.24	U^{235}, CdR		

No correction was made for epithermal activation of the dysprosium foils. In the treatment of the data for copper and U^{235}, the cadmium ratio for the foil material inside the fuel rod was used to correct both the fuel and moderator data for the epithermal component of the activation. This involves the assumption that there is no depression of the epithermal flux by the fuel. In the autoradiographic technique with gold and manganese foils, both the bare and cadmium-covered activities were observed throughout the unit lattice cell, and the variation of the epithermal flux within a single lattice cell was found to be slight.

The observed differential flux distributions were weighted by the radial location with respect to the unit cell, to allow for the variation in differential area. For the integral foil method, the sum of the activities of the segmented parts of the copper foils was used, but the dysprosium foils in the $2a_0$ and $3a_0$ lattices of 15/1 fuel were counted without cutting. In these cases, it was necessary to apply a geometry correction due to the relation between detector crystal and foil sizes. The correction was based on the whole and segmented activities of a foil that was uniformly irradiated, rather than that of the actual case in which a variation of flux was present throughout the foil. Correction factors in the two cases amounted to 1.04 and 1.48, respectively. This is believed to be the reason for the slight inconsistency between the values for the $3a_0$ and $4a_0$ lattices of 15/1 fuel.

The values reported for the 50/1 fuel were actually obtained from irradiations in loading No. 184, a mixed lattice of 190 50/1 fuel rods and 742 25/1 rods. Details of the geometrical arrangement and the

observed dysprosium foil activities in these determinations are presented in Figure 26. In the cadmium-ratio method for the $6a_0$ lattices, only a single foil, at the position of maximum cell flux, was irradiated in the moderator. However, the relatively flat flux distribution, except in the immediate vicinity of the fuel rod, makes small the error introduced by not using a weighted flux distribution for the values reported. Here the cadmium ratios for 0.025-mm U^{235} foils were 58 in the moderator, 52 in the 25/1 fuel, and 47 in the 50/1 fuel. Definition of the disadvantage factor as $(CdR)_M - 1/(CdR)_F - 1$ implies no epithermal flux depression within the fuel rod.

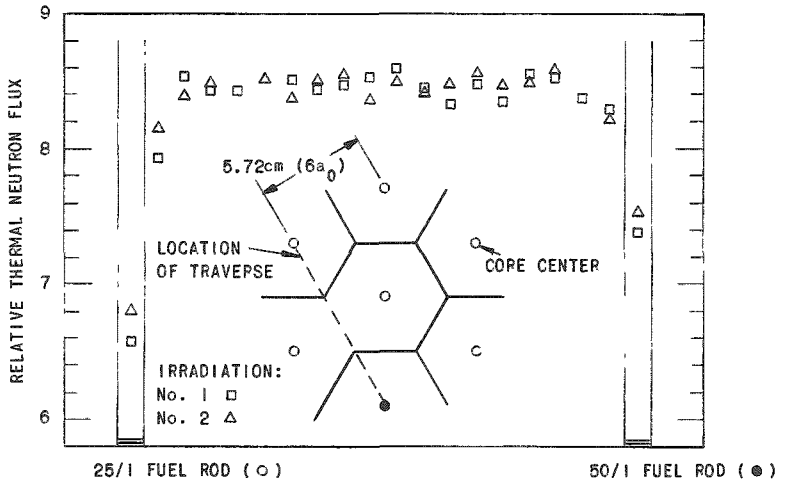

Fig. 26. Neutron Flux Distribution in $6a_0$ Lattice of Fuel Rods with Two Enrichments

The measurements by the photographic or autoradiographic technique were actually performed in the EBWR geometry, rather than in uniform geometry. However, the two probably are similar within experimental error limits, since the foils were placed near the center of a cluster which contained a total of 27 other fuel rods with the $2a_0$ triangular pitch. Typical results of the microdensitometer readings are shown in Figure 27. Foils were irradiated in equivalent flux locations, one bare and one cadmium-covered foil per run. The lower image pair were exposed for 4 hr, and the intermediate pair for the following $17\frac{1}{2}$ hr, by the same bare and cadmium-covered foils. The lower pair is not useful because of difficulty in determining a true zero point, and the highest exposure bare image is overexposed. Kodak Type M photographic plates were used.

The left-hand edge of the trace obtained for the overexposed image shows a peak typical of the border effect (Mackie lines). This is inherent in development of dark images, but is limited to a very narrow region. These so-called "adjacency effects" are reported to seldom exceed a few percent for ordinary photographic images.[18] Absence of a similar peak at the right-hand edge is due to recorder lag.

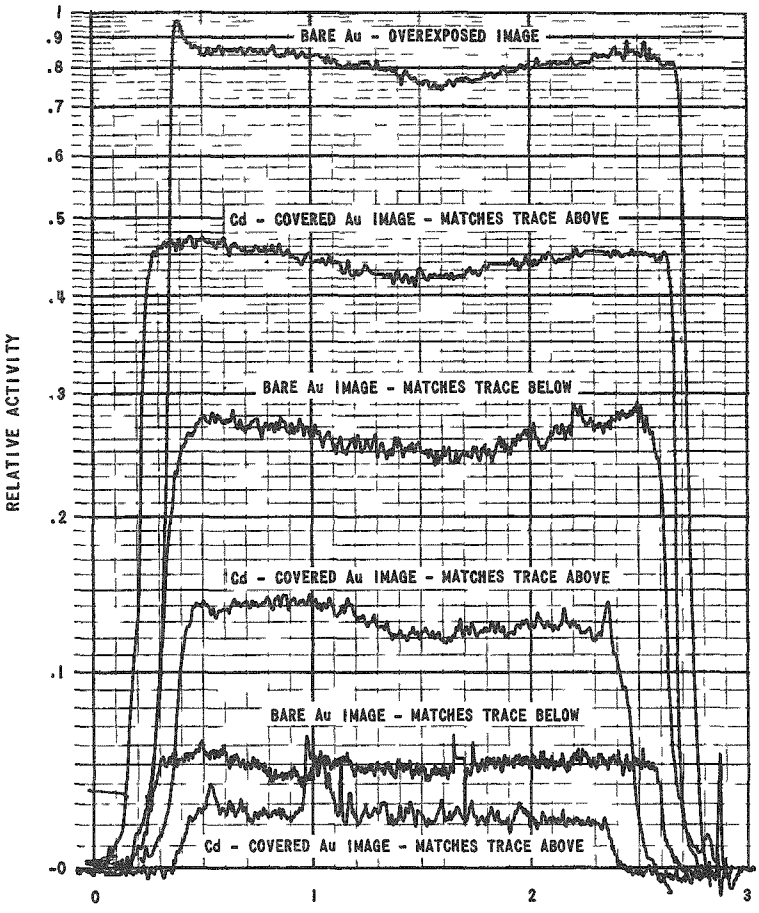

Fig. 27. Typical Results of Autoradiographic Measurements on Activated Foils

3. Results for Clustered Lattices

Disadvantage factor measurements were made for the single clustered assembly in EBWR geometry, four clustered patterns in the uniform grid, and nine arrangements in the practical clustered geometry. The results, method, and loading number are given in Table XXVII. The loadings are described in more detail in the chapter on clean criticals, but for convenience the major characteristics of these loadings are included here also. The single measurement in a cluster containing H_2O was made in a loading not described previously. It consisted of a 3 x 3 array of H_2O-filled clusters surrounded by 39 D_2O-filled clusters having the same pitch, fuel, and rods per cluster. The foils were placed in and around the central H_2O-filled cluster.

Table XXVII

EXPERIMENTAL DISADVANTAGE FACTORS FOR CLUSTERED LATTICES

Description					Value	Method
EBWR Clustered (Loading No. 82, 25/1 Fuel)					1.55	U^{235}, diff.
Uniform Clustered (25/1 Fuel)						
Loading No.	△ Pitch	Rods/cluster				
163	$2\sqrt{3}a_0$	3			1.19	Cu, Integral
167	$6a_0$	9			1.32	Cu, Integral
177	$6\sqrt{3}a_0$	27			1.66	Cu, diff.
234	$15a_0$	37			1.97, 1.99	Dy, diff.
Practical Clustered						
Loading No.	□Pitch	Rods/cluster	Fuel	Cluster Contents		
322	10.8 cm	19	25/1	D_2O	1.68, 1.71	Dy, diff.
334	10.8 cm	31	25/1	D_2O	1.77	Dy, diff.
-	10.8 cm	31	25/1	H_2O	2.06	Dy, diff.
439	13.0 cm	19	15/1	D_2O	2.51	Dy, diff.
436	13.0 cm	19	15/1	Void	2.32	Dy, diff.
313	13.0 cm	19	25/1	Void	1.70	Dy, diff.
308	13.0 cm	25	25/1	D_2O	1.69	Dy, diff.
425	13.0 cm	31	15/1	D_2O	2.34	Dy, diff.
419	13.0 cm	31	15/1	Void	2.44	Dy, diff.

Sufficient foils were placed within the fuel rods forming the cluster to establish the variation of flux with position, except for the single measurement in EBWR geometry. There a single foil was placed in the central rod and the variation was determined from foils placed in the moderator within the cluster of fuel rods. For the dysprosium and U^{235} measurements, foils were placed along radii extending to the flat portions and corners of the unit cells. In the copper activations, single large foils were used to cover a symmetric portion of the entire cell. These large copper foils also extended into the fuel zone for the clusters of 3 and 9 rods.

The average relative thermal neutron flux in the fuel was determined by assigning a measured or interpolated flux value to each fuel pin, adding contributions from individual pins, and dividing by the total number of fuel pins. All segments of the copper foil used in the clusters of three and nine rods were counted to determine the average

moderator flux. The copper foil used for the 27-rod cluster was cut to yield two radial distributions, just as was obtained for all of the differential measurements. To compute the average relative thermal neutron flux in the moderator region, a representative area was assigned to each moderator foil, the product of this area, and the corrected flux for each foil determined, and the sum of all such products divided by the total moderator area.

Except for the two measurements involving integral foil activation and counting, an assumption must be made for the ratio of fluxes in the moderator and fuel portions of the cluster. For the $1a_0$ triangular pitch which existed for the fuel rods within all of the clusters, the D_2O occupies 38% of the fuel rod cell volume. Since the volume of the fuel cluster is small compared with that of its cell, the D_2O contained within the immediate vicinity of the fuel rods is a very small fraction of the total moderator. Thus any error in the ratio assigned for the cluster moderator relative to the fuel will be of minor consequence, except for the EBWR-type cluster in which only a single measurement of the fuel flux was made. Based on an extrapolation of the results obtained for lattices of single fuel rods, fuel cluster disadvantage factors of 1.07 and 1.10 have been assumed for the treatment of the data for clusters of 25/1 and 15/1 fuel, respectively. The value reported for the single EBWR cluster is based on the 1.07 value. Use of the value 1.32 obtained from the single measurement in a rod within the EBWR cluster would yield a disadvantage factor of 1.98, instead of the 1.55 reported.

For all of the clusters of 25/1 fuel, the D_2O contained within the fuel zone was considered as moderator in the calculation of disadvantage factor. The aluminum cladding and that contained in the cluster tubes were ignored in all of the calculations for 25/1 fuel, as was the H_2O in the one clustered lattice of this type measured. A slightly different treatment of the observed flux pattern was made for the clusters of 15/1 fuel. The disadvantage factor was taken as the ratio of the average relative neutron flux in the moderator region outside the equivalent area of the cluster to the average relative neutron flux within the equivalent area of the cluster. Within the cluster, it was assumed that $\phi_{fuel} = \phi_{void} = 1.00$, $\phi_{Al\ clad} = 1.05$, and $\phi_{D_2O} = 1.10$.

The effect of epithermal activation was ignored for the dysprosium data. For the copper and U^{235} data, it was assumed that no epithermal flux depression existed, and so the cadmium ratio observed for foils placed in the fuel rods were used to separate the epithermal component.

A representative set of observations of the thermal flux distributions in shown in Figure 28. The patterns observed in the direction of the side and corner of the square cell of loading No. 308 are shown.

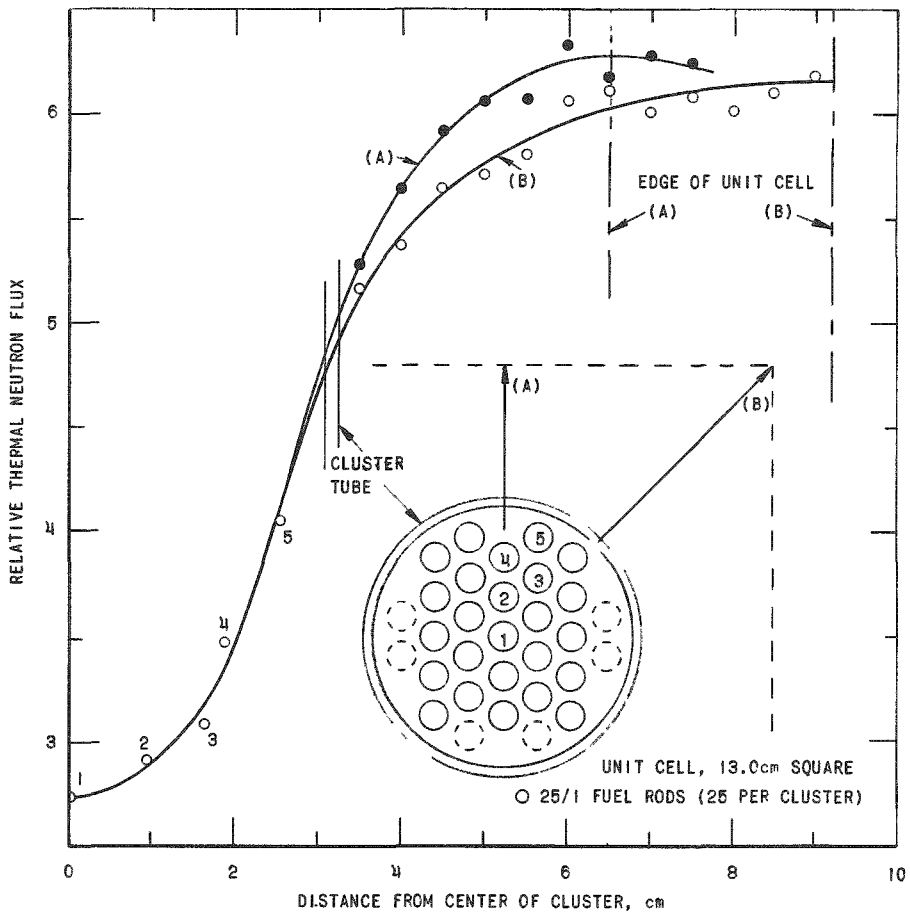

Fig. 28. Typical Flux Distributions in a Clustered Lattice Cell

F. Fast Fission Factor

Comparisons of the fast fission cross section and threshold energy for thorium and U^{238}, coupled with a knowledge of the magnitude of the fast effect for U^{238}-bearing systems similar in geometry to the THUD assemblies, led to the conclusion that $(\epsilon - 1)$ was approximately zero. This was verified experimentally, through measurements made in two lattice arrangements favorable for the occurrence of thorium fission.

The first measurement was performed in an assembly of 21 clusters of 25 fuel rods each, arranged in a square array of 13.0-cm pitch. The second determination was made in a cluster of 25 fuel rods surrounded by 31 clusters of 19 fuel rods with all of the clusters arranged in a 10.8-cm-sq pattern.

Samples of Th^{232} and U^{235} were irradiated in the central and outermost fuel rods of a central cluster, as indicated in Figure 29. The arrangement of the samples within the fuel rods and the size of the samples

are also shown in that figure. The larger mass of Th^{232} was necessary to preserve the 25/1 thorium to U^{235} atom ratio of the fuel rods. Each sample was wrapped in aluminum foil to prevent contamination by fission products from adjacent samples or from the fuel. The samples were irradiated for about an hour at a reactor power level of a few watts.

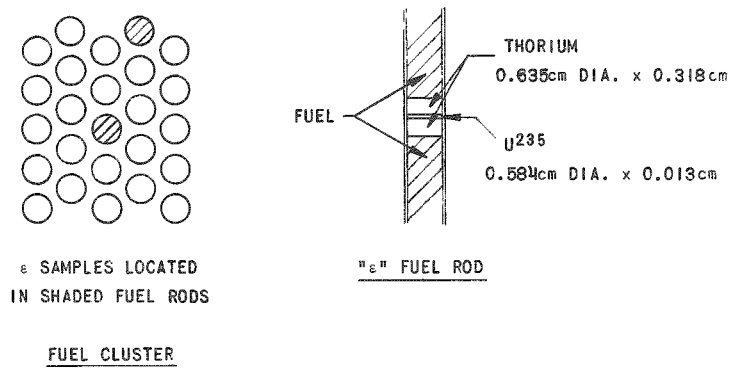

Fig. 29. Experimental Configuration in the Fast Fission Factor Determination

The number of fissions which occurred in each sample was determined by radiochemical analysis of the concentration of the fission product Mo^{99} ($t_{1/2}$ = 66.4 hr). The results are presented in Table XXVIII. The observed counting rates for the samples are given as a guide to the statistical uncertainties involved. The thorium values have been corrected for a background of approximately 13 cpm. Correction of these count rate data was made for decay time, chemical yield of the Mo^{99} extraction procedure, and the counter efficiency. Mo^{99} fission yields of 6.1% for U^{235} and of 2.9% for Th^{232} were used to obtain the tabulated values for the number of fission per gram.

Table XXVIII

RADIOCHEMICAL DETERMINATION OF

Loading Number	Location in Cluster	Material	Mo^{99} Counting Rate (cpm)	Fissions per Gram	Fast Fission Factor
307	Center	U^{235}	15,000	5.40×10^{11}	1.0066
		Th^{232}	89	2.28×10^{8}	
	Edge	U^{235}	23,000	7.52×10^{11}	1.0045
		Th^{232}	80	2.14×10^{8}	
322*	Center	U^{235}	20,000	9.42×10^{11}	1.0064
		Th^{232}	105	3.90×10^{8}	
	Edge	U^{235}	31,000	1.24×10^{12}	1.0063
		Th^{232}	136	5.06×10^{8}	

*Modified by the addition of six fuel rods to the cluster in which measurement was made.

Also included in Table XXVIII is an approximate value for the fast fission factor ϵ. Since ϵ is defined as the ratio of the number of fast neutrons produced by all fissions to those of thermal fission origin, consideration must be given for the THUD system to fast fission of Th^{232}, U^{238}, and U^{235}. Since each fission neutron makes a net contribution of

$$C = \left[\nu_f - \left(1 + \frac{\sigma_c}{\sigma_f}\right)\right]$$

to the fast neutron population, the fast fission factor may be written in terms of the fission rates of the various isotopes, F_i, as

$$\epsilon = \frac{\nu_{25}^{th} F_{25}^{th} + C_{02} F_{02} + C_{25} F_{25} + C_{28} F_{28}}{\nu_{25}^{th} F_{25}^{th}} .$$

Here all quantities except those having a superscript indicating thermal energy pertain to fast fission.

The quantities determined experimentally were F_{02} and $(F_{25}^{th} + F_{25})$. Values for F_{25} and F_{28} relative to F_{02} were obtainable from known fission cross sections and atom densities. In terms of such quantities the above expression for ϵ may be written as

$$\epsilon = 1 + \frac{N_{02}}{\nu_{25}^{th} N_{25}} \quad \frac{C_{02} + C_{25}\left(\frac{N_{25}\ \sigma_{f,25}}{N_{02}\ \sigma_{f,02}}\right) + C_{28}\left(\frac{N_{28}\ \sigma_{f,28}}{N_{02}\ \sigma_{f,02}}\right)}{\frac{235}{232} R - \frac{\sigma_{f,28}}{\sigma_{f,02}}}$$

Here N designates relative atom densities in the THUD fuel and R is the ratio of fission per gram for U^{235} to that for Th^{232}.

The values used to calculate ϵ are given in Table XXIX. The relatively small concentration of U^{238} in the THUD fuel makes its contribution to ϵ insignificant. The fast fission portion of the U^{235} fission rate amounts to less than $\frac{1}{2}$% of the observed amount, and hence is an unimportant correction in the denominator of the expression for ϵ. However, its large fast fission cross section compared with that for Th_{232} offsets in part its lower concentration. In addition, C_{25} is almost twice as large as C_{02}. The combined effect is that fast fission in U^{235} accounts for 40% of the value of $(\epsilon - 1)$.

The values obtained from the two measurements at the center of a cluster of 25 fuel pins are in good agreement. The cause of the discrepancy in the values for fuel pins at the edge of these clusters is unknown, but geometrical considerations favor the lower value. The magnitude of the measured values is consistent with that expected from theoretical considerations, and the lack of similar measurements for other THUD fuel geometries should not handicap the interpretation of the THUD critical experiments.

Table XXIX

PARAMETERS USED IN ϵ CALCULATIONS

Isotope	σ_f (b)	σ_c (b)	ν	ν^{th}	N
Th^{232}	0.135	0.06	2.35		24.65
U^{235}	1.25	0.07	2.7	2.43	1.00
U^{238}	0.532	0.05	2.8		0.058

V. REACTOR DESIGN INFORMATION

Initially, the THUD program of critical experiments was oriented toward providing design information for a proposed loading of the Experimental Boiling Water Reactor. Consequently, it was appropriate to investigate configurations of the THUD system which could be related to conditions existing in a practical reactor. In a boiling water reactor, there is a decrease in water density as the moderator is heated to its boiling point, and a further drastic reduction in density due to formation of steam in the core region. Although the water density varies with position, data on the reactivity effect of a uniform distribution of voids in a core loading representative of an EBWR type system provide a convenient check on the design calculations. Consequently, measurements were made with voids uniformly dispersed in unclustered cores having the EBWR geometry. In Section A, the results of these measurements are presented.

In addition, there was interest in establishing the effectiveness of control rods and how that would change with variation in water density. In Section B is reported a number of experiments with blade- and cross-type control rods in unclustered cores of the EBWR geometry. Also included in Section B is some information on the effectiveness of thorium sheet as a possible control material in clustered core arrangements.

A. EBWR Geometry Cores with Uniform Voids

The reactivity effect of a poison or void introduced into a core representative of the EBWR was determined through the measurement of control rod positions or water levels for clean and poisoned or voided cores. Differences could be translated into corresponding reactivity worths through the use of reactor parameters established in other measurements. Uncertainties in the determination of the actual core dimensions, deviations from uniform distribution of material, and uncontrollable drifts in the total reactivity constituted the principal sources of error. Advantages of the method are the simplicity of the preparations and ease of the measurements.

1. Procedure

Voids were introduced by interspersing thin-wall aluminum tubes, as described in Section II-B, among the fuel rods in lattices having the EBWR core geometry. The uniformity of the distribution was limited by the mechanical design of the clusters which held the fuel rods. When filled with heavy water, the void tubes constituted a distributed aluminum poison. With the heavy water removed from these tubes, a combination of void and aluminum poison was present in the core. The difference in critical configurations between a core containing water-filled aluminum tubes and the one containing an equal number of empty aluminum tubes yielded information on the reactivity effect of voids.

Two methods of reactivity compensation were employed in these measurements of void coefficients. In some cases the effect of poison and voids was offset by adjustment of the position of the central 25.4-cm-span cross-type control rod. In others, the water level was varied to restore criticality.

For the control rod criticals, the water level was held at 192.2 cm, thereby providing a 40-cm-thick top reflector. For this arrangement, the void tubes were either completely filled or empty. The critical position for the central control rod was determined, and the differential worth of this control rod near criticality was observed in order to relate the change in control rod setting for criticality to reactivity.

In the water level criticals, a reduction in void density was accomplished by uncapping a preselected number of void tubes so that water would enter the open tubes when the moderator level exceeded approximately 157 cm. As clean critical was established, the water which had flowed into the open void tubes remained trapped, so that its level exceeded that of the moderator. However, it was desirable that the water level in the void tubes coincide with the moderator water level. Consequently, criticality was approximated by first observing the critical water level with heavy water completely filling the uncapped tubes, next removing an amount of water calculated to yield a water level in the tubes identical with the critical water level of the moderator, and then redetermining the critical water level. In the final measurement with void tubes, the empty void tubes were replaced by identical ones which had a small hole at the base. This allowed the moderator to flow into these void tubes and thereby eliminated the need for determining criticality by successive approximations.

2. Description of Experiments

First a sequence of void-coefficient experiments was made in a reflected core of 836 unclustered 25/1 fuel rods in the EBWR geometry. In the first measurement, nine void tubes were inserted in each cluster, which was completely filled with fuel pins having a $2a_0$ triangular pitch and a proportionate number in the peripheral clusters. For all other measurements 33 void tubes were inserted in each full cluster, and hence these cores had a ratio of 33 void tubes to 28 fuel rods. A typical arrangement of the void tubes and the fuel rods within a cluster is shown in the upper right hand corner of Figure 5.

Criticality for the core containing no void tubes had been established prior to the insertion of these tubes. After the first measurements with 268 empty and filled void tubes in the core, the number of void tubes was increased to 1004, resulting in approximately 17% void in the moderator. The critical conditions observed for a sequence of steps between the fully voided and the unvoided condition are given in Tables XXX and XXXI.

Table XXX

ROD CRITICALITY AND WORTH FOR REFLECTED CORE OF 836 25/1 FUEL RODS CONTAINING VOID TUBES

Loading Number	Void Tubes		No. 9 Rod Critical Position, (cm)	No. 9 Rod Calibration	
	Empty	Full		Increment, (cm)	Doubling Time, (sec)
14*	0	0	56.97	0.686	64.5
			56.95	0.940	44.0
20	0	268	63.72		
30	0	1004	82.30	1.270	35.62
28	188	816	88.89	1.270	42.2
26	372	632	96.11	1.270	50.5
25	588	416	107.04	1.676	44.35
24	828	176	123.83	2.591	40.8
23	1004	0	145.31	5.080	49.1
			145.14	5.080	52.7
			144.83		

*47.2-cm top reflector. For other loadings, 39.8 cm.

Table XXXI

UNIFORM VOID DISTRIBUTION IN CLEAN CRITICAL ASSEMBLIES

Loading Number	Fuel Rods	Void Tubes		Critical D_2O Level H_c (cm)
		Empty	Full	
19	836	0	0	109.64
20	836	268	0	121.08
31	836	0	1004 to 127.95 cm	127.72
29	836	188	816 to 136.08	133.83
27	836	372	632 to 141.67	140.40
25	836	588	416 to 149.29	149.34
24	836	828	176	106.69
52	1616	0	0	72.55
50	1616	1908	0	99.71
51	1616	0	1908 to 80.67	81.33
56	1012	0	0	94.84
57	1012	1212	0	141.64
58	1012	0	1212 to H_c*	109.40, 109.03
59	1012	0	0	95.35

*Use of pierced tubes

The first summarizes those experiments in which the critical position of the central control rod was determined with a fixed water level, whereas the second contains the data for clean critical configurations. Even with all of the void tubes filled with water, there still was an appreciable fraction of the heavy water displaced from the core by the void tube material. Consequently, the reactivity effect associated with the displacement of additional water while the number of void tubes and hence the aluminum content remained unchanged must be used to separate the reactivity effect associated with the aluminum poison.

The doubling time associated with upward displacement of the central control rod is included with the rod critical observations reported in Table XXX. For the clean critical conditions reported in Table XXXI, the water level in the filled void tubes is specified. It is approximately equal to the critical water level, that is, the level existing in the moderator region outside of the void tubes. These data were obtained in normally a second approximation to the critical configuration. Also included in Table XXXI are the less extensive results of the introduction of voids and aluminum poison in large steps in two assemblies during the course of measurements of control rod worths, as reported in Section B of this chapter.

To assist in the interpretation of the clean critical data for the poisoned and voided assemblies, several measurements of the differential water worth were made. These results are assembled in Table XXXII.

Table XXXII

DIFFERENTIAL WATER WORTH IN ASSEMBLIES CONTAINING VOID TUBES

Loading Number	Fuel Pins	Void Tubes		Initial H_c (cm)	Increment (cm)	Final H_c (cm)	Doubling Time (sec)
		Empty	Full				
20	836	268	0	121.082	0.508	-	78.5
				-	1.016	-	28.5
				-	0.762	121.107	46.5
30	836	0	1004	126.85	0.762		60.34
					1.143		31.62
28	836	188	816	133.07	0.762		67.3
					1.524		23.6
29	836	188	816 to 136.08	133.83	0.762		66.8
					1.524		24.7
26	836	372	632	139.83	0.762		72.8
					1.524		26.6
27	836	372	632 to 141.67	140.40	0.762		82.5
25	836	588	416	148.98	0.660		107.6
					1.308		42.1
					2.540		13.2
25	836	588	416 to 149.29	149.34	1.270		44.8
24	836	828	176	160.69	1.036		63.0
50	1616	1908	0	99.670	0.254	99.657	126.85
				99.657	0.597	99.733	36.385
				99.733	0.775	99.720	25.22
				99.573	0.681	99.581	29.0
				99.581	0.927		18.15
57	1012	1212	0	141.635	1.270	141.554	35.90
				141.554	2.032	141.554	17.55
				141.554	2.540	141.554	11.48
				141.554	2.540	141.554	11.59
58	1012	0	1212 to H_c	109.398	1.016		19.86
					1.194	109.220	19.19
				109.220	1.270		15.70
				109.032	1.016	109.017	22.39
				109.017	1.270	109.030	15.40
				109.030	1.270		15.25

Note that several of these measurements are associated with systems for which the void tubes were completely filled with water. This represents the first approximation from which an estimate was made of the amount of heavy water which should be removed from the filled void tubes in order that the level within the tubes approximate the critical water level, as reported in the preceding table. Data about differential water worth for clean assemblies to which the void tubes were added have already been reported in Table XXI (loadings Nos. 14, 19, 52, 56 and 59).

B. Control Experiments

Early in the THUD program the objective shifted from the design of a loading for EBWR to an investigation of idealized assemblies, and so most of the information on effectiveness of control rods was obtained solely to verify compliance with the rules regarding shutdown reactivity available to the operator. The limited precision of those measurements makes them of questionable value for the purposes of this report. However, two experiments of general interest were performed, one a comparison of the worth of single cross- and blade-type control elements in cores having EBWR geometry, and the other an investigation of the reactivity effect of thorium sheets sectioning clustered core criticals.

1. Inserted Cross and Blade Control Elements

Criticality was established for a number of $2a_0$, slightly clustered assemblies (EBWR geometry) of 25/1 fuel with either a 25.4-cm-span cadmium cross or a blade of the same width inserted at the center. The cadmium was 0.51-mm thick, clad in 1.59-mm thick aluminum. Measurements were made in unpoisoned cores of several radii, in an aluminum-poisoned core, and in an aluminum-poisoned and voided core. The critical water level with the control element inserted is compared with that for the clean critical assembly in Table XXXIII.

In this sequence of measurements, some additional information was obtained. In loading No. 50, the following corresponding positions of the 25.4-cm-span central cross rod and the critical water height were observed:

Central Cross:	0	38.91 cm	59.11 cm	out
Water Level:	142.30 cm	124.21 cm	109.65 cm	99.71

In loading No. 52, the critical height was also observed for a core containing an off-center cross-type control element. The center of this rod was located 32.39 cm from the center in a core of 46.70-cm radius, at control rod position No. 7. Thus it was completely surrounded by core material. The critical water height was 82.85 cm. No further measurements were made of the effectiveness of an off-center rod, since one or more wings of the cross rod at any of the fixed positions of the rod guides would extend into the reflector for the other (smaller) assemblies.

Table XXXIII

WATER LEVEL COMPENSATION FOR INSERTED CENTRAL CROSS AND BLADE CONTROL ELEMENTS

Core Description					
Loading Number	Fuel Rods	Void Tubes	Radius (cm)	Control Element	Critical Water Level (cm)
55	1164	0	39.40	None	85.71
				25.4-cm cross	139.40
54	1316	0	41.94	None	80.15
				25.4-cm cross	118.16
53	1468	0	44.19	None	75.73
				25.4-cm cross	104.94
52	1616	0	46.70	None	72.55
				25.4-cm cross	96.40
				25.4-cm blade	87.05
51	1616	1908 (filled)	46.70	None	81.29
				25.4-cm cross	110.70
50	1616	1908 (empty)	46.70	None	99.71
				25.4-cm cross	142.30
				25.4-cm blade	124.21

2. Thorium Sheets in a Clustered Core

Interest in thoria-urania-D_2O systems arises partly because of the possibility of achieving a thermal breeder with U^{233}. For this reason it was considered worthwhile to determine whether thorium might be useful as a combination control rod and fertile material. Because of its low thermal capture cross section, it is obvious that such control elements would be far more bulky than the usual cadmium or boron rods. However, the use of surplus neutrons to make U^{233} rather than nonproductive capture might improve the neutron economy sufficiently to offset the mechanical disadvantages.

Several measurements of the change in water height required to compensate for the presence of large thorium sheets in a clustered lattice were performed. Clusters composed of 31 of the 25/1 fuel rods were used in a square lattice of 10.8-cm pitch. Measurements were made in cores composed of both a 6 x 6 and a 6 x 8 array of these clusters. Operation with the bottom plugs of the cluster cans removed allowed the heavy water to fill the cluster tubes to the same level existing in the moderator region.

Plates of thorium, 6.99 cm x 61 cm x 0.193 cm, were available, and sheets of thorium were constructed from these plates held within an aluminum border. These sheets extended the entire width and height of the core in a plane, usually separating it into two halves, each with either a 3 x 6 or a 4 x 6 pattern of clusters. The critical water heights required for the various configurations of thorium sheets were determined, and the doubling time produced by the addition of a small amount of water was observed, to provide a basis for interpreting the change in critical water height. Flux depression due to central thorium sheets was established from flux plots, and measurements of the relative contribution of photoneutrons were made.

The first experiments were made in a core composed of 36 clusters, but sufficient excess reactivity was not available to extend these measurements to systems with more than two sheets of thorium bisecting the core. An additional row of six clusters was added at each end of the core, to determine the poisoning effects of additional layers of thorium. In this second core, the limited supply of thorium plates precluded measurements for thicknesses greater than five layers. The results are assembled in Table XXXIV.

Table XXXIV

CRITICAL CONDITIONS AND DIFFERENTIAL WATER WORTH WITH THORIUM SHEETS IN CLUSTERED CORES

Number of Layers of Thorium	Location (y-plane, x coordinate) (cm)	Critical Height (cm)	Increment (cm)	Doubling Time (sec)
31 rod clusters of 25 1 fuel, 10.8-cm-sq pitch, 6 x 6 array				
0	0	101.53	0.635	38.82
			0.889	22.07
1	0	122.17	1.27	26.95
2	0	144.84	2.03	26.74
2	+0.635, -0.635	147.10	2.03	27.53
2	0, -10.80	152.86	2.54	24.17
31 rod clusters of 25 1 fuel, 10.8-cm-sq pitch, 6 x 8 array				
0	0	85.78	0.508	33.08
1	0	96.34	0.762	28.35
2	0	105.72	0.889	28.64
2	+10.80, -10.80	108.98	0.762	41.02
3	0	113.87	0.965	31.61
			1.07	25.64
4	0	119.21	1.27	26.17
			1.12	30.36
5	0	126.00	1.52	23.69

Also included in this table are the results of separating two layers by 1.27 cm at the median plane and moving one of the sheets to the next channel between rows of clustered elements. In addition, a few measurements were made of the effect of removing individual plates from a single layer of thorium. These results are given in Table XXXV.

Table XXXV

PERTURBATION CAUSED BY REMOVAL OF ONE PLATE FROM SINGLE LAYER THORIUM SHEET CENTERED IN 6 x 8 ARRAY OF CLUSTERS

Gap Location (z coordinate, cm)	Change in Critical Water Height, cm
0 to 6.99	-0.460
34.93 to 41.91	-1.359
83.82 to 90.81	-0.008

Figure 30 shows typical results for dysprosium flux traverses made perpendicular to the thorium sheet. Data for a clean core and one containing a single layer of thorium are shown. The depression of the flux caused by the rows of fuel clusters is evident. From these and similar flux plots, the thermal flux depression caused by various thicknesses of thorium sheet at the center of the core was obtained. The results are displayed in Figure 31.

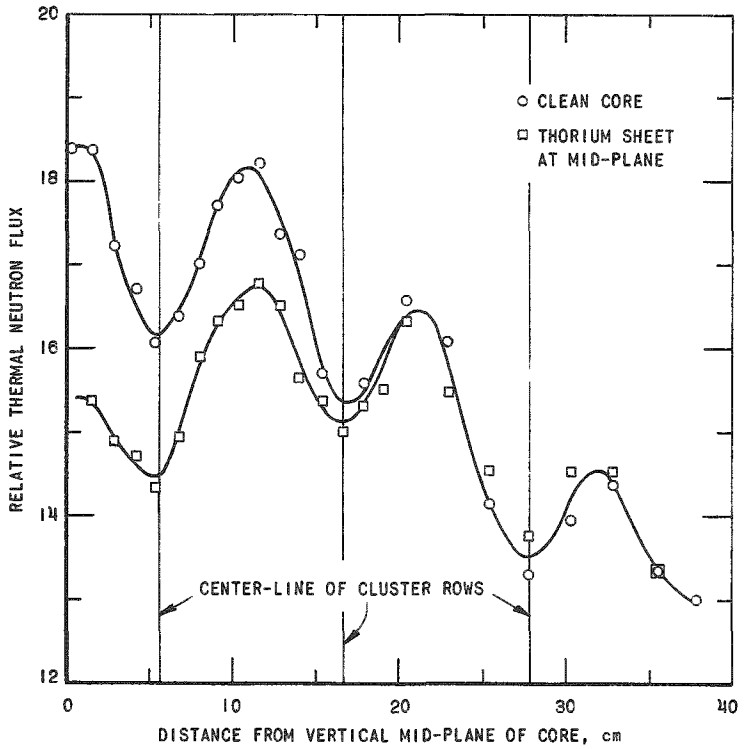

Fig. 30

Depression of Thermal Neutron Flux by a 0.19 cm Thick Thorium Sheet at the Core Center

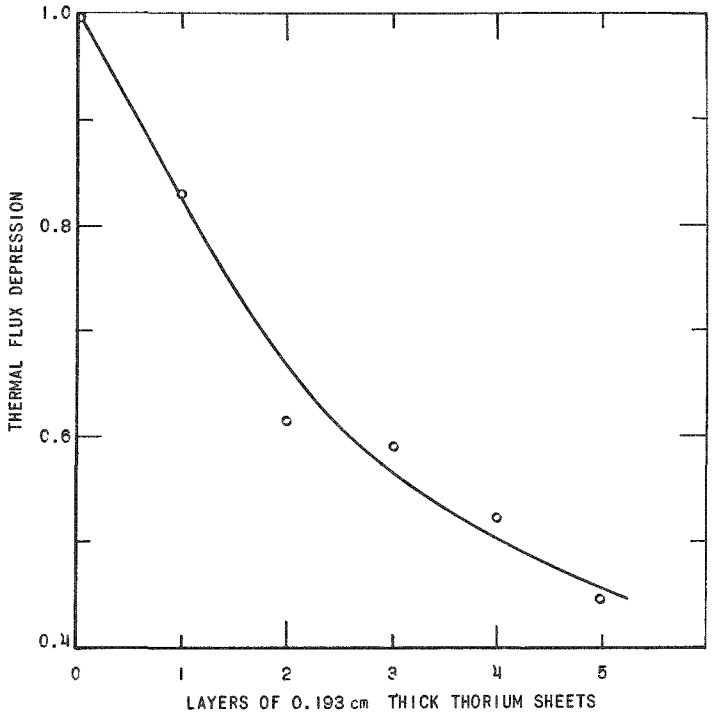

Fig. 31. Thermal Flux Depression by Thorium Sheets at Core Center

Determinations of photoneutron effectiveness were made for the larger core containing both a three-layer sheet and a five-layer sheet. These results are included with similar data in Table XXXIX.

VI. SUPPLEMENTAL DATA

Additional available data of use for the analysis, interpretation, and standardization of the experimental results reported in the preceding chapters are discussed in this final chapter.

A measure of the degree of neutron thermalization is given by the cadmium ratio of materials for which the dependence of cross section on energy is known. Such data obtained during the THUD program are assembled here. Because of the presence of heavy water, there was a second source of delayed neutrons in the THUD criticals. Since the photoneutron production depends upon fuel composition within a representative lattice cell and also on the geometrical form of the assembly, the interpretation of observed reactivity data requires a knowledge of the variation of the photoneutron production. Consequently, a summary of experiments in which the relative yields of photoneutrons and delayed neutrons were determined for a variety of cores is presented here. Observations on two time-dependent variables, the heavy water purity and the core temperature, are also included. Related to the latter is a description of the measurement of the temperature coefficient of reactivity for uniform cores with two different lattice spacings.

A. Spectral Indices

An indication of the degree of neutron thermalization existing in the THUD lattices is available from the ratio of thermal to epicadmium activation of a variety of materials irradiated in the critical assemblies. In Table XXXVI are assembled the cadmium ratios observed in a position of neutron energy equilibrium. Measurements were made in both the moderator and fuel near the center of most of the types of uniform lattices studied. The investigation of clustered lattices was less thorough, and so only fragmentary data exist for this class of assemblies. In addition, the switch to dysprosium as the detector for the disadvantage factor measurements eliminated the cadmium ratio information which occurred as a by-product during the earlier determinations of disadvantage factor.

Except where indicated otherwise in the table, all measurements were made with 0.58- or 0.63-cm-diameter foils covered by 0.51-mm-thick cadmium in lattices of 25/1 fuel. Those with smaller diameter were used for measurements within the fuel rods, with the detector material sandwiched between cadmium disks identical in diameter with the foil and the fuel pellets. For cadmium-covered activations in the moderator, the edges of each size of foil were also protected from thermal activation by insertion in pill boxes stamped from 0.51-mm-thick cadmium. The one value for 50/1 fuel was obtained from foils placed inside such a fuel pin in an assembly in which 20% of the fuel rods had this lower enrichment.

Table XXXVI

OBSERVED CADMIUM RATIOS

Lattice	Pitch	Foil Material	Cd R_{Mod}	Cd R_{Mod}	Remarks
Uniform	$2a_0\Delta$	U^{235}	6.9		Fission counter
Uniform	$2a_0\Delta$, EBWR	U^{235}	8.9		Fission counter
		25-μ U^{235}		4.8	
		Au	2.9		1.02-mm-dia wire, 0.25-mm Cd
		25-μ Au		1.42	
		89-μ Mn		3.3	
		127-μ In		1.9+	
		25-μ Cu		3.5	
		25-μ Cu		3.0	
Uniform	$3a_0\Delta$	U^{235}	14.2		Fission counter
		25-μ Cu		3.9	
Uniform	$6^+a_0\Delta$	25-μ U^{235}	58	47	
		89-μ Mn	32		
		127-μ In	9.7		
		25-μ U^{235}		52	50/1 fuel pin
		25-μ Cu	>25		
		203-μ 3 wt-% Dy-Al	165		
28 rod cluster	10.2 cm □(EBWR)	25-μ U^{235}	4.35	4.55	Center of cluster
27 rod cluster	$6\sqrt{3}a_0\Delta$	25-μ Cu		4.6	Center of cluster, 0.25-mm Cd
				3.9	Edge of cluster, 0.25-mm Cd

Some values obtained during flux distribution measurements with a 0.95-cm-diameter by 5-cm-long U^{235} fission counter are also included in the Table XXXVI. These data were obtained during determinations of reflector savings. For the epithermal flux measurements, the counter was wrapped in 0.25-mm cadmium, with sufficient overlap to give an average thickness of 0.41 mm. Three of the four experimental values given in Figure 32, which shows the variation of cadmium ratio with the moderator-to-fuel volume ratio, were obtained with the fission counter. The air gap and aluminum clad of the fuel rod were ignored in calculating the values of V_M/V_F used in the figure.

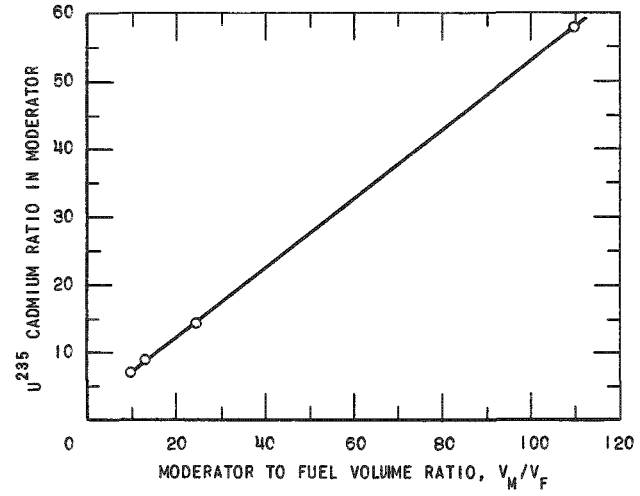

Fig. 32. Dependence of U^{235} Cadmium Ratio on Moderator to Fuel Volume Ratio.

B. D_2O Purity

As mentioned previously, the duration of the THUD experimental program was appreciably greater than had been anticipated at the start, and so the failure to include a system for maintaining heavy water purity in the ZPR-VII facility resulted in a significant variation in the amount of light water contamination in the D_2O during the course of these experiments.

Water samples were withdrawn periodically during the experimental program and submitted for mass spectrographic analysis. The results of some 26 analyses are plotted as a function of the time at which the sample was withdrawn in Figure 33. Some of the scatter in the values is due to fluctuations in the quality of the vacuum in the spectrometer. Some light water contamination of the samples may have resulted in the early part of the THUD program because of inexperience in withdrawing samples.

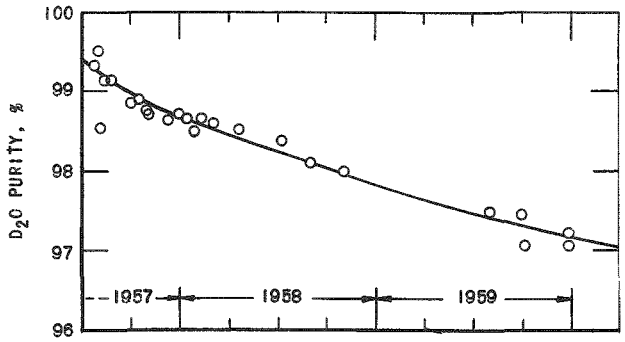

Fig. 33. Variation of D_2O Moderator Purity

The trend line drawn through the data points indicates a gradual deterioration in D_2O purity with time. Over a two-and-one-half-year period there was a 2% decrease in the heavy water content of the moderator. Possible sources of this addition of light water are contact with the air, perspiration during the many major core loading changes, leakage from the light water-filled clusters, and inadequate drying of these clusters before restoring a heavy water filling.

There is a possibility of a systematic error in the mass spectrometric determinations of the heavy water concentration. At the completion of the experimental program, the heavy water was shipped to the Savannah River site. The analysis of the heavy water content on receipt was 1.6% below the average reported for three samples withdrawn during the unloading operation at the end of 1959. The explanation for this discrepancy is not known.

Occasionally, a water sample was submitted for chemical analysis. A typical spectrochemical analysis report is given in Table XXXVII. The accuracy is estimated as a factor of two. The cadmium concentration is no more than the detectable minimum, and so its presence is questionable. The quantities of impurities detected are not sufficient to account for the changes in reactivity observed when previously assembled systems were reconstructed.

Table XXXVII

SPECTROCHEMICAL ANALYSIS REPORT FOR D_2O SAMPLE

Element	Micrograms/ml	Element	Micrograms/ml
Al	0.5	Li	0.05
Ba	0.02	Mg	1
Ca	2	Mn	0.02
Cd	0.02	Na	1
Cr	0.01	Pb	0.03
Fe	0.1	Sr	0.005

C. Relative Photoneutron Effectiveness

1. The THUD Inhour Equation

The analysis of those THUD experiments which required the measurement of the differential water level and control rod worths requires an accurate knowledge of reactivity as a function of reactor period. The inhour equation, which gives this relationship, is in turn, a function of the abundance and half-life of delayed neutrons from two main sources, delayed neutron emitters among the U^{235} fission products, and deuterium. The principal source of the gamma rays for the photoneutron process is the

U^{235} fission products. The threshold of the deuterium photoneutron process is 2.2 Mev.

From the fast effect measurement, it is known that the number of thorium fissions in the THUD reactor is negligible compared with the number of U^{235} fissions. In the conversion of Th^{233} into U^{233}, the delayed gamma rays are in every case below 2.2 Mev, thus eliminating the possibility of deuterium photoneutrons from this source. Furthermore, the possibility of delayed photoneutrons from Al^{28} radioactivity is also ruled out because the gamma-ray energy of this process is only 1.8 Mev.

The conventional inhour equation is given[19] by

$$\rho = \frac{\ell}{Tk_{eff}} + \sum_{i=1}^{m} \frac{\beta_i}{1 + \lambda_i T} \quad ,$$

where ρ is the reactivity, defined by

$$\rho = \frac{k_{ex}}{k_{eff}} = \frac{k_{eff} - 1}{k_{eff}} \quad ,$$

T is the period, and β_i is that fraction of the total neutrons emitted in the fission process which have a mean delay time of λ_i^{-1}.

For the THUD reactor, with two different sources of delayed neutrons, the inhour equation becomes

$$\rho = \frac{\ell}{Tk_{eff}} + \sum_{i=1}^{m} \frac{\beta_i}{1 + \lambda_i T} + \sum_{j=1}^{n} \frac{\beta_j}{1 + \lambda_j T} \quad .$$

Here β_i and λ_i have the same meaning as above, and β_j and λ_j are corresponding quantities derived from observation of the decay of the photoneutron production when fission products are in contact with heavy water.

Reported values for the delayed and photoneutron constants required for the inhour equation are given in Table XXXVIII. The six delayed neutron groups were obtained from the data of Keepin and Wimett.[20] The first (longest-lived) photoneutron group was obtained from the data of Ergen,[21] and the remaining eight groups derived from the data of Bernstein et al.[22] The β_j values for the photoneutrons are quoted in the literature in terms of the β_i for the 22-sec delayed neutron activity, so the actual β_j values given were obtained from the Keepin and Wimett data.

For use in the inhour equation, the β_i values of Table XXXVIII require a correction, because the fission product delayed neutrons are of slightly lower energy than the prompt neutrons and hence have a lower leakage probability.

Table XXXVIII

CHARACTERISTICS OF DELAYED AND PHOTONEUTRONS

Half-life (sec)	Transformation Constant, $\lambda_{i,j}$ (sec^{-1})	Yield, $\beta_{i,j}$
Delayed neutrons:		
54.6	1.27×10^{-2}	2.47×10^{-4}
21.9	3.17×10^{-2}	1.3845×10^{-3}
6.03	1.15×10^{-1}	1.222×10^{-3}
2.23	3.11×10^{-1}	2.6455×10^{-3}
0.50	1.40	8.32×10^{-4}
0.18	3.87	1.69×10^{-4}
		$\Sigma\beta_i = 6.50 \times 10^{-3}$
Photoneutrons:		
1.11×10^{6}	6.26×10^{-7}	4.07×10^{-7}
1.91×10^{5}	3.63×10^{-6}	1.02×10^{-6}
1.58×10^{4}	4.37×10^{-5}	3.213×10^{-6}
5.94×10^{3}	1.17×10^{-4}	2.327×10^{-5}
1.62×10^{3}	4.28×10^{-4}	2.064×10^{-5}
462	1.50×10^{-3}	3.352×10^{-5}
144	4.81×10^{-3}	6.980×10^{-5}
41.0	1.69×10^{-2}	2.036×10^{-4}
2.50	2.77×10^{-1}	6.496×10^{-4}
		$\Sigma\beta_j = 1.051 \times 10^{-3}$

The effectiveness factor E_i is defined for a reactor as the ratio between the value of β_i which would appear in the kinetic equations describing that reactor and the value of β_i given in the literature as characteristic of the fission process. On the age formulation for epithermal leakage, this effectiveness factor is of the form $E_i = e^{c_i \tau B^2}$. It is customary to use a single value for c_i, of the order of $\frac{1}{3}$.

For THUD-type cores, which consist of a heterogeneous mixture of thorium, U^{235}, aluminum, and heavy water, the delayed photoneutrons yields observed for fission products dispersed in heavy water are not applicable because some of the gamma rays sufficiently energetic to produce photoneutrons are absorbed or scattered by the other components and degraded below the threshold energy of 2.2 Mev for the (γ,n) reaction in deuterium. Thus it is desirable to introduce a second effectiveness factor, E, defined as the ratio of the effectiveness of photoneutrons to that for delayed neutrons in a specific THUD core.

This relative photoneutron effectiveness E will be unity for infinitely dilute fuel, provided the photoneutrons have the same energy as the delayed neutrons. Since the THUD fuel elements are of finite size, and thus absorb some of the photoneutron-producing gamma rays, E will tend to be less than unity. A counter effect will exist if, as is suspected, the photoneutrons are of lower energy than the delayed neutrons, and thus have a lower leakage probability during slowing down in a finite core. A second factor which would increase E is the possibility that the photoneutron yield reported by Bernstein et al.,[22] is low. Hughes[23] has reported a value 75% higher.

The experimental determination of the relative photoneutron effectiveness for many of the THUD cores is reported in this section. The importance of an accurate determination of this quantity is demonstrated by results presented in Figure 34. The inhour equation has been evaluated by means of the parameters reported in Table XXXVIII for values of E from 0 to 1.5. From the graph of reactivity as a function of reactor period, the effect of an uncertainty in E can be evaluated.

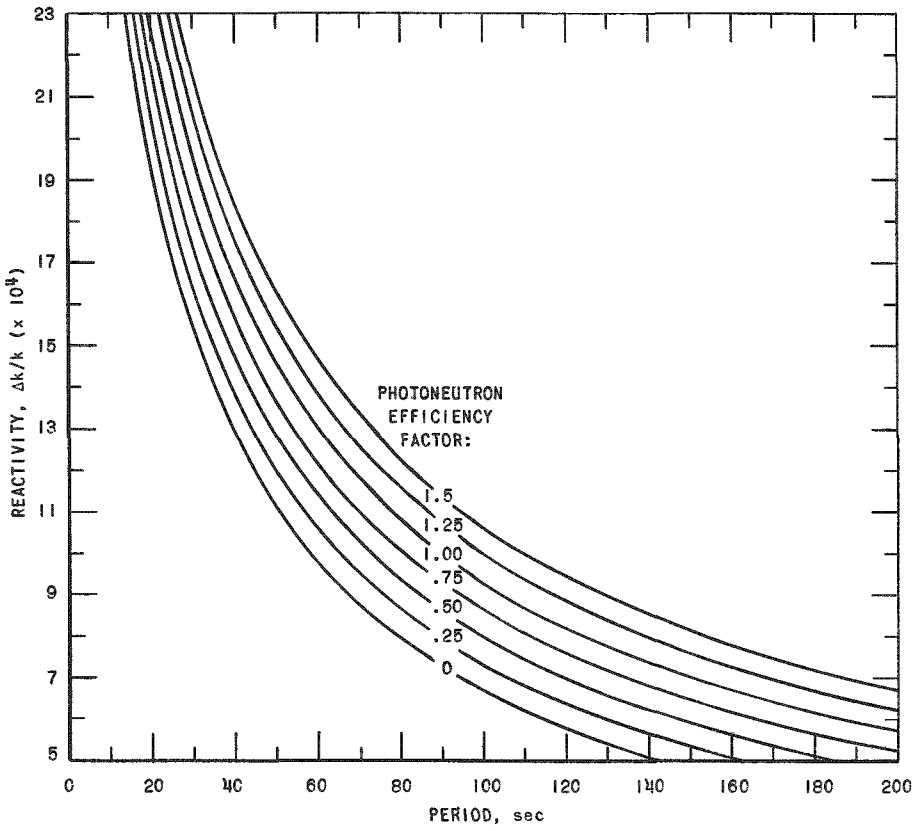

Fig. 34. Influence of Relative Photoneutron Abundance on the Period-Reactivity Relation.

For the results presented in Figure 34 a value of 1.042 was used to correct both delayed and photoneutron yields for the reduced probability of leakage. This factor is dependent upon the age and buckling as well as upon the assumed energy of these neutrons, and hence will vary with the composition of the THUD cores. A value of 695 μsec was used for the prompt neutron lifetime, which is also influenced by the nature of the core. For the THUD systems, this is given approximately by $[\Sigma_a v\ (1 + L^2B^2)]^{-1}$. The reactivity-period relationship is influenced only slightly by the neutron lifetime, since the second term in the inhour equation is dominant for the range of doubling times observed.

2. Experimental Procedure

The effectiveness of photoneutrons relative to delayed neutrons was measured by a modification of the method used by M. Johns and B. Sargent[24] to determine the yields and half-lives of photoneutrons and delayed neutrons in the ZEEP reactor. From measurements of the neutron intensity as a function of time from shutdown and certain reactor kinetics equations, they were able to obtain the various absolute yields and half-lives.

In the THUD experiments, the reactor was held at steady power for a period of time, T_B, usually about 20 min, to allow the longer-lived photoneutron-producing gamma rays to build up to some fraction of equilibrium concentration. Bernstein reports that the two groups of shortest half-life yield 85% of the photoneutrons. To this irradiation time, T_B, is added an increment equal to the period on which the reactor was brought to power, in order to account for the precursors generated during startup. Rapid shutdown was achieved by releasing a control rod and the register pulses from the scaler of a BF_3 counter channel monitoring the reactor flux (Channel 1 or 2) were recorded on a high-speed strip-chart recorder.

Before bringing the reactor to power the water was raised to operating height, the control rods were placed in the shutdown configuration, the source was removed, and a background count taken. This background, which was assumed constant during the measurements, takes account of any residual source produced by the long-lived activity of the fuel or other causes. A shutdown time of several hours usually preceded each measurement, to minimize the effect of previous irradiations of the fuel.

The neutron decay rates observed in the first two experiments, performed with loading No. 60, are given in Figure 35. A practice was made of restricting the maximum counting rate used in the analysis of results to about 3000 per second. For a counting circuit dead-time of about 5 μsec, the correction for counting loss is less than 1% and therefore negligible.

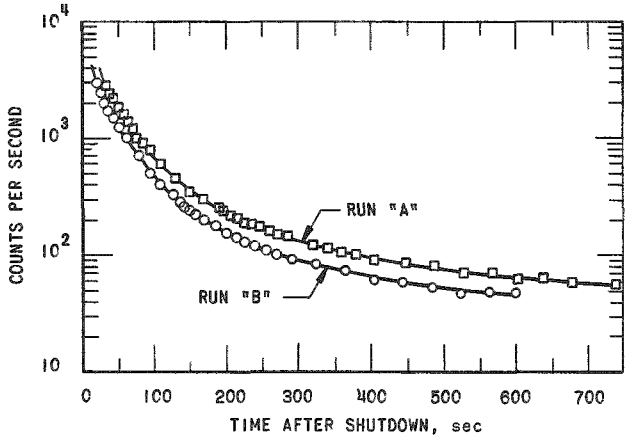

Fig. 35. Decay of Neutron Population Following Reactor Shutdown.

3. Data Analysis and Results

The equations describing the combined delayed and photoneutron intensity as a function of time from shutdown have been derived by Johns and Sargent.[24] For the analysis of the THUD measurements, the behavior of the flux after a rod drop worth Δk can be expressed by the sum

$$\phi(t) = \phi_0 \sum E_i A_i \, e^{-\alpha_i t} \quad ,$$

with one term for each delayed and photoneutron group. Here

$$A_i = \frac{\beta_i}{\sum \beta_i + \Delta k}\left[1 - e^{-\lambda_i T_B}\right]; \; \alpha_i = \lambda_i \left[1 - \frac{\beta_i}{\sum \beta_i + \Delta k}\right] \quad ,$$

ϕ_0 is the flux before the drop, and E_i is the effectiveness factor of each group.

For analysis of the decay curves, it was assumed that all delayed neutron groups had the same effectiveness factor E_d and all photoneutron groups have the same effectiveness factor E_p. Then putting $D = \phi_0 E_d$ and $P = \phi_0 E_p$, the equation for the time-dependent flux may be written

$$\phi(t) = D \sum_{i=1}^{6} A_i \, e^{-\alpha_i t} + P \sum_{j=1}^{9} A_j \, e^{-\alpha_j t} \quad .$$

For convenience, the units of ϕ were taken as register clicks per second.

An IBM-704 code, RE-155, was used to provide a least-squares fit of the experimental data. Using the group constants given in Table XXXVIII, it takes as input the locations of the register pulses read off the recorder chart in arbitrary units, calculates the time intervals using the recorder time calibration, and furnishes the values and errors of D, P, and P/D. The ratio P/D is the relative photoneutron effectiveness $E = E_p/E_d$.

It is not possible to determine E_p and E_d absolutely. The reason for this is that the A_i, which determine what values of E_p and E_d will fit the data, are themselves strongly dependent on the value of Δk assumed. However, ascertaining Δk involves the interpretation of a reactivity measurement in terms of an effective set of delayed neutron constants, whereas the compilation of this effective set presupposes knowledge of E_p and E_d. Thus, any attempt to get E_p and E_d absolutely leads to a circular argument which invalidates the attempt. Since a change in Δk changes all A_i by the same ratio and leaves the α_i essentially unaffected, valid determinations of E can be made.

The Δk involved in the rod drop which initiates the flux decay enters into the calculations as a correction factor for λ_i, which takes account of the precursors generated after the shutdown. The appropriate value was determined either from an estimate of the worth of the control rod or from the trace of a count rate meter connected to the scaler. The correction factor is small, and a sequence of calculations, for loading No. 184 data, with a range of values for Δk showed only a very slight dependence of E on the value of Δk, namely, a 0.1% decrease in E for a change from 0.25 to 0.35 for Δk.

The values of the relative photoneutron effectiveness obtained from analysis of the decaying flux in a variety of THUD cores are assembled in Table XXXIX. The loadings are described in other tables in this report. The comments on the cores included in this table will serve as a guide to the location of the detailed descriptions. Excluding the value for loading No. 223, the values for E vary by about a factor of 2. A definite trend with degree of dilution of the fuel is evident.

In order to use these data for conversion to reactivity of the doubling times observed in cores other than those listed here, some evaluation of these results is required. It is for this reason that the observations of differential water worth are presented in this report in terms of doubling times. The value of E is a combination of a volume and a surface effect, since gamma rays originating in those fuel elements near the core-reflector boundaries have a greater probability of producing photoneutrons because of the greater effective dilution. The relative contributions from surface and volume depend on the core size. Clustered and flux-trap lattices represent a further complication in trying to separate the surface and volume effects in order to derive values of E for other cores.

Table XXXIX

EXPERIMENTAL VALUES FOR RELATIVE PHOTONEUTRON EFFECTIVENESS E

Loading Number	E	Comment on Core
EBWR Geometry		
60	0.702 ± 0.019	Clean critical (cc)
Uniform, 15/1 Fuel		
381	0.617 ± 0.005	$2a_0$ cc
403	0.729 ± 0.003	$3a_0$ cc
407	0.888 ± 0.011	$4a_0$ cc
411	0.989 ± 0.009	$6a_0$ cc
Uniform, 25/1 Fuel		
262	0.669 ± 0.013	$2a_0$ cc
265	0.706 ± 0.010	#262, less 148 central rods
270	0.726 ± 0.006	#269 ($2a_0$ cc), less 258 central rods
271	0.809 ± 0.006	#269, less 556 central rods
249	1.237 ± 0.025	$6a_0$, fuel substitution
184	1.138 ± 0.029	6^+a_0, fuel substitution
	1.130 ± 0.090	
Clustered Fuel		
223	0.040 ± 0.035	$8a_0$ △ pitch, 19 rods/cluster
306	0.661 ± 0.004	13.0-cm □ pitch, 25 rods/cluster
322	0.642 ± 0.011	10.8-cm □ pitch, 19 rods/cluster
293	0.654 ± 0.027	10.8-cm □ pitch, 31 rods/cluster, H_2O filled
334	0.558 ± 0.004	10.8-cm □ pitch, 31 rods/cluster
344	0.660 ± 0.011	10.8-cm □ pitch, 31 rods/cluster, + 0.579-cm Th sheet
354	0.567 ± 0.005	10.8-cm □ pitch, 31 rods/cluster, + 0.965-cm Th sheet

D. Temperature Variation

A seasonal fluctuation in temperature occurred in the cell which contained the ZPR-VII facility. Furthermore, since the water was stored in a dump tank below floor level and was transferred to the core tank only during the actual operation of the system, there existed smaller daily variations in the reactor temperature.

A thermocouple was located in the core tank, adjacent to the instrument thimble attached to the inner side of the tank wall. The thimble is visible in the lower right-hand corner of Figure 2. The sensitive end of the thermocouple was at approximately mid-height of the fuel, and displaced slightly from the wall of the instrument thimble. Approximately 0.6 liter of water flowed through the assembly per second during operation, and so some degree of mixing was achieved. For temperature coefficient measurements, additional thermocouples were located near the top and bottom of the core structure and in the dump tank.

At times the thermocouple or its recorder was inoperative, and so a chart of the temperature variation with time has been constructed from available data, as a means to estimate the temperature applicable to the critical configurations for which no temperature was recorded. The range of temperatures observed in successive 10-day intervals is shown in Figure 36. The range of temperature for the entire period of operation was 12.2°C, from 17.8 to 30.0°C.

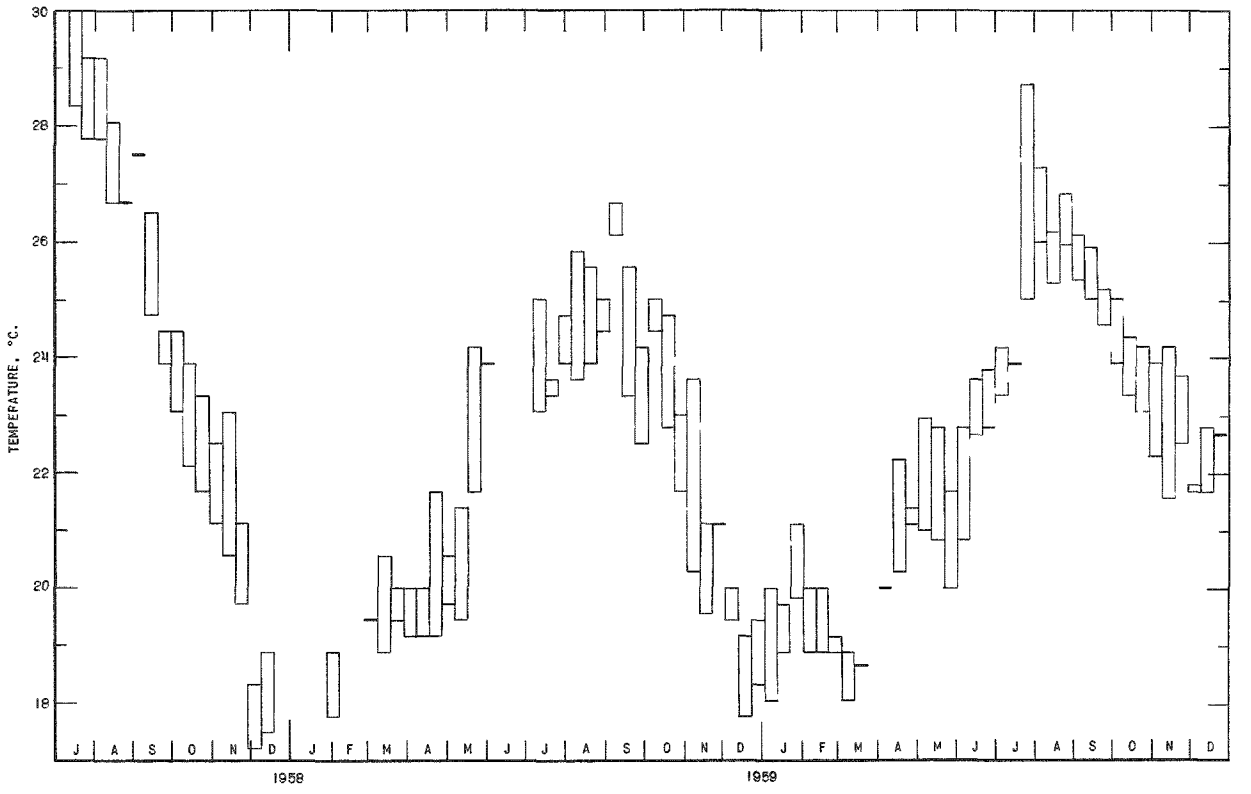

Fig. 36. Seasonal Variation of Moderator Temperature

The temperature chart of the recorder was divided in single-degree increments over a range from 0 to 300°F. Tenths of a degree were usually estimated, but the width of the pen line was approximately half a degree and so this, coupled with slight differences in successive charts, limits the accuracy of the readings to approximately ± 0.5°F (0.3°C). Frequently, the

system was shut down several times in a day, and hence temperature data are available showing the variation of temperature with amount of pumping of the water from the storage tank to the core tank. On the average, an increase of approximately 1°C was observed during the course of a day's operation.

In addition to the normal seasonal changes, there were a number of experiments performed in ZPR-VII which influenced the D_2O moderator temperature. During May, June, and October of 1958, temperature coefficient experiments in which the entire moderator was heated were performed. These are described in the following section. During the month of February, 1958, a steam generator was inserted in the core for measurement of the dynamic response of the assembly to bubble formation.

Because of the moderate magnitude of the temperature coefficient for the assemblies measured, it is likely that the temperature variations contribute less to the observed changes in critical dimensions than certain variables of unknown magnitude, such as the degree of reproducibility of the core geometry and the variation of fuel content among the rods used.

E. Effect of Temperature on Criticality

Measurements were made to establish the temperature coefficient of reactivity for cores composed of uniform lattices of single fuel rods with $3a_0$ and $6^{+}a_0$ triangular pitch.

For the first measurement, the immersion-type heaters available in the ZPR-VII system were placed in the reactor tank. It was hoped that this would eliminate the need for dumping the water after a criticality determination, thereby eliminating the possibility of an abrupt reactivity change due to shifting of core components. A core composed of 348 of the 25/1 fuel rods was assembled (loading No. 144) with a triangular lattice pitch of $3a_0$. Four thermocouples were inserted at three different heights in the tank; one was in the core and three in the reflector region. The water was heated intermittently over a period of 6 hr. The thermocouple readings demonstrated that convective circulation was not adequate to achieve a uniform temperature throughout the system. Adequate mixing was obtained by dumping the water before each determination of criticality. Table XL summarizes the critical water levels observed as the temperature was increased during these measurements.

At the termination of these temperature coefficient measurements, the differential water worth was measured. This result is also included in Table XL, together with several similar measurements made on the same core before and after the sequence of water-heating measurements. From this information on the differential water worth, the temperature coefficient of reactivity for this core can be evaluated.

Table XL

TEMPERATURE DEPENDENCE OF CRITICALITY AND DIFFERENTIAL WATER WORTH IN A $3a_0$ PITCH CORE

Temperature (°C)	Initial Critical Height (cm)	Increment (cm)	Doubling Time (sec)	Final Critical Height (cm)
23.33	145.39			
26.29	145.99			
28.98	146.76			
33.15	147.90			
33.61	148.06			
37.69	149.23			
37.78	149.23			
42.15	150.77	1.270	48.70	150.65
23.89	145.42	1.778	27.12	145.36
23.89	145.36	1.016	69.93	
25.56	146.27	1.270	46.75	
26.83	146.56	1.778	27.55	146.52
26.83	146.52	1.270	49.93	

Several months later this same type of measurement was repeated, for a core containing 190 of the 50/1 fuel rods and 742 of the 25/1 fuel rods. This core, loading No. 184, was one in a sequence of fuel substitution experiments with a lattice pitch of $6^{+}a_0$, as described in Section IV, C. The experimental procedure was modified slightly, as a result of the experience gained in the first measurement. The heavy water was heated and stirred in the storage tank until a single thermocouple in that tank registered a temperature rise of approximately 3°C. The heated water was then pumped into the main core tank and temperatures were read on three thermocouples mounted at approximately 30-cm spacings along a vertical line inside the core. Agreement of the temperature readings at the three levels implied that the temperature distribution in the core was uniform. Water worth data obtained for several of these heated criticals.

The results of these measurements are assembled in Table XLI. The first sequence was discontinued after a period of approximately 3 hr, when a short circuit occurred in one of the heaters. The first two entries in the table were obtained at that time. The difficulty was remedied, and the measurements resumed. The data obtained in this second series of measurements, as reported in Table XLI, were obtained on two successive days. The reversal in the temperature in this series resulted from overnight cooling.

Table XLI

TEMPERATURE DEPENDENCE OF CRITICALITY AND DIFFERENTIAL WATER WORTH IN A $6\frac{+}{a_0}$ PITCH CORE

Temperature (°C)	Critical Height (cm)	Increment (cm)	Doubling Time (sec)
21.17	141.06		
28.56	142.93	2.032	13.27
24.65	142.99		
30.87	144.83	1.778	17.22
28.78	144.25		
33.89	145.82	1.524	23.30
38.61	147.14		
40.39	147.68	1.524	23.86

Appendix A

PERFORMANCE AND MODIFICATIONS OF THE ZPR-VII FACILITY

Prior to the initial loading of fuel into the ZPR-VII system, some pre-operational testing of the system and training of the operating crew was performed. These activities resulted in some data of interest for comparison with the calculated results reported in the Hazards Summary Report.[10] In addition, it became apparent that some modification of procedures and mechanical details was desirable to increase the ease of operation with no significant reduction in the safety of the use of the ZPR-VII facility. Rate information on water flow, control rod movement, and heating and cooling of the moderator are reported here, for comparison with the estimates made during the design of the system. In addition, the important modifications in the operating procedure and mechanical structure are discussed here, for reference purposes in connection with the continued use of the facility for investigation of other nuclear systems. Changes made in the instrumentation and control circuitry have been reported previously.[11]

Control Element Drive Units

Several changes have been made in the control rod drive system to enhance the safety and/or convenience of operation.

The control element guides are 182.9 cm in height, the cadmium elements 152.4 cm. The elements are limited by switches to travel from 2.86 to 166.8 cm above the base plate. The lower value corresponds to the bottom of the fuel within the fuel rods and the higher to a distance 11.4 cm above the top of the fuel. At the maximum height, the elements extend 16.2 cm into the guide. Clamps have been attached to the control rod cables to function as a mechanical stop on control element withdrawal in the event that the upper limit switch fails and this failure is not observed by the operator. Each clamp is set so that motion more than 2.5 cm beyond the normal upper limit of withdrawal is prevented by contact between the clamp and pulley. Thus, the element cannot be withdrawn from its guide.

A setting of 65 on the Variac of the armature voltage supply is required to withdraw a control rod in the specified minimum time of 5 min. Only 2.8 min is required at maximum voltage (100 on Variac). A time of 0.8 sec is required for a control rod to drop the full range. A mechanical stop has been added at a setting of 65 on the Variac as a reminder of the maximum allowed speed of withdrawal during operation. The maximum available speed can be used when there is no water in the core tank. This is controlled by an interlock with the dump valve clutch power and serves to reduce the time consumed by the daily checkout and withdrawal of safety elements prior to startup, with no reduction in the safety of operation. The control elements can be inserted at maximum rate at all times.

Sheet metal guides have been added in the control element drive units to prevent fouling of the cable in the shock-absorbing system as it winds up during a rod drop. A spring has been added to supplement the action of the existing spring in the shock absorber arm, to offset the effect of any loss of resiliency in the original springs. A sheet metal housing has been added to the drive units and external pulleys, to prevent possible fouling by miscellaneous misplaced hardware or debris.

Flow Rates

With only the control elements and guides in the tank, 13.2 min are required to fill the tank at the high flow rate. This compares favorably with the estimated minimum fill time of 11 min. In 1.5 min the water level reaches the core-support plate; an additional 10 min are required for the water to submerge the 182.9-cm-high control element guides, and the water reaches the fixed overflow, corresponding to a 61-cm top reflector, in an additional 1.7 min. Thirty-five seconds are required for the water to drain through the 30.5-cm-diameter dump line from this level to the base plate with the top cover removed, 36.5 sec with the cover on. The estimated time was 28 sec.

With the manually operated flow-control needle valve in the 2.5-cm-diameter, low-flow line fully open position, 57 sec are required for a 1-cm increase in water level. This corresponds to a flow rate of 0.606 liter/sec, to be compared with the authorized maximum low flow rate of 0.631 liter/sec.

Zero Correction for Standpipe Selsyn

The water is recirculated at the low flow rate during operation, resulting in a meniscus at the overflow of the standpipe. Thus a difference exists between the water level and height of the overflow standpipe as read from the selsyn indicator at the control console. In order that a correction could be applied, a determination of the significance of the position-indicator readings at the standpipe in terms of the actual water level was made by means of probes suspended from the upper tank structure. Initially, a flat weir plate was used on the standpipe. For this, a correction factor of +1.50 cm was necessary to convert the selsyn reading to actual water height as measured from the bottom of the fuel. A change to a crested weir plate after loading No. 20 resulted in a new factor of +1.70 cm. For the experiments with the clustered geometry, the fuel was positioned 1.27 cm lower in the core tank and so the factor then was +0.43 cm.

Heating and Cooling Rates

During the testing of the system at elevated temperature, it was found that the two 36-kw immersion heaters were able to heat the water in the dump tank at a rate of approximately 5°C/hr with the cell exhaust fans running and no circulation of the water.

Source Interlock

The source interlock was provided to prevent startup before the source had been inserted. As initially wired, withdrawal of the source at any time would shut the reactor down, and, conversely, any shutdown signal would deactivate the magnetic clutch for the source drive, causing the source to drop into its storage well.

As originally designed, it was necessary to bypass the source interlock by a key-operated switch when the source was removed for establishing criticality. The wording in the Hazards Summary Report anticipated this situation, as follows: "Operation of the assembly may not begin as long as interlocks are shorted out. Any exception must be approved in the log book by both of the qualified operators." While the word "begin" provides for the routine operational procedure regarding the source, it was not intended to apply to the other interlocks. Shorting of any of the other interlocks at any time during operation must be justified in the log book.

Interruption of clutch power for the source drive at shutdown was provided to insure that the source had been returned to its shield before a person entered the reactor cell. This could be accomplished equally well by interlocking the source drive clutch power with the door to the cell. This change was made to reduce the possibility of damage to the source or the drive unit due to the shock associated with the source drop. With this change, the operator has the opportunity to withdraw the source (if still in the core) following a shutdown. If he forgets, it drops into a shielded pit when the cell door is opened, thus achieving the same result provided by the original arrangement.

Power Keys

The Hazards Summary Report stated: "Power for operation of the facility may be turned on through the combination of two keys. Only two keys will be in existence and the number of personnel authorized for possession of a key will be limited. Presence of the key in its proper switch will indicate knowledge and approval of the current operation by the qualified operator supplying the key."

Usually there are more than two qualified operators for the ZPR-VII system, and so a practical difficulty exists in making available a key to any two of the qualified operators without having any one able to obtain both keys. Assignment of a registered key to each of the qualified operators is the present procedure. It is believed that this actually provides more assurance that each operation of the assembly is properly supervised.

Miscellaneous Mechanical Modifications

Several mechanical modifications have been made in the ZPR-VII system. The plastic porthole in the top cover plate has been replaced by a thin rubber sheet to serve as a pressure-relief device. The standpipe which provides a coarse indication of water level has been moved from the side of the core tank to the control room and a second standpipe added in parallel for precise measurement of water level, supplementing the variable standpipe selsyn indicator. Adjustable projections were added to the void holddown plate to minimize lateral motion of the element clusters. The bolts which held the core tank cover in place have been replaced by toggle clamps.

Appendix B

CHARACTERISTICS OF FUEL PELLETS

Physical and chemical measurements on the fuel pellets of 25/1 and 50/1 thorium-to-uranium ratio have provided the information on the dimensions and composition required for the interpretation of the results of the critical experiments performed with this fuel. The nature of these measurements and the results are reported below.

The records on transfer of materials, as maintained by the Special Materials Department, provide a consistent set of data on the composition of the fuel elements. This information is presented in Table XLII for comparison with the values obtained from the measurements described in this Appendix.

Table XLII

PROPERTIES OF REPRESENTATIVE THUD FUEL ELEMENTS FROM ACCOUNTABILITY DATA

	25/1	50/1
Total weight (gm)	356.24	349.64
Thorium (gm)	301.05	301.26
U^{235} (gm)	12.037	6.01
U (gm)	12.943	6.47
Th, wt-%	84.51	86.16
U^{235},* wt-%	3.38	1.72
U, wt-%	3.63	1.85
Th-U^{235} atom ratio	25.33	50.77
Th-U weight ratio	25.01	50.12

*Based on a 93% isotopic content.

Variation of Fuel Weights

The number of fuel elements having net fuel weights in successive half gram intervals is indicated in Figure 37, for both ratios of fuel. These results are based on weighings made by the supplier. For the 25/1 fuel, three well-defined Gaussian type distributions exist, indicating significant changes in the processing of the material during the production of successive batches of the 25:1 fuel. The average weight for 1630 rods was 357.2 gm. A single broad distribution of weights occurs for the 50/1 fuel. This single peak is more than twice the width of the peaks observed for the 25:1 fuel, indicating that perhaps that here too the fabrication was not well

controlled, but that two or more batches having peaks fairly close together resulted in the processing of the 50:1 fuel. The average weight for 1525 50/1 fuel rods was 349.8 gm. These average weights are slightly less than the values obtained from the Special Materials' records. The small difference may be attributed to cumulative errors in weighing, intentionally added binder, and small amounts of other material which may be present.

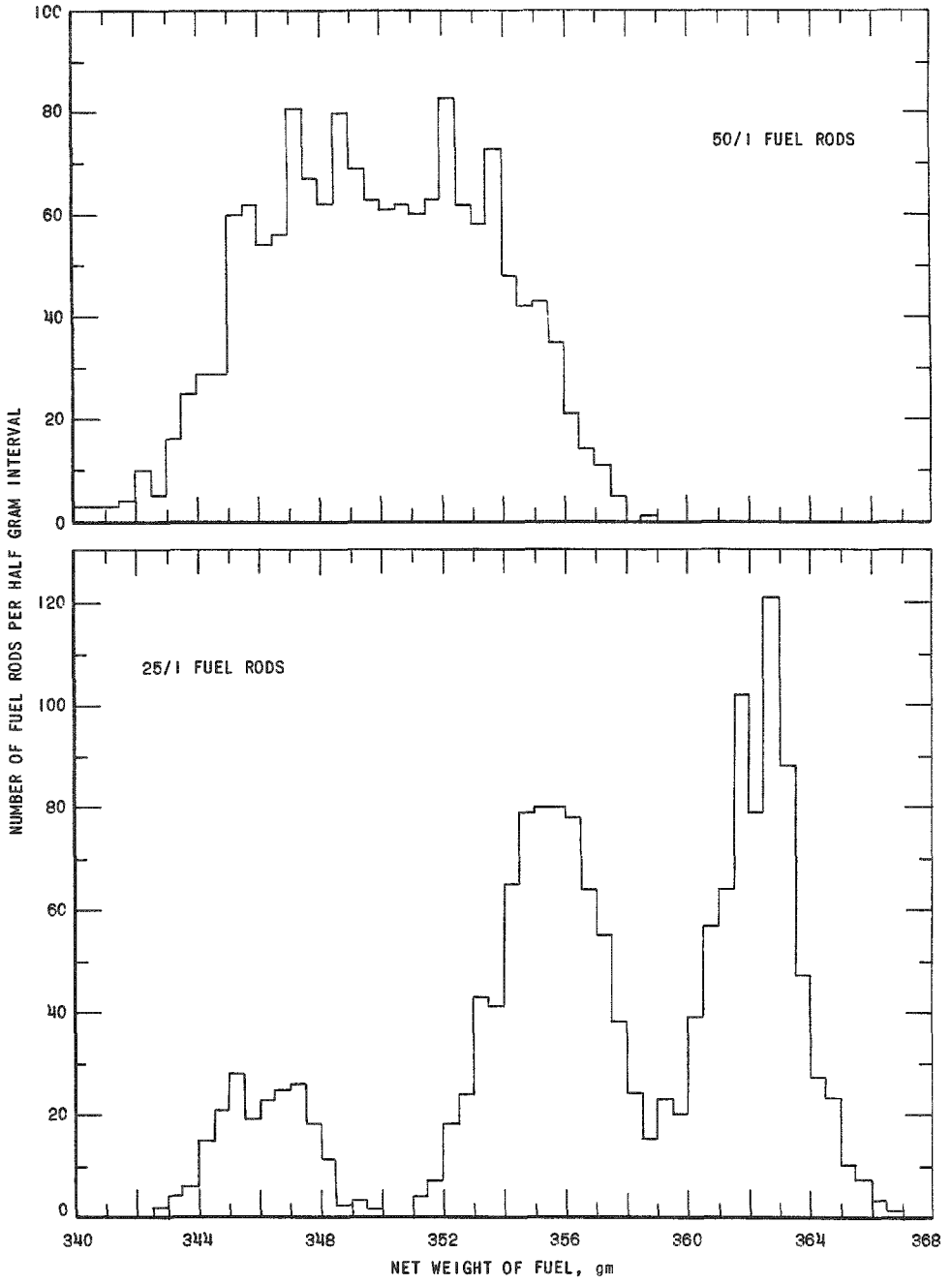

Fig. 37. Weight Distribution of THUD Fuel Rods

Pellet Faults

In an effort to explain the variation in weight among the 25/1 fuel elements, an X-ray examination was made of 32 of these elements. It was found that damaged, malformed, and separated pellets occurred in about 3 to 5% of the total. There were a few badly damaged pellets and a few widely separated pellets. The separations were usually found near the top of the fuel rod. Most separations were unobstructed; however, a few pellets could not meet because of loose fragments between the pellets. The light fuel rods had as good or better appearance than the heavier ones, possibly because of less pellet shrinkage during fusing.

Dimensions and Weight of Individual Pellets

The physical characteristics of individual pellets of the fuel were measured, in order to evaluate any effect on the experimental program. Localized measurements such as disadvantage factor, resonance escape probability, and foil activations would be influenced by local fuel variations. A group of 103 near-perfect pellets were selected from seven fuel pins for individual measurements. Ninety-one of these pellets were picked from six of the 25/1 fuel elements. The remaining 12 were from a single 50/1 one. Results are given, with standard deviations, in Table XLIII. The weight and length measurements were determined with high precision. However, the density measurements are relatively sensitive to the error in measuring diameter. Diameters were quite consistent for a given pellet, but showed about 1/2% standard deviation from pellet to pellet.

Table XLIII

WEIGHT AND DIMENSIONS OF SELECTED PELLETS

	25/1	50/1
Gm/cm, average	2.341 ± 0.031	2.311 ± 0.039
Range of length, cm	1.149 - 1.667	1.520 - 1.570
Range of diameter, cm	0.579 - 0.594	0.579 - 0.584
Density, gm/cm^3	8.63 ± 0.15	8.71 ± 0.17

Chemical and Mass Spectrometric Analysis

Uranium Content

Samples of the THUD fuel were analyzed chemically as a check on the reported concentration of thorium and uranium. The first eight pellets submitted for analysis of uranium content were selected from among the 91 pellets of 25/1 fuel on which weight and dimensional measurements were made.

These eight fuel pellets covered the entire range of densities observed from 8.37 gm/cm^3 to 8.90 gm/cm^3, and the concentrations of seven pellets agreed to 1%. Also, the values for these pellets agreed reasonably well with a value based on the 25:1 atom ratio of thorium to U^{235}. The one remaining pellet had a uranium concentration 10% higher. Each analysis was done twice except for that pellet having the high concentration. This analysis was repeated four times. The uranium concentrations, weight per unit length, and density of each pellet are given in Table XLIV. Although the pellet having the high uranium content also has the highest density, the other samples seem to indicate that there is no relationship between uranium content and density.

Table XLIV

URANIUM CONTENT OF SELECTED 25/1 FUEL PELLETS

Sample No.	Rod No.	Weight/Length (gm/cm)	Density (gm/cm^3)	Average Uranium Concentration (Wt-%)
1	941	2.376	8.64	3.67
2	1525	2.302	8.37	3.72
3	1525	2.310	8.47	3.68
4	1525	2.366	8.90	4.18
5	1585	2.332	8.41	3.68
6	1595	2.358	8.72	3.70
7	1625	2.344	8.82	3.70
8	1625	2.388	8.68	3.72
9	Unknown	Not Measured	Not Measured	4.11
10	↓	↓	↓	4.21
11				3.71
12				3.74
13				3.74
14				3.72

Confirmation of the existence of pellets with a uranium content appreciably higher than the specified value was obtained in a subsequent analysis of six additional pellets, selected by measurement of the fission rate. Results of the analysis of these pellets are also included in Table XLIV. The fission rates of the two (rod unknown) pellets with 4.11 and 4.21 wt-% analyses were about 11% higher than normal and such pellets occurred with less than 1% frequency. The remaining four pellets were selected as being normal representatives of the 300 25/1 pellets tested for fission rate.

Thorium and Uranium Isotopic Content

The fission rate measurements on a smaller sampling of 50/1 pellets indicated no abnormalities, but two of these pellets were included among four samples submitted for a chemical determination of thorium content and a mass spectrometric measurement of the relative abundance of the uranium isotopes. The values reported by the Special Materials Analytical Laboratory, together with its estimate of errors, are collected in Table XLV. Reference to the table of data based on accountability records reveals a slight inconsistency.

Table XLV

WT-% OF THORIUM, URANIUM, AND URANIUM ISOTOPES IN THUD FUEL SAMPLES

Sample	A	B	C	D
Fuel Type	25/1	25/1	50/1	50/1
Thorium	84.06 ± 0.17	84.20 ± 0.17	85.98 ± 0.17	85.87 ± 0.17
Uranium	3.72 ± 0.06	3.70 ± 0.06	1.90 ± 0.03	1.91 ± 0.03
U^{234}	0.99 ± 0.01	0.814 ± 0.008	1.00 ± 0.01	1.04 ± 0.02
U^{235}	93.28 ± 0.05	93.29 ± 0.05	93.28 ± 0.05	92.85 ± 0.08
U^{236}	0.467 ± 0.008	0.443 ± 0.004	0.474 ± 0.005	0.480 ± 0.005
U^{238}	5.26 ± 0.05	5.45 ± 0.05	5.25 ± 0.05	5.63 ± 0.08

Impurities

A spectrochemical analysis of each of the first eight pellets analyzed for uranium content indicated the presence of trace amounts of several elements other than thorium and uranium. A typical result yielded the following weight percents of certain elements: Al, 0.07%; Ca, 0.07% (?); Fe, $< 0.05\%$; and Mg, 0.05% (?). Note that the estimated accuracy is a factor of two, and that the presence of two of the four elements detected is considered questionable. There was no pellet-to-pellet variation in the concentration of these elements. No chemical analyses were made of the 50/1 fuel.

Relative U^{235} Content by Neutron Irradiation

As alternates to the chemical procedure, the variation in uranium content among the fuel pellets was investigated by observation of the relative number of fast neutrons emitted by pellets placed in a neutron beam from the thermal column of CP-5 and also by measurement of the fission product decay activity of irradiated pellets. Using a background correction based on the counting rate observed with a pure thoria pellet, a proportionality was observed between the corrected counting rate and the pellet

weight, for an initial batch of 36 pellets. Only two pellet activities fell more than 1% off the established line. The data indicated uniform mixing of thoria and urania batches before pelleting. A self-shielding correction for absorption of neutrons brought the extrapolated curve nearer zero counting rate at zero pellet weight; however, it appeared that further study was needed to construct the exact shape of the curve.

Following the chance discovery of a pellet with an abnormally high uranium content, sample No. 4 of Table XLIV, an additional 250 or so pellets of the nominal 25/1 fuel were measured by this technique.

The fixture in which the pellets had been mounted for the first irradiations was replaced with one of much less mass. The data obtained with this fixture extrapolated through the (zero,zero) intercept. Only three pellets in this second batch indicated an unexpected fast neutron emission rate, the two whose high value of uranium content was confirmed by chemical analysis, (samples No. 9 and No. 10 of Table XLIV) and one with a rate about midway between that for these two pellets and the remainder.

About 50 pellets of 50/1 fuel were also investigated. Fast neutron emission and fission product decay activity both agreed with the accountability information within the accuracy of the self-shielding corrections. Less variation among pellets was found in 50/1 fuel than in 25/1 fuel. However, this may have resulted from the sampling of only two fuel rods.

ACKNOWLEDGMENT

The complexity of a program of critical experimentation and the extended nature of the THUD program in both scope and duration have necessitated an appreciable effort by a large number of individuals. The authors are extremely appreciative of the support given by many of our associates in following through on the plans and the execution of the program of measurements undertaken with thoria-urania fuel in heavy water.

To some extent it is possible to cite specific contributions made by those who have contributed to the work reported in this summary of the experimental results. The determination of relative photoneutron effectiveness reported in Section VI, C has been made mainly by C. E. Cohn. J. L. Helfrich, while on loan from Frankford Arsenal, Philadelphia, Pennsylvania, was responsible for establishing the techniques and performing the initial measurements of the thorium-cadmium ratio, as described in Section IV, D. E. Hellstrand from AB Atomenergi, Stockholm, Sweden, participated in the determination of disadvantage factors discussed in Section IV, E during his brief association with the THUD program. J. A. Beidelman was responsible for much of the work performed in connection with the measurements of reflector savings (Section IV, A) and fast fission factor (Section IV, F).

Important contributions in the operation of the ZPR-VII facility for the acquisition of critical assembly data had been made by J. W. Armstrong, D. Daavettila, R. M. Mattson, and A. B. Rothman, in addition to their part in special measurements made using the THUD system but not included in this report. L. R. Dates has provided valuable support for the THUD program through the design of special mechanical devices and the modifications necessary to the original system described in the Hazards Summary Report.

Several individuals not listed as co-authors have performed valuable services in support of the program of measurements carried out on this system. W. R. Robinson participated in most of the measurements based on foil-activation techniques, and Ingeborg K. Olson handled most of the data processing associated with the measurements. In addition, these two individuals have been very helpful in the preparation of this report through their assistance in the organization of the data presented. S. Skladzien was responsible for the radiochemical procedures involved in the fast fission factor measurement. R. A. Meschke of the Reactor Operations Division performed the numerous analyses of the heavy water purity. J. H. Handwerk of the Metallurgy Division provided advice and guidance to the supplier of the thoria-urania fuel pellets. A. F. Engfer directed the crew responsible for the maintenance and modifications of the instrumentation and control circuitry.

REFERENCES

1. W. C. Redman, Age and Resonance Escape Probability for the THUD Critical, in Thorium-U^{233} Symposium, Jan. 9-10, 1958, BNL-483 (C-26), pp. 61-72..

2. W. C. Redman and J. A. Thie, Properties of Exponential and Critical Systems of Thoria-Urania and Heavy Water, and Their Application to Reactor Design, Proceedings of the Second United Nations International Conference on the Peaceful Uses of Atomic Energy, Geneva, Switzerland, 12, 402-413 (1958).

3. W. C. Redman, S. G. Kaufmann, and J. W. Armstrong, Heterogeneous Critical Experiments with ThO_2, UO_2 and D_2O, 2nd Winter ANS Meeting, N. Y., Oct. 28-31, 1957, Session 2, Paper 8.

4. J. W. Armstrong, J. A. Beidelman, S. G. Kaufmann, and K. E. Plumlee; Experiments in Thoria-Urania D_2O Criticals, Trans. ANS 1, No. 1, 98-99 (1958).

5. R. A. Mattson and J. L. Helfrich, Resonance Integral and Escape Probability for a Thoria-Urania-D_2O System, Trans. ANS 1, No. 1, 99-100 (1958).

6. W. C. Redman, B. S. Maxon, and D. A. Daavetilla, Determination of Neutron Age and Resonance Escape Probability, Trans. ANS 1, No. 1, 100 (1958).

7. K. E. Plumlee and S. G. Kaufmann, Flux to Fission Rates in Annular Cores, Trans. ANS 2, No. 1, 166-167 (1959).

8. W. C. Redman and J. A. Beidelman, Clustering Experiments with ThO_2-UO_2 Fuel in D_2O, Trans. ANS 2, No. 1, 167-168 (1959).

9. A. B. Rothman and E. M. Pennington, Water Worth Methods in Determining M^2 in THUD Cores, Trans. ANS 2, No. 1, 170-171 (1959).

10. W. C. Redman, J. A. Thie, and L. R. Dates, Hazards Summary Report on the Oxide Critical Experiments, ANL-5715 (April 1957).

11. C. A. Pesce, Nuclear Instrumentation and Control of the D_2O-Moderated Thoria-Urania Critical Assembly (ZPR VII), ANL-5942 (May 1959).

12. N. L. Snidow, R. C. Anderson, M. L. Batch, G. A. G. deCoulon, R. H. Lewis, and W. M. Vannoy, Thorium-Uranium Physics Experiments - Final Report, BAW-1191 (May 1960).

13. K. E. Plumlee and M. T. Wiggins, Foil Activation Data Handling with Automatic Counters and a High Speed Computer, Trans. ANS 4, No. 1, 63-64 (1961).

14. S. Krasik and A. Radkowsky, PWR Critical Experiments, Proceedings of the International Conference on the Peaceful Uses of Atomic Energy, 5, 203-214 (1956).

15. H. Kouts, Analysis of p Measurement, BNL-2095 (1954).

16. D. Klein, A. Z. Kranz, G. G. Smith, W. Baer, and J. DeJuren, Measurements of Thermal Utilization, Resonance Escape Probability, and Fast Effect in Water Moderated, Slightly Enriched Uranium and Uranium Oxide Lattices, Nuclear Science and Engineering, 3, 403-427 (1958).

17. R. Sher, BNL, private communication (1960).

18. Eastman Kodak Co., Kodak Photographic Plates for Scientific and Technical Use, 7th ed., Rochester, N. Y. (1953), p. 15.

19. S. Glasstone and M. C. Edlund, The Elements of Nuclear Reactor Theory, D. Van Nostrand Co., Inc., Princeton, New Jersey (1952), p. 301.

20. G. R. Keepin and T. F. Wimett, Reactor Kinetics Functions: A New Evaluation, Nucleonics 16 (10), 86-90 (1958).

21. W. K. Ergen, Hard Gamma Emitters Among Fission Fragments, ANP-59 (1951).

22. S. Bernstein, W. M. Preston, C. Wolfe, and R. E. Slattery, Yield of Photoneutron from U^{235} Fission Products in Heavy Water, Phys. Rev., 71, 573-581 (1947).

23. W. D. B. Spaatz, D. J. Hughes, and A. Cahn, Photoneutrons Produced in D_2O and Beryllium by Fission Product Gamma-Rays, CP-3472 (MDDC-764) (1946).

24. M. Johns and B. Sargent, Photoneutrons in a Heavy Water Pile, CRP-416 (PD-238), (1949).